NASA CONTRACTOR REPORT

NASA CR-2805

NASA CR-2 C.1

DETERMINATION OF CONSTANT-VOLUME BALLOON CAPABILITIES FOR AERONAUTICAL RESEARCH

Frank B. Tatom and Richard L. King

Prepared by
SCIENCE APPLICATIONS, INC.
Huntsville, Ala. 35805
for George C. Marshall Space Flight Center

NATIONAL AERONAUTICS AND SPACE ADMINISTRATION • WASHINGTON, D. C. • MARCH 1977

TECHNICAL REPORT

1. REPORT NO. NASA CR-2805	2. GOVERNMENT ACCESSION NO.	3. RECIPIENT'S CATALOG NO.
4. TITLE AND SUBTITLE Determination of Constant-Volume Balloon Capabilities for Aeronautical Research		5. REPORT DATE March 1977
		6. PERFORMING ORGANIZATION CODE
7. AUTHOR(S) Frank B. Tatom and Richard L. King		8. PERFORMING ORGANIZATION REPORT # M-208
9. PERFORMING ORGANIZATION NAME AND ADDRESS Science Applications, Inc. Huntsville, Alabama 35805		10. WORK UNIT NO.
		11. CONTRACT OR GRANT NO. NAS8-31173
12. SPONSORING AGENCY NAME AND ADDRESS National Aeronautics and Space Administration Washington, D.C. 20546		13. TYPE OF REPORT & PERIOD COVERED Contractor
		14. SPONSORING AGENCY CODE

15. SUPPLEMENTARY NOTES

This report was prepared under the technical monitorship of the Aerospace Environment Division, Space Sciences Laboratory, NASA/Marshall Space Flight Center.

16. ABSTRACT

The report is concerned with determining the proper application of constant-volume balloons (CVB) for measurement of atmospheric phenomena and with the proper interpretation of the resulting data. A literature survey covering 176 references is included. The governing equations describing the three-dimensional motion of a CVB immersed in a flow field are developed. The flow field model is periodic, three-dimensional, and nonhomogeneous, with mean translational motion. The balloon motion and flow field equations are cast into dimensionless form for greater generality, and certain significant dimensionless groups are identified. An alternate treatment of the balloon motion, based on first-order perturbation analysis, is also presented. A description of the digital computer program, BALLOON, used for numerically integrating the governing equations is provided. The numerical results based on the program are presented and discussed together with a number of general observations regarding the balloon motion. Conclusions based on the results of the literature study, the development of the governing equations, the dimensional analysis, and the numerical results are provided together with certain recommendations.

17. KEY WORDS Constant Volume Balloons, Wind Measurements, Tetroon		18. DISTRIBUTION STATEMENT Category: 47	
19. SECURITY CLASSIF. (of this report) Unclassified	20. SECURITY CLASSIF. (of this page) Unclassified	21. NO. OF PAGES 185	22. PRICE $7.50

* For sale by the National Technical Information Service, Springfield, Virginia 22161

FOREWORD

This report was prepared for the National Aeronautics and Space Administration, Marshall Space Flight Center, as a summary report on one phase of the work on Contract NAS8-31173, "Determination of Constant-Volume Balloon Capabilities for Aeronautical Research". The work described herein was performed by Science Applications, Incorporated, Huntsville Division with Dr. Frank B. Tatom as Principal Investigator.

The NASA Contracting Officer's Representative for this work is Dr. George H. Fichtl, MSFC Space Sciences Laboratory (ES-43).

ACKNOWLEDGEMENTS

Special acknowledgements for their continuing interest and support of this and other aviation safety tasks, are due Mr. William McGowan of the Office of Aeronautics and Space Technology, NASA Headquarters and Mr. John Enders, formerly of the same organization, and currently of the Federal Aviation Administration.

TABLE OF CONTENTS

TABLE OF CONTENTS
(continued)

TABLE OF CONTENTS
(continued)

LIST OF ILLUSTRATIONS

LIST OF ILLUSTRATIONS
(continued)

LIST OF TABLES

LIST OF SYMBOLS

Symbol	Definition
	English Symbols
a	$\frac{36\mu}{(2\sigma+\rho)D^2}$ (Appendix B only)
a	first constant in linearized approximation for Basset term (Appendix M only)
$\tilde{a}$	$\frac{\gamma D}{T_o}$ (Appendix C only)
A	fluid wave amplitude for x_1-direction
A_{ij}	element of experiment matrix in Phase I
b	$\frac{3\rho}{2\sigma+\rho}$ (Appendix B only)
b	second constant in linearized approximation for Basset term (Appendix M only)
$\tilde{b}$	$g/R\gamma$ (Appendix C only)
B	fluid wave amplitude for x_2-direction
$B(k,\omega;x_3)$	Fourier transform of $u'_1(x_1,t,x_3)$
$B_{\ell k}$	element of experiment matrix in Phase II
c	$\frac{18}{(2\sigma+\rho)D}\sqrt{\frac{\rho\mu}{\pi}}$ (Appendix B only)
c	phase velocity, ω/k
C	fluid wave amplitude for x_3-direction

Symbol	Definition
C_D	drag coefficient
$C_{D\ell}$	drag coefficient (10^3<Re<10^5)
C_{22}	cruciform arrangement about element A_{22} in matrix A_{ij}
C_{33}	cruciform arrangement about element A_{33} in matrix A_{ij}
d	$\frac{2(\sigma-\rho)}{2\sigma+\rho}$ (Appendix B only)
D	diameter of spherical body (balloon)
D_{iim}	m-th element in lower arm of cruciform arrangement C_{ii}
f( )	function of ( )
$F(k,\omega;X_{30})$	$\langle B(k,\omega;X_{30})B^*(k,\omega;X_{30})\rangle$
$(F_B)_i$	i-th component of force based on Basset term
$(F_D)_i$	i-th component of drag force
$(Fg)_i$	i-th component of gravitational force
$(Fp)_i$	i-th component of pressure force (dynamic buoyancy)
g	gravitational acceleration
G_1	nonlinear contribution to the drag term (Appendix M only)
$H_L(\tau;X_{30})$	quasi-Lagrangian time auto-correlation function for stationary turbulence

LIST OF SYMBOLS

(Continued)

Symbol	Definition
$\hat{i}$	the longitudinal component (x_1-direction) of the unit vector
k	wave number in stationary coordinate system
K	spatial wave number in transformed coordinate system
ℓ	length
L_{iim}	m-th element in left arm of cruciform arrangement C_{ii}
L_1	first dimensionless group, $\frac{\rho}{2\sigma+\rho}$
L_2	second dimensionless group, $\frac{\sigma}{2\sigma+\rho}$
L_3	third dimensionless group, $\frac{12\nu}{AD}$
L_4	fourth dimensionless group, $\frac{1}{2} C_{D\ell}$
L_5	fifth dimensionless group, $\frac{2}{3} g \frac{(g/R-\gamma)D^2}{A^2 T_o}$

LIST OF SYMBOLS

(Continued)

Symbol	Definition
L_6	sixth dimensionless group, $6\sqrt{\nu/(AD\pi)}$
m	mass of spherical body (balloon)
m_a	apparent mass of the displaced fluid
M	mass
N^2	linear component of buoyancy term (Appendix M only)
p	pressure in the flow field
R	specific gas constant
R_{iim}	m-th element in right arm of cruciform arrangement C_{ii}
Re	the Reynolds number for flow past the balloon
t	elapsed time
T	atmospheric temperature
u_i	wind velocity component in x_i-direction
U_{iim}	m-th element in upper arm of cruciform arrangement C_{ii}
v_i	velocity component of spherical body (balloon) in x_i-direction
V	volume of spherical body (balloon)
x_i	component of Cartesian coordinate system
x_3	vertical position relative to equilibrium altitude, x_{30}

LIST OF SYMBOLS

(Continued)

Symbol	Definition
x_{30}	equilibrium altitude at which $\sigma=\rho_o$
X_i	balloon coordinate

Greek Symbols

α	linear drag term used in first-order theoretical analysis (Appendix M only)
β	latitudinal derivative of Coriolis force, appearing in phase velocity relation for Rossby wave (Appendices H, I and J only)
β	ratio of Eulerian frequency to quasi-Lagrangian frequency
γ	constant temperature lapse rate
γ_p	lapse rate of air parcel
Γ_s	adiabatic lapse rate
Γ_ρ	constant density lapse rate
$\delta(\ )$	Dirac delta function
δ_{ij}	Kronecker delta function
ζ	$k(x_1+x_2+x_3)$
Θ_i	phase angle for i-th component of fluid velocity
λ	frequency for case #2 in linear analysis (Appendix M only)

LIST OF SYMBOLS

(Continued)

Symbol	Definition
λ_j	micro-scale of turbulence
μ	dynamic viscosity
ν	kinematic viscosity
Π	dimensionless group
ρ	density of ambient fluid
σ	density of spherical body (balloon)
σ^2	variance
τ	period of oscillation according to first-order theory
τ	time relative to some elapsed time t (Appendix H only)
τ_o	$2\pi/N$ (Appendix M only)
τ_α	$2\pi/\alpha$ (Appendix M only)
$\phi_E(k,\omega,x_1,t;x_3)$	general Eulerian space-time power spectrum
$\phi_E(K,K\bar{u}_1-\Omega,x_{30})$	Eulerian space-time power spectrum at equilibrium altitude x_{30}
$\Phi_E(k;x_{30})$	Eulerian space power spectrum at equilibrium altitude x_{30}
$\psi_L(K,\Omega;X_{30})$	Lagrangian two-dimensional space-time spectrum
$\Psi_L(\Omega,x_{30})$	quasi-Lagrangian time power spectrum at equilibrium altitude x_{30}
ω	Eulerian frequency of the wind

LIST OF SYMBOLS

(Continued)

Symbol	Definition
Ω	transformed frequency in coordinate system moving with the mean wind
Ω'_L	quasi-Lagrangian frequency of the balloon

Superscripts

$\tilde{}$	dimensionless
*	conjugate
$\bar{}$	mean value
$\rightarrow$	vector
'	quasi
'	fluctuating quantity (Appendix H only)
$\hat{}$	unit vector

Subscripts

a	apparent
B.V.	Brunt-Väisälä
CVB	constant-volume balloons
(DISPERSIVE)	characteristic of a dispersive medium
E	Eulerian
(GRAVITY)	gravity waves
i	i-th component
j	j-th component

LIST OF SYMBOLS

(Concluded)

Symbol	Definition
L	Lagrangian
o	equilibrium altitude
(ROSSBY)	Rossby waves
(TAYLOR)	according to Taylor's hypothesis
1	longitudinal direction in horizontal plane (normally alligned with mean wind direction)
2	transverse direction in horizontal plane
3	vertical direction

Miscellaneous Symbols

< >	ensemble average
$\Longrightarrow$	implies

1. INTRODUCTION AND SUMMARY

The use of constant-volume balloons (CVB) has proven a popular method of measuring atmospheric phenomena. Certain questions, regarding the proper application of such balloons and the proper interpretation of resulting data, have arisen. Thus a need has developed for determining the true capabilities of the CVB for aeronautical research. This study described in this report was designed to satisfy this need.

The initial phase of the study involved a literature survey concerned with CVB. A description of this survey is contained in Section 2.

Examination of the literature revealed the need for a more rigorous mathematical treatment of the dynamics of CVB in a fluctuating flow field. Accordingly a mathematical model was developed which describes the response of the CVB to three-dimensional periodic non-homogeneous flow. A description of this model is provided in Section 3.

The mathematical model previously noted was incorporated into a digital computer program. Section 4 provides a description of this program, which is called BALLOON.

By means of BALLOON, over 84 numerical runs were conducted with the NASA/MSFC UNIVAC 1108. These runs produced both digital and graphical results as discussed in Section 5. Because of the considerable bulk involved, most of the computer plots are not included. They are available in a separate document [1].

Analysis of the numerical results obtained, combined with a study of the work of other investigations has resulted in certain observations and conclusions. Section 6 contains such observations and conclusions. Because of limitations in the scope of the investigation these conclusions are not considered to be completely general with regard to CVB behavior.

At the same time they do provide some insight into the nature of the problem of properly interpreting data collected by CVB's.

References cited and included in Section 7. In addition there are 16 appendices containing supplementary material. Of special significance is a first-order perturbation analysis contained in Appendix H.

2. LITERATURE SURVEY

The survey of literature consisted of three separate activities. The first involved an inspection of existing balloon literature from the files of the NASA Contracting Officer's Representative, Dr. George H. Fichtl, representing approximately 600 papers and reports. Such an inspection revealed 60 pertinent documents. The second activity involved utilization of the computerized information retrieval system at Redstone Scientific Information Center. The third activity consisted of a personal review of journals pertaining to meteorology and atmospheric physics back to 1969. Because Dr. Fichtl's files appeared to adequately cover all earlier years, the personal review did not proceed back to any earlier journals. The journals review included:

Journal of Meteorology
Journal of the Atmospheric Sciences
Journal of Applied Meteorology
Quarterly Journal of the Royal Meterological Society
Journal of Geophysical Research
Beiträge zür Physik der freien Atmosphüre
Journal of Japanese Meteorology Society

In the process of reviewing the literature some distinction had to be made between different types of balloons. Clearly not all literature concerning balloons is pertinent to the study. At the same time it was recognized that there exist a number of types of balloons which are closely related or nearly equivalent to CVB's. These include tetroons, constant-altitude balloons, constant level balloons, transondes, horizontal-sounding balloons and certain types of super-pressure balloons. A description of each of these types is provided in Appendix A. The decision was made to include in the survey literature pertaining to all of these types of balloons so long as the application of the balloon was consistent with the general application of CVB's.

The results of the survey revealed four categories of articles or reports. The first category is concerned with the general theory, design, and operation of constant-volume balloons as discussed in subsection 2.1. The second category, which is described in subsection 2.2, is concerned with the use of constant-volume balloons to determine the mean wind velocity. The third category, which is of primary interest in the current study, is similar to the second except that, in addition to the mean wind velocity, some measurement of turbulent fluctuations is recorded. This category is presented in subsection 2.3. Within the third category of literature, it is appropriate to recognize two subcategories labeled 3-A and 3-B. In subcategory 3-A, the measurements of turbulent phenomena are presented in their simplest form, involving variation with respect to spatial position or time. In 3-B such data may be present, but in addition, some spectral analysis or correlation of such data is provided. Clearly subcategory 3-B is of special interest in the current investigation. The fourth category which is presented in subsection 2.4, pertains to theoretical studies of the motion of constant-volume balloons and related objects immersed in a turbulent flow field, and also to the theory of atmospheric turbulence.

2.1 Category 1 Literature - General Theory, Design and Operation of Constant-Volume Balloons

For the current investigation, literature describing the general characteristics of constant-volume balloons (CVB) was not of primary importance. At the same time such literature was of some value in providing background material and in developing an understanding of the various uses to which the balloons have been put. More than seventy papers, reports, and articles [2-75] were identified in this category. Some of these also contained information pertinent to other categories as discussed in other subsections. For the sake of brevity the discussion of Category 1 literature which follows will be limited to material of special significance.

The first CVB investigation was reported over sixty-five years ago by Ley [2] and concerned the use of "balanced pilot balloons." The objectives of the study were to obtain a better picture of:

"(a) Periodic oscillations of stratum as apart from variations due to altitude.

(b) Vertical currents or rising winds.

(c) Local eddies or other phenomena."

These objectives correspond quite closely to those of more recent studies. Ley in a separate article [3] also reported on an automatic valve for maintaining such pilot balloons at a constant altitude.

The first apparent use of CVB's in conjunction with radio transmitters was reported by Akerman and Piccard [4] shortly prior to World War II. During the fifteen years following the war a number of articles appeared describing various methods of improving balloon performance [5-17] . The initial works of Lally [14,16] and Angell [15] are included in this group as are some of the works of Hopper [7,13,17] and Laby [13,17].

During the ten-year period from 1961 through 1970, more than 40 category 1 articles were written [18-61]. One of the most useful of these was a summary of the state-of-the-art in 1961 written by Angell [18]. The introduction of Mylar as a material for the balloon skin was probably the most significant development in CVB operations in this period. Both the Ghost balloon experiment [26,27,29,30,31,36,39,43,50,53,57,58] and the EOLE experiment [28,34,35,38,44,54,57] began operations during this period.

Category 1 literature during the period 1971 - 1975 consisted of thirteen articles [62-74]. Several of these were concerned with the EOLE experiment [62,66-68]. One of the most significant articles was concerned with tetrocn drag coefficients over a range of Reynolds number from 10^4 to 6×10^5 [71]. Typical drag coefficient values were .73.

2.2 Category 2 Literature - The Use of the CVB's to Measure the Horizontal Mean Wind

The literature survey uncovered 68 articles, reports, and papers dealing with the use of CVB's to measure the horizontal mean wind velocity. Of these, 23 also contained category 1 material, including the initial work of Ley, and have already been noted [2,12,15,17,18,20,21,26,29,34,43,44,48,53,55,57-59, 63,68,69,72,74]. The remaining 42 papers [75-117] cover a twenty-five year span (1950-1974) and describe various programs in which CVB's were utilized to track the mean horizontal wind. One of these papers [80] was not actually so much concerned with measuring the mean wind as with utilizing such a wind to send "balloon bombs" from Japan to the United States during World War II. A number of investigations involved flights over urban areas [82-84,92,101,105,109,114] while others dealt with the GHOST program [87,89-91,94-96,100,117] and still others with the EOLE experiment [98,99,102,111,112,116,117]. Balloon trajectories at various altitudes were analyzed including 500mb [85], 200mb [116], 50mb [86], and 50km [108]. Clustering phenomena were studied in some cases [85,97] while the relationship between the dispersing of CVB's and turbulent diffusion in the atmosphere was investigated in others [102,104,115]. A number of studies were concerned with balloon trajectories in the planetary boundary layer [97,103,109,110]. Still others were directed toward measurements of rain clouds and thunderstorms [93,113].

In essentially all the studies noted the basic assumption was made that the mean motion of the balloon corresponded to the mean motion of the atmosphere.

2.3 Category 3 Literature - The Use of CVB's to Measure Turbulent Fluctuations

Category 3 literature can be divided into two groups, as noted previously. All literature which contained some measurement of turbulent fluctuations, either vertical or horizontal, was considered Sub-Category 3-A if it did not provide for some form of spectral analysis or correlation of the fluctuations. Sub-Category 3-B consisted of all literature which contained both measurement of fluctuations and spectral analysis or correlation of the data.

2.3.1 Sub-Category 3-A Literature - Without Spectral Analysis of Correlation

Twenty-two different studies provided basic measurements of turbulent fluctuations [2,18,20,25,74,75,83,92,108,110,111, 112,115,118-126]. The majority of these studies were concerned with vertical fluctuation [2,18,20,25,74,83,92,108,110,115, 120,122-126]. The data were generally presented in the form of a plot of altitude, temperature or pressure versus time. The period of oscillation were generally relatively short, being measured in minutes.

Ten studies provided measurement of horizontal fluctuations [75,110-112,118-121,124,125]. As with vertical fluctuation the data were generally presented in the form of a plot of displacement versus time. Two separate groups could be identified. The first of these was concerned with large-scale fluctuation with periods of oscillation measured in hours or even days [111,112] while the second group dealt with small-scale fluctuations with periods of oscillation measured in minutes [110,118-121].

Sub-Category 3-A literature contains a wealth of information but time and manpower limitations precluded any attempt to carry out any detailed analysis of the measured data.

2.3.2 Sub-Category 3-B Literature - With Spectral Analysis or Correlation

The most significant group of literature bearing on the current study consisted of twenty-one articles which provide both turbulence measurements and spectral analysis or correlations of measured data [68,72,78,84,127-143]. It was appropriate to identify two groups within Sub-Category 3-B. In the first of these, the authors generally provided turbulence measurements, based on tracking the CVB, and some analysis of the resulting data [68,72,78,84,127,129,130,135,136,138-141,143]. These types of analyses produced Lagrangian or quasi-Lagrangian representations of turbulence. It is important to note that a wide range of frequencies and wave numbers were covered in these studies. A number of the studies were primarily concerned with low frequency oscillations (.001 to 0.1 cycles/hr) of the horizontal winds [68,130,139,140,143]. The remaining dealt with intermediate to high frequency oscillations (0.1 to 100 cycles/hour) of the vertical winds [72,78,84,127,129,135,136, 138]. In several of these cases the natural frequency of oscillation was detected [72,84,129,136]. One study utilizing neutrally buoyant floats for measuring vertical velocity fluctuations in the ocean (in the spectral range from 10^{-2} to 1 cycle/hour), also detected the natural frequency of oscillation [141].

The seven remaining Sub-Category 3-B papers [128,131-134, 137,142] were especially pertinent to the current investigation because in addition to turbulence measurements and analysis based on the motion of CVB's they also provide corresponding data and analysis based on measurements taken at a stationary point. Thus both Lagrangian (or quasi-Lagrangian) and Eulerian descriptions of turbulence were available for comparison.

The first of these studies is especially noteworthy because of its completeness. Gifford [128] calculated the vertical velocity energy spectra over the range from 3 to 200 cycles/hour at a height of 300 feet based on measurement, by fixed anemometers, CVB's and gust equipment mounted aboard an airplane. He demonstrated that in terms of the frequency, (corresponding to the spectral maxima), the data could be correlated by the relation

$$\omega = \Omega_L' + k\,\bar{u}_1 \qquad (2\text{-}1)$$

where

ω = Eulerian frequency (measured by the fixed anemometer)

Ω_L' = (quasi) Lagrangian frequency (measured by the CVB)

k = wave number (measured by the airplane)

$\bar{u}_1$ = mean wind velocity

Angell and Pack [131], in a study of low-level CVB flights from Wallops Island, obtained measurements of vertical, longitudinal, and transverse fluctuations. Based on such measurements they calculated values of transverse velocity variance and transverse turbulence intensity at altitudes from 2500 - 3000 feet. They provided a comparison of such values with Eulerian values (obtained at heights from 6 to 300 feet) and with other Lagrangian values (obtained at altitudes from 1000 to 3000 feet). In general the values of Lagrangian variance and intensity obtained by Angell and Pack were less than the corresponding Eulerian values and were also less than the other Lagrangian values. Because the mean wind velocities were not provided and because of differences in height at which the various measurements were obtained, it is difficult to draw quantitative conclusions from these comparisons.

Angell [132] in another study carried out an analysis of the trajectories of CVB's launched from Cardington at altitudes ranging from 1200 to 4200 feet. Based on measurement of vertical fluctuations, vertical velocity spectra were derived extending from .01 to 1.0 cycles/minute. The spectral peaks of these quasi-Lagrangian spectra were then compared with corresponding peaks from Eulerian spectra, derived from measurements by wind vanes attached to a barrage-balloon cable at heights ranging from 600 to 3500 feet. The ratio, β, of the frequency for the Eulerian spectral peak to the frequency for the Lagrangian spectral peak was computed and tabulated. Values of β ranged from 1.1 to 8.5. An approximate correlation of β with turbulence intensity was developed.

Kao and Bullock [133] performed a comparison of Lagrangian and Eulerian correlations and energy spectra of geostrophic velocities. The frequency range for the spectra extended from .001 to .07 cycles/hour. The curves for the Eulerian auto correlation coefficients of both horizontal velocity components resembled their Lagrangian counterparts but displayed larger integral time scales. The Eulerian velocity spectra also resembled the Lagrangian but were shifted toward lower frequency. The value of β based on the ratio of the integral time scale was 0.53.

In a separate paper Kao [134] computed and analyzed the Eulerian and Lagrangian autocorrelations and energy spectra of large-scale turbulent motion at the 300 mb level. The results were similar to those presented in the preceding study. The frequency range was the same and the same resemblance of the Eulerian autocorrelation curves and spectra to their Lagrangian counterparts was again observed. The value of β was found to be 0.33. It is important to note that the Lagrangian values were based on data collected by Angell [15] from CVB flights from Japan to the United States while the Eulerian values were based on data collected by Kao over Salt Lake City. The mean wind speeds were not equal in the two experiments.

Angell, Pack, Hoecker, and Delver [137] performed a comparison of Lagrangian and Eulerian time-scales based on CVB flights past a 460 meter tower in Nevada equipped with a bidirection wind vane. The range of frequencies extended from ∿.0003 to .01 cycles/sec. Based on the frequencies corresponding to the spectral peaks, values of β from 1.5 to 4.7 were obtained. A limited correlation of β as a function of turbulence intensity was developed.

In a closely related study, Angell [142] calculated the Lagrangian and Eulerian time scales based on CVB flights past a 460-meter television tower near Oklahoma City. The time scales were based on the spectral peaks of composite Lagrangian and Eulerian spectra with a frequency range from .0001 to 1.0

cycles/second. Values of β ranged from 2.4 to 13. Angell suggested that the presence of an urban area might reduce the Lagrangian time scale, thus causing larger values of β. Correlation of β with turbulence intensity was demonstrated to a limited degree.

2.4 Category 4 Literature - Theoretical Studies of CVB's and Other Bodies Immersed in a Turbulent Flow Field

Many of articles, papers, and reports already described also provided some theoretical treatment regarding the behavior of CVB's [2,20,22,46,58,65,72,72,97-99,102,103,119,122,124, 126,127,136]. Some of these dealt with predicting the expansion of the balloon due to pressure differences and predicting the equilibrium altitude [58,65,72]. Others dealt with predicting the natural frequency of vertical oscillation for the CVB and/or an air parcel [20,58,72,127,136]. Still others were concerned with the response of the CVB to oscillations in the flow field [22,46,97,126]. Two papers dealt with the numerical simulation of the dispersion of CVB [98,99], while two others were concerned with relating balloon dispersion to atmospheric diffusion [102,119]. The behavior of CVB's in the vicinity of mountains was the subject of two other studies [122,124].

Much of the remaining Category 4 literature was concerned with the behavior of a body immersed in a fluid [144-167]. One of the earliest treatments of this problem was that by Bassett [144], who took into account transient viscous effects. For the case of low Reynolds numbers, corresponding to small particles, a sizeable number of studies have been performed [145-154]. These studies generally involved particle densities which were much greater than the fluid density and thus differed significantly from the CVB problem. The rigor with which the governing equations were derived, however, proved useful in establishing the governing equations for CVB motion. Two other papers [155,156] dealt with the behavior of bubbles in fluids, when the density of the bubble is much less than the density of the fluid. The basic question of the natural vertical oscillation in a stratfied fluid has been addressed in a number of studies [20,58,72,127,136] as previously noted. In addition to these, the original work of Brunt [157], for vertical oscillations of an air parcel in the atmosphere, and the work of Larsen [158], for a neutrally buoyant sphere oscillating in a stratified fluid, are worthy of note.

Clearly the most relevant studies involving immersed bodies were those dealing with balloon motion [159-167]. Two papers [161,163] were especially pertinent. The paper by Hirsch and Booker [161] dealt with the response of superpressure balloons to vertical air motions. In developing the governing equation for the balloon response, however, the authors apparently neglected apparent mass and pressure gradient effects as well as the Bassett terms. In addition the equations describing the motions of the air and the balloon, as presented in the paper, appear erroneous. For these reasons the resulting balloon trajectories are of questionable value.

The paper by Hanna and Hoecker [163] was concerned with the response of constant-density balloons to sinusoidal variations of vertical wind speeds. The equation governing the balloon motion was derived with more rigor than noted above, but several important assumptions and/or simplifications were made which were not clearly stated. First, the follow-the-fluid-particle total derivative was assumed identical to the follow-the-balloon total derivative. Second the Bassett term was neglected. The first assumption is valid because the authors considered only a periodic velocity field, which was spatially homogeneous. The second simplification appears acceptable for large Reynolds numbers. The authors presented dimensionless plots for calculating phase lag and amplitude response as a function of the properties of the atmosphere and the balloon.

It is important to note that the authors did not predict any frequency shift of the balloon motion with respect to the air motion.

In addition to literature dealing with the behavior of immersed bodies, certain other Category 4 literature was identified. This included certain studies dealing with CVB trajectories [168-170]. Also, a number of important references dealing with atmospheric turbulence [171-180]. Especially useful in this regard were the works of Lumley and Panofsky [175] and Slade [176].

3. ANALYTICAL DEVELOPMENT

In order to gain a better understanding of the behavior of a constant-volume balloon immersed in a flow field, a mathematical model has been developed based on the appropriate governing equations. The equations describing the balloon motion and the fluid velocity field are presented in subsection 3.1. These equations are presented in both dimensional and dimensionless form. By means of dimensional analysis, as described in subsection 3.2 certain important dimensionless groups can be identified, which are useful in presenting results with more general application.

As an alternative method of treating the problem, a first-order perturbation analysis of a perfectly responding CVB has been performed as discussed in subsection 3.3.

3.1 Governing Equations for Balloon Motion

The governing equations for the motion of a balloon submerged in a turbulent flow field consist of the equations for the conservation of momentum of the balloon coupled with the equations for conservation of momentum of the fluid.

3.1.1 Conservation of Momentum Equations for the Balloon

The conservation of momentum equations were originally derived for small Reynolds numbers (>0.1) as discussed in Appendix B. Based on the derivation provided in that appendix, but without the assumption of low Reynolds numbers, the conservation of momentum equations for a balloon can be written as

$$m\frac{dv_i}{dt} + m_a\frac{d(v_i-u_i)}{dt} = \frac{1}{2}\rho(u_i - v_i)|\vec{u} - \vec{v}|C_D\frac{\pi D^2}{4} - \frac{m}{\sigma}\frac{\partial p}{\partial x_i} + mg\delta_{i3} - \frac{3}{2}\rho D^2\sqrt{\pi\nu}\int_0^t \frac{\frac{d(v_i-u_i)}{dt'}dt'}{\sqrt{t - t'}} \tag{3-1}$$

If viscous stresses in the fluid are neglected,

$$\frac{\partial p}{\partial x_i} = \rho g\delta_{i3} - \rho\frac{Du_i}{Dt} \tag{3-2}$$

A combination of Equations (3-1) and (3-2) yields

$$m \frac{dv_i}{dt} + m_a \frac{d(v_i - u_i)}{dt}$$

$$= \frac{1}{2} \rho (u_i - v_i) \left| \vec{u} - \vec{v} \right| C_D \frac{\pi D^2}{4} - \frac{m}{\sigma} \left(\rho g \delta_{i3} - \rho \frac{Du_i}{Dt} \right)$$

$$+ mg\delta_{i3} - \frac{3}{2} \rho D^2 \sqrt{\pi \nu} \int_o^t \frac{\frac{d(v_i - u_i)}{dt'}}{\sqrt{t - t'}} dt' \tag{3-3}$$

Rearrangement yields

$$(m + m_a) \frac{dv_i}{dt}$$

$$= \frac{1}{2} \rho (u_i - v_i) \left| \vec{u} - \vec{v} \right| C_D \frac{\pi D^2}{4} + \left(m_a + \frac{m\rho}{\sigma} \right) \frac{Du_i}{Dt}$$

$$+ m_a (v_j - u_j) \frac{\partial u_i}{\partial x_j} - (1 - \rho/\sigma) \, mg \, \delta_{i3}$$

$$- \frac{3}{2} \rho D^2 \sqrt{\pi \nu} \int_o^t \frac{\frac{d(v_i - u_i)}{dt'}}{\sqrt{t - t'}} dt' \tag{3-4}$$

Division by $\frac{V\sigma A^2}{D}$ yields

$$\left(\frac{m}{\sigma V} + \frac{m_a}{\sigma V}\right) \frac{d\,(v_i/A)}{d\,(At/D)}$$

$$= \frac{1}{2}\ \frac{\rho}{\sigma}\left(\frac{u_i}{A} - \frac{v_i}{A}\right)\left|\frac{\vec{u}}{A} - \frac{\vec{v}}{A}\right| \frac{C_D\ \pi D^3}{4V}$$

$$+\left(\frac{m_a}{\sigma V} + \frac{m\rho}{\sigma^2 V}\right) \frac{D(u_i/A)}{D(At/D)} + \frac{m_a}{\sigma V}\left(\frac{v_j}{A} - \frac{u_j}{A}\right) \frac{\partial(u_i/A)}{\partial(x_j/D)}$$

$$-\ (1 - \rho/\sigma)\ \frac{m}{\sigma V}\ \frac{gD}{A^2}\ \delta_{i3}$$

$$-\ \frac{3}{2}\ \frac{\rho}{\sigma}\ \frac{D^3}{V}\ \sqrt{\frac{\pi\nu}{AD}} \int_0^{At/D} \frac{\dfrac{d(v_i/A - u_i/A)}{d(At'/D)}}{\sqrt{At/D - At'/D}}\ d(At'/D) \tag{3-5}$$

The following relations hold:

$$m = \sigma V \tag{3-6}$$

$$m_a = \frac{1}{2}\ \rho\ V \tag{3-7}$$

and

$$V = \frac{1}{6}\ \pi D^3 \tag{3-8}$$

With these identities Equation (3-5) can be written

$$(1 + \frac{\tilde{\rho}}{2})\ \frac{d\tilde{v}_i}{d\tilde{t}} = \frac{3}{4}\ (\tilde{u}_i - \tilde{v}_i)\ |\vec{\tilde{u}} - \vec{\tilde{v}}|\ C_D\ \tilde{\rho} + \left(\frac{\tilde{\rho}}{2} + \tilde{\rho}\right)\frac{D\tilde{u}_i}{D\tilde{t}} + \frac{\tilde{\rho}}{2}\ (\tilde{v}_j - \tilde{u}_j)\ \frac{\partial \tilde{u}_i}{\partial \tilde{x}_j}$$

$$-\ (1 - \tilde{\rho})\ \tilde{g}\ \delta_{i3}\ - 9\ \tilde{\rho}\sqrt{\frac{\tilde{\nu}}{\pi}} \int_0^{\tilde{t}} \frac{\dfrac{d(\tilde{v}_i - \tilde{u}_i)}{d\tilde{t}'}}{\sqrt{\tilde{t} - \tilde{t}'}}\ d\tilde{t}' \tag{3-9}$$

where

$$\tilde{\rho} = \rho/\sigma \tag{3-10}$$

$$\tilde{v}_i = v_i/A \tag{3-11}$$

$$\tilde{u}_i = u_i/A \tag{3-12}$$

$$\tilde{t} = At/D \tag{3-13}$$

$$\tilde{x}_j = x_j/D \tag{3-14}$$

$$\tilde{g} = gD/A^2 \tag{3-15}$$

$$\tilde{\nu} = \nu/(AD) \tag{3-16}$$

Division by $\left(\frac{2 + \tilde{\rho}}{2}\right)$ yields

$$\frac{d\tilde{v}_i}{dt} = \frac{3}{4}\left(\frac{2\tilde{\rho}}{2+\tilde{\rho}}\right)C_D\ (\tilde{u}_i - \tilde{v}_i)\ |\vec{\tilde{u}} - \vec{\tilde{v}}| + \frac{3}{2}\left(\frac{2\tilde{\rho}}{2+\tilde{\rho}}\right)\frac{D\tilde{u}_i}{D\tilde{t}}$$

$$+ \frac{1}{2}\left(\frac{2\tilde{\rho}}{2+\tilde{\rho}}\right)(\tilde{v}_j - \tilde{u}_j)\ \frac{\partial\tilde{u}_i}{\partial x_j} - \frac{2(1-\tilde{\rho})}{2+\tilde{\rho}}\ \tilde{g}\ \delta_{i3}$$

$$- \frac{18\tilde{\rho}}{(2+\tilde{\rho})}\sqrt{\frac{\tilde{\nu}}{\pi}}\int_o^{\tilde{t}} \frac{\frac{d(\tilde{v}_i - \tilde{u}_i)}{d\tilde{t}'}}{\sqrt{\tilde{t} - \tilde{t}'}}\,d\tilde{t}' \tag{3-17}$$

Now the drag coefficient C_D can be approximated by the relation

$$C_D = \frac{24}{Re} + C_{D\ell} \qquad (Re < 10^3) \tag{3-18}$$

where

$$C_{D\ell} \simeq .5 \tag{3-19}$$

$$Re = \frac{|\vec{u} - \vec{v}|\ D}{\nu}$$

$$= \frac{|\vec{\tilde{u}} - \vec{\tilde{v}}|}{\tilde{\nu}} \tag{3-20}$$

A combination of Equations (3-17), (3-18) and (3-20) yields

$$\frac{d\tilde{v}_i}{d\tilde{t}} = \frac{3}{2}\left(\frac{\tilde{\rho}}{2+\tilde{\rho}}\right)\frac{24\ \tilde{\nu}}{|\vec{\tilde{u}} - \vec{\tilde{v}}|}\ (\tilde{u}_i - \tilde{v}_i)\ |\vec{\tilde{u}} - \vec{\tilde{v}}|$$

$$+ \frac{3}{2}\left(\frac{\tilde{\rho}}{2+\tilde{\rho}}\right) C_{D\ell}\ (\tilde{u}_i - \tilde{v}_i)\ |\vec{\tilde{u}} - \vec{\tilde{v}}| + 3\left(\frac{\tilde{\rho}}{2+\tilde{\rho}}\right)\frac{D\tilde{u}_i}{D\tilde{t}}$$

$$+\left(\frac{\tilde{\rho}}{2+\tilde{\rho}}\right)(\tilde{v}_j - \tilde{u}_j)\ \frac{\partial\tilde{u}_i}{\partial\tilde{x}_j} - \frac{2(1-\tilde{\rho})}{2+\tilde{\rho}}\ \tilde{g}\ \delta_{i3}$$

$$- 18\left(\frac{\tilde{\rho}}{2+\tilde{\rho}}\right)\sqrt{\frac{\tilde{\nu}}{\pi}}\int_o^{\tilde{t}} \frac{\frac{d(\tilde{v}_i - \tilde{u}_i)}{d\tilde{t}'}}{\sqrt{\tilde{t} - \tilde{t}'}}\ d\tilde{t}'$$

$$= 36\left(\frac{\tilde{\rho}}{2+\tilde{\rho}}\right)\tilde{\nu}\ \ (\tilde{u}_i - \tilde{v}_i) + \frac{3}{2}\left(\frac{\tilde{\rho}}{2+\tilde{\rho}}\right) C_{D\ell}\ (\tilde{u}_i - \tilde{v}_i)\left|\vec{\tilde{u}} - \vec{\tilde{v}}\right|$$

$$+ 3\left(\frac{\tilde{\rho}}{2+\tilde{\rho}}\right)\frac{D\tilde{u}_i}{D\tilde{t}} + \left(\frac{\tilde{\rho}}{2+\tilde{\rho}}\right)(\tilde{v}_j - \tilde{u}_j)\ \frac{\partial\tilde{u}_i}{\partial\tilde{x}_j} - \frac{2\ (1-\tilde{\rho})}{2+\tilde{\rho}}\ \tilde{g}\ \delta_{i3}$$

$$- 18\left(\frac{\tilde{\rho}}{2+\tilde{\rho}}\right)\sqrt{\frac{\tilde{\nu}}{\pi}}\int_o^{\tilde{t}} \frac{\frac{d(\tilde{v}_i - \tilde{u}_i)}{d\tilde{t}'}\,d\tilde{t}'}{\sqrt{\tilde{t} - \tilde{t}'}} \tag{3-21}$$

Further development of the dimensionless form of the equation is provided in Appendix C.

3.1.2 Mathematical Model for the Flow Field

The equations governing the motion of fluid are commonly referred to as the Navier-Stokes equations. Although numerical solutions of these equations are possible, such a procedure is beyond the scope of the current study. Accordingly a simple mathematical model was developed representing a periodic three-dimensional flow field which conserves mass, as described in Appendix D. The final dimensional form of the model is:

$$u_i = \bar{u}_1 \, \delta_{i1} + A \sin \left(\zeta - \omega t + \theta_i \right) \tag{3-22}$$

where

$$\zeta = k \left(x_1 + x_2 + x_3 \right) \tag{3-23}$$

$$\left. \begin{aligned} \theta_1 &= 0 \\ \theta_2 &= 2\pi/3 \\ \theta_3 &= -2\pi/3 \end{aligned} \right\} \tag{3-24}$$

It is important to note that the flow field model is three-dimensional and does contain a mean translational velocity.* To increase the generality of the model it can be cast in dimensionless form as described in Appendix E. In such form the model can be written:

$$\tilde{u}_i = \tilde{\bar{u}}_1 \, \delta_{i1} + \sin \left(\zeta - \tilde{\omega} \tilde{t} + \theta_i \right) \tag{3-25}$$

where

$$\tilde{u}_i = u_i / A \tag{3-26}$$

$$\tilde{\bar{u}}_1 = \bar{u}_1 / A \tag{3-27}$$

---

* These two features of the flow field model distinguish it from the model of Hanna and Hoecker [163] , who, as already noted in Section 2.4, employed a model which contained no mean translational motion and was spatially homogeneous.

$$\zeta = \tilde{k}\ (\tilde{x}_1 + \tilde{x}_2 + \tilde{x}_3) \qquad (3\text{-}28)$$

$$\tilde{k} = k\ D \qquad (3\text{-}29)$$

$$\tilde{x}_i = x/D \qquad (3\text{-}30)$$

$$\tilde{\omega} = \omega D/A \qquad (3\text{-}31)$$

$$\tilde{t} = At/D \qquad (3\text{-}32)$$

3.2 Dimensional Analysis

Inspection of Equation (3-21) reveals certain dimensionless groups. As shown in Appendix C these groups can be written as:

$$L_1 = \frac{\rho}{2\sigma + \rho} \qquad (3\text{-}33)$$

$$L_2 = \frac{\sigma}{2\sigma + \rho} \qquad (3\text{-}34)$$

$$L_3 = \frac{12\ \nu}{AD} \qquad (3\text{-}35)$$

$$L_4 = \frac{1}{2}\ C_{D\ell} \qquad (3\text{-}36)$$

$$L_5 = \frac{2}{3}\ g\ \frac{(g/R-\gamma)D^2}{A^2\ T_o} \qquad (3\text{-}37)$$

$$L_6 = 6\ \sqrt{\nu/(AD\pi} \qquad (3\text{-}38)$$

A comparison of Equations (3-35) and (3-38) reveals

$$L_6 = \sqrt{3L_3/\pi} \qquad (3\text{-}39)$$

For a CVB the balloon density is essentially equal to the atmospheric density. Thus,

$$L_1 \cong 1/3 \qquad (3\text{-}40)$$

and

$$L_2 \cong 1/3 \qquad (3\text{-}41)$$

For simplicity the balloon is assumed to have a spherical shape. For this case

$$C_{D\ell} \cong 1/2 \qquad (3\text{-}42)$$

and

$$L_4 \cong 1/4 \qquad (3\text{-}43)$$

Thus the six dimensionless groups are reduced to two: L_3 and L_5. Furthermore, the dimensionless group, L_3, can be approximated as:

$$L_3 \cong \frac{12\nu_o}{AD} \qquad (3\text{-}44)$$

where ν_o = kinematic viscosity at the equilibrium altitude. This parameter is clearly the reciprocal of a type of Reynolds number as shown in Appendix F. It is important to note that the two dimensionless groups, $12\,\nu_o/(AD)$ and $\frac{2}{3}\,g\,(g/R - \gamma)D^2/(A^2T_o)$ are essentially constant for any given balloon problem and appear sufficient (to first-order accuracy) for characterizing the balloon motion. At the same time, the six original dimensionless groups are not truly constants and the numerical solution of Equations (3-21) described in Section 4, has allowed for the actual variation of these groups to achieve higher-order accuracy.

Examination of Equation (3-25) indicates that the flow field model contains five dimensionless parameters: $\tilde{\bar{u}}_1$, $\tilde{k}$, $\tilde{x}_i$, $\tilde{\omega}$, and $\tilde{t}$. Two of these, $\tilde{x}_i$ and $\tilde{t}$, represent the balloon coordinates in space and time as obtained from the solution to the equation governing the balloon motion, and thus these two parameters

The true significance of Equation (3-45) can best be understood in terms of certain examples as presented in Appendix H. The example based on Taylor's Hypothesis is especially noteworthy. For this case the relation between the two spectra becomes

$$\psi_{L(TAYLOR)}(\Omega,\ x_{30}) = \delta(\Omega) \int_{-\infty}^{\infty} \phi_{E(TAYLOR)}(K;\ x_{30})dK \qquad (3\text{-}48)$$

According to Equation (3-48) the quasi-Lagrangian power spectrum is simply a spike at $\Omega=0$, and is thus independent of the shape of the Eulerian space-time power spectrum. It therefore appears according to the first-order perturbation analysis, that the quasi-Lagrangian power spectrum, obtained from observing the balloon motion, could not be used to describe the Eulerian spectrum, if Taylor's Hypothesis holds.

4. COMPUTER PROGRAM BALLOON

The equations presented in Section 2 were incorporated into a digital computer program entitled "BALLOON". Essentially, the program utilizes a fourth-order Runge-Kutta technique to integrate the differential equations governing the balloon motion. The program consists of a driver routine (MAIN); 9 subroutines (GEOMET, INTEG, ACCEL, PROPTY, BUOYNT, APARNT, DRAG, BASSET, and POTFLU); and 2 functions (DVAL and MREF). The basic orginization of BALLOON is indicated in Figure 4-1.

A copy of the source program is contained in Appendix K. A description of each subroutine or function is contained in Table 4-1. In subsection 4.1 an explanation of all input parameters is provided including the input format. A description of the output is contained in subsection 4.2.

4.1 Inputs

All inputs to the program are read in through MAIN. These inputs can be divided into two segments or blocks. To facilitate explaining the sequence and format for each input item, the actual FORTRAN statements (both READ and FORMAT) associated with the inputs are provided as part of the discussion which follows.

4.1.1 Block #1 Inputs

The first set of inputs consists of data setting up certain initial parameters. The form of the input is as follows:

```
      READ (5,7002) NNN
      READ (5,7001) BCDX,BCDY1,BCDY2,BCDY3,FLDY1,FLDY2,FLDY3
      READ (5,100) G,X,K,THETA,UB,V
      READ (5,100) A,ØMEGA,SIGMA,D,MUREF,TEMREF,T,TLIM,DELTAT,
     *TEMPO,PO,TEMLAP,R,X30
  100 FØRMAT (8E10,3)
 7001 FØRMAT (12A6.8X)
 7002 FØRMAT (12)
```

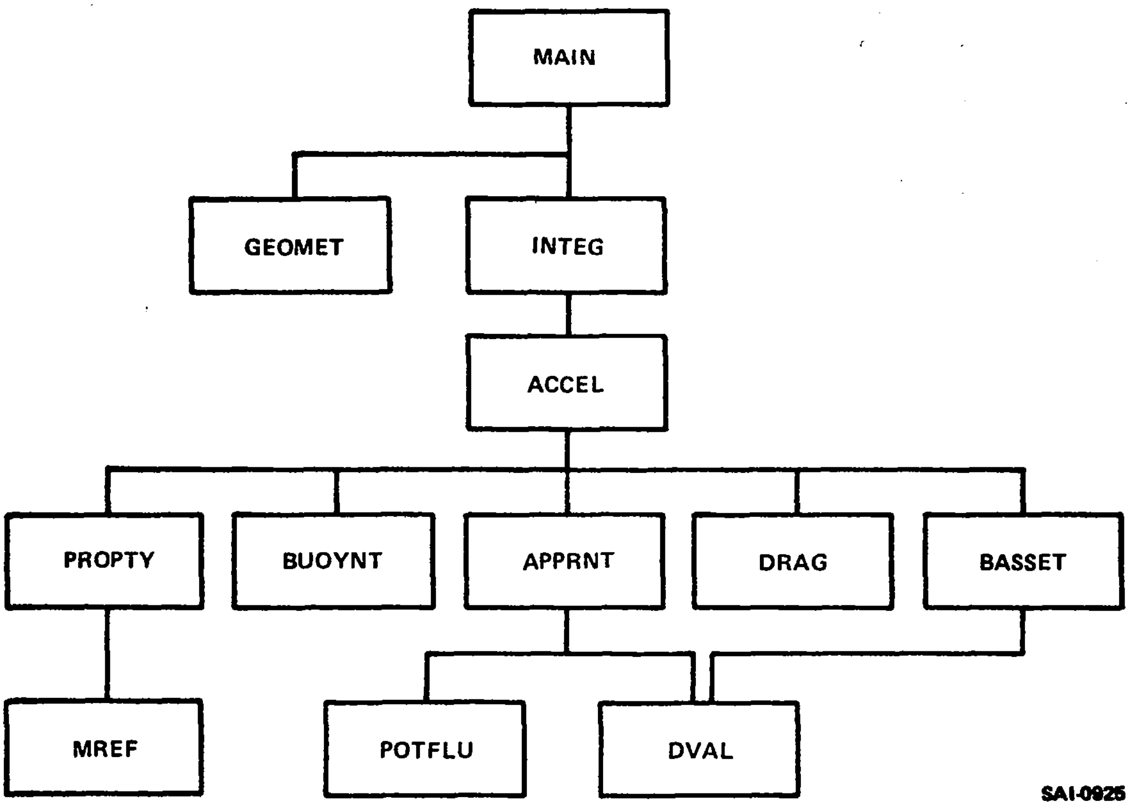

Figure 4-1. Organization of Balloon Program

Table 4-1

Summary of Subroutines and Functions in BALLOON

Name	Purpose	Called by	Calls Up
ACCEL	Calculates acceleration of balloon	INTEG	APPRNT BASSET BUOYNT DRAG PROPTY
APPRNT	Calculates forces due to apparent mass and pressure gradients in the fluid	ACCEL	DVAL POTFLU
BASSET	Calculates Bassett force	ACCEL	DVAL
BUOYNT	Calculates force due to buoyancy	ACCEL	
DVAL	Calculates correction to convection term due to difference in balloon and fluid velocities	APPRNT BASSET	
DRAG	Calculates drag	ACCEL	
GEOMET	Calculates time-independent geometric factors	MAIN	
INTEG	Performs numerical integration	MAIN	ACCEL
MAIN	Serves as driver and provides for input and output		GEOMET INTEG
MREF	Calculates viscosity as a function of temperature	PROPTY	
POTFLU	Calculates flow field derivatives	APPRNT	
PROPTY	Calculates temperature and density as a function of altitude	ACCEL	MREF

Table 4-2 provides a definition of each input item. Notice should be taken than the table is arranged in the same order as the items are read.

4.1.2 Block #2 Inputs

The second set of data occur in the following form:

```
     READ (5,101)XD(2),XD(5),BCDX(11),BCDX(12),T,TLIM,DELTAT,IDT,IDS
101  FØRMAT (2E10.3,10X,2A6,8X,3F5.0,2I5)
```

The data in Block #2 are somewhat redundant of Block #1 data. This redundancy results from certain modifications to the program to permit dimensionless results and to provide for multiple cases to be run in sequence. The meaning of each Block #2 input is provided in Table 4-3. As before, the items in the table are listed in the same order as they are read into the program. One set of these inputs must be provided for each case to be run in sequence.

4.2 Outputs

All outputs to the program occur in MAIN. These outputs can be divided into 4 blocks. As with the description of inputs, to aid in explaining the sequence and format of each output item, the actual FORTRAN statements (both WRITE and FORMAT), associated with the outputs are provided as part of the discussion which follows.

4.2.1 Block #1 Outputs

The first output set occurs in the following form:

```
     WRITE(6,9004) A,B,C
9004 FØRMAT(///10X,1P3E12.4)
```

The variables A, B, C, refer to the amplitudes of the u_1, u_2 and u_3 velocity components. The variable A is read in, but B and C are computed. Sample values of this output is included in Appendix L.

Table 4-2

Definitions of Block #1 Inputs

Variable	Meaning
NNN	The number of different cases to be run in sequence
BCDX	alphanumeric label for abscissa of all plots
BCDY1	alphanumeric label for ordinate of first plot (normally x_i-component of velocity)
BCDY2	alphanumeric label for ordinate of second plot (normally x_2-component of velocity)
BCDY3	alphanumeric label for ordinate of third plot (normally x_3-component of velocity)
FLDY1	alphanumeric label for ordinate of fourth plot (normally x_1-coordinate of balloon)
FLDY2	alphanumeric label for ordinate of fifth plot (normally x_2-coordinate of balloon)
FLDY3	alphanumeric label for ordinate of sixth plot (normally x_3-coordinate of balloon)
G	gravitational acceleration vector
X	position vector for initial position
K	wave number vector for the fluid
THETA	phase angles for the components of the fluid velocity model
UB	initial fluid velocity vector
V	initial balloon velocity vector
A	fluid wave amplitude for x_1 direction
OMEGA	Eulerian frequency for the fluid
SIGMA	balloon density
D	balloon diameter
MUREF	reference dynamic viscosity coefficient
TEMREF	reference temperature
T	initial time of balloon fluid
TLIM	final time of balloon flight
DELTAT	time step for numerical integration
TEMPO	temperature at altitude x_{30}
PO	pressure at altitude x_{30}
TEMLAP	temperature lapse rate
R	gas constant
X30	initial balloon altitude

Table 4-3

Definitions of Block #2 Inputs

Variable	Meaning
XD(2)	dimensionless wave number, $\tilde{k}$
XD(5)	dimensionless frequency, $\tilde{\omega}$
BCDX(11) BCDX(12)	alphanumeric label to permit identifying each run by a "test" caption
T	initial time of balloon flight
TLIM	final time of balloon flight
DELTAT	time step for numerical integration
IDT	number of integration time steps between output data generations
IDS	factor for increasing TLIM (final time = IDS*TLIM)

4.2.2 Block #2 Outputs

The second set of output provides a label for each case and provides a list of most inputs in the following form:

```
     WRITE(6.0915) BCDX(11),BCDX(12),(XD(L2),L2=1.5)
     WRITE(6,INPUT)
9015 FØRMAT(1H1,25X,'TEST CASE'2A6//' DIMENSIØNLESS GRØUPS'//' N7='1PE1
   .12.4/' N8='E12.4/              ' N9='E12.4/' N10='E12.4/' N11='E12.4)
     NAMELIST/IMPUT/G,X,K,THETA,UB,V,A,ØMEGA,SIGMA,D,MUREF,TEMREF,T,
    *TLIM,DELTAT,TEMPO,PO,TEMLAP,R,X30
```

The definition of all of these items are provided in Tables 4.2 and 4.3. A sample set of this output is included in Appendix L.

4.2.3 Block #3 Outputs

The form of this output is as follows:

```
     WRITE(6,9002)
     WRITE(6,9003) ((WRA(I,J),J=1,11),I=1,50)
     WRITE(6,9008)
     WRITE(6,9009) ((WRB(I,J),J=1,6),I=1,50)
     WRITE(6,9006)
     WRITE(6,9007) ((WRC(I,J),J=1,17,I=1,50)
9002 FORMAT('1 TIME  SCALED TIME     SCALED ATMØSPHERIC WIND
    1SCALED BALLØØN VELØCITIES     VELØCITY RATIØS,//)
9003 FØRMAT(1X,OPF8.2,1P10E11.3)
9008 FØRMAT('1 TIME   SCALED TIME    X          Y          DZ          RE
    1'//)
9009 FØRMAT(1X.OPF8.2,1PS5E11.3)
9006 FØRMAT('1 TIME  SCALED TIME          FDRAG/FBUØY
    1      FAP1/FBASS                          FAP2'//)
9007 FØRMAT(1X,OPF8.2,1P10E11.3/20X,1P6E11.3)
```

Basic data describing the computed wind and balloon motion are stored in the fields WRA, WRB, and WRC. The WRA field provides a tabulation of wind and balloon velocity as a function of time. The WRB field contains the balloon coordinates and the Reynolds number as a function of time. The WRC field contains a tabulation of the various forces acting on the balloon as a function of time. Sample values of block #3 data are included in Appendix L.

4.2.4 Block #4 Outputs

This output set consists of calls to the NASA/MSFC UNIVAC 1108 plotting routines as follows:

```
YB = 8.8
YT = 11.2
CALL  QUIK3L(-1,XL,XR,YB,YT,1H+,BCDX,BCDY1,-IDX,PT,PY1)
CALL  QUIK3L(C,XL,XR,YB,YT,IHO,BCDX,BCDY1,-IDX,PT,PZ1)
YB = -1.5
YT = 1.5
CALL  QUIK3L(-1,XL,XR,YB,YT,1H+,BCDX,BCDY2,-IDX,PT,PY2)
CALL  QUIK3L(0,XL,XR,YB,YT,1HO,BCDX,BCDY2,-IDX,PT,PZ2)
CALL  QUIK3L(-1,XL,XR,YB,YT,1H+,BCDX,BCDY3,-IDX,PT,PY3)
CALL  QUIK3L(0,XL,XR,YB,YT,1HO,BCDX,BCDY3,-IDX,PT,PZ3)
CALL  QUIK3V(-1,1HO,BCDX,FLDY2,-IDX,PT,PY)
CALL  QUIK3V(-1,1HO,BCDX,FLDY3,-IDX,PT,PZ)
```

The fluid velocity components are stored in the PY1, PY2 and PY3 fields while the balloon velocity components are stored in the PZ1, PZ2, and PZ3 fields. The lateral and vertical coordinates of the balloon position are stored in the PY and PZ fields respectively. The preceding parameters are plotted as a function of time which is stored in the PT field. Examples of the plots generated by this block of output data are found in Section 5.

5. NUMERICAL RESULTS

The computer program, BALLOON, has been used to numerically solve the equations governing the motion of the balloon in a periodic, three-dimensional flow field. The numerical results can be grouped in two categories. The first category contains the results of test runs to validate the numerical model incorporated into the program. This category is presented in subsection 5.1. The second category represents the results of a series of runs, which are designed to provide general insight into the balloon response to the flow field. This category is described in subsection 5.2

Based on these numerical results certain observations concerning the behavior of constant-volume balloons have been made. These observations are presented in subsection 5.3

5.1 Test Case Results

Several types of test runs were carried out. The first were designed to provide a means of initially validating the model for certain simple conditions for which first-order theoretical solutions exist. These runs are described in subsection 5.1.1. The second type of test run was designed to verify the generality of the dimensionless form of the numerical solution. The results of these runs are presented in subsection 5.1.2. A number of other test cases were conducted to determine the effect of changing or omitting certain features in the program. The results of these tests are discussed in subsection 5.1.3.

5.1.1 Initial Test Cases

A series of four test cases were carried out which were simple enough to permit comparison with first-order theory. The simplifications employed in these four cases are summarized in Table 5-1. For each of these cases, as discussed in Appendix M, the period of oscillation based on first-order theory agreed closely with the results of the numerical solution. One additional test case (#5) was conducted to ensure that the simplification involving an isothermal atmosphere was not a special case. The period of oscillation for this test run, according to first-order theory, and the period obtained from the numerical solution were nearly identical.

Table 5-1

Summary of Simplifications for Initial Test Runs

Test Run #	Simplifications: Drag Force	Apparent Mass	Bassett Force	Fluid Acceleration Force	Atmosphere
1	zero	zero	zero	zero	isothermal
2	linear	zero	zero	zero	isothermal
3	zero	½ balloon mass	zero	zero	isothermal
4	zero	zero	linear	zero	isothermal
5	zero	zero	zero	zero	nonisothermal

5.1.2 Dimensionless Test Cases

In order to verify the dimensionless formulation of the governing equations and the resulting dimensionless solution, two test cases (#6 and #7) were conducted with the program BALLOON. The dimensional input values for the two cases are presented in Table 5-2. While the dimensional inputs are clearly different for the two cases, the values of the five dimensionless parameters developed in Section 3.3 are the same for both cases. Values of the dimensionless groups are presented in Table 5-3.

In terms of dimensionless time, space, and velocity the differences in the numerical solutions for the two cases were less than 1%. The dimensionless plots of the vertical components of the balloon and wind velocities versus time for these cases are presented in Figure N-1 of Appendix N. Thus the validity of the dimensionless formulation was confirmed.

5.1.3 Other Test Cases

Because of the fact that evaluation of the Bassett term represents 90% of the computation time in BALLOON, a test run (test case #8) was conducted, in which the Bassett term was set to zero with the same inputs as given for test case #6. The results are presented in Figure N-2 of Appendix N. As indicated in the figure, the absence of the Bassett term caused an 11% reduction in the period of the balloon motion. Although such a reduction is considered significant, the general shape of the plots of both balloon and wind vertical velocity components closely resemble those shown in Figure N-1. Furthermore, the Reynolds number associated with this test case was $\sim$480 which is considerably above the Stokes flow regime in which the Bassett term is rigorously applicable. For these reasons, computation of the Bassett term was omitted in subsequent runs unless the Reynolds number was $\sim$1.

Table 5-2

Dimensional Input Values for Test Cases #6 and #7

Variable	Case #6	Case #7	Units
T_o	218	300	^oK
R	$2.870224\text{x}10^6$	$2.870224\text{x}10^6$	$cm^2/sec^2\ ^oK$
γ	0	0	$^oK/cm$
g	980.6	980.6	cm/sec^2
μ_o	$1.40646\text{x}10^{-4}$	$1.84540\text{x}10^{-4}$	g/cm sec
ω	$3.20036\text{x}10^{-2}$	$2.72746\text{x}10^{-2}$	rad/sec
A	15.44	19.15	cm/sec
D	12.0616	17.5562	cm
k	$2.072693\text{x}10^{-3}$	$1.42399\text{x}10^{-3}$	cm^{-1}
$\bar{u}_1$	45.7555	56.75966	cm/sec
σ	$3.61494\text{x}10^{-4}$	$2.626856\text{x}10^{-4}$	gm/cm^3
ρ_o	$3.61494\text{x}10^{-4}$	$2.626856\text{x}10^{-4}$	gm/cm^3

Table 5-3

Values of Dimensionless Parameters for Test Cases #6 and #7

Variable	Definition	Value
L_3	$\frac{12\nu_o}{AD}$	2.5×10^{-2}
L_5	$\frac{2}{3} \frac{g\,(g/R-\gamma)D^2}{A^2 T_o}$	6.25×10^{-4}
$\tilde{\bar{u}}_1$	$\bar{u}_1/A$	2.96
$\tilde{k}$	kD	2.5×10^{-2}
$\tilde{\omega}$	$\frac{\omega D}{A}$	2.5×10^{-2}

In the setup of test cases #6 and #7, the initial balloon velocity was set equal to the mean wind velocity and, in the flow field model, the phase angle Θ_1 was set to 0, with Θ_2 set to $2\pi/_3$, and Θ_3 set to $-2\pi/_3$. In examining the results obtained, the question arose as to whether or not a change in the value of the phase angle would have a significant effect on performance of the balloon. This question is equivalent to the question of the influence of the initial phase relation between balloon and wind velocity on the periodic solution.

To resolve this issue, three additional test cases (#9, 10, and 11) were conducted with phase angles as indicated in Table 5-4. All other input variables in test cases #9, 10 and 11 were the same as case #6. The results obtained are presented in Figures N-3 through N-5 of Appendix N. Examination of these figures reveals that for each different phase angle immediately following time zero there is a different transient buildup for the balloon motion. Subsequent to the transient buildup, a periodic pattern occurs. Comparison of Figures N-1, N-3, N-4, and N-5 indicated that the periodic motion of the balloon relative to the wind, following the transient buildup, is essentially independent of the phase angle.

5.2 Results of Numerical Experiments

Based on the results of test cases #1 - #11, the computer program BALLOON was considered acceptable for conducting a series of numerical experiments. To provide maximum results with a minimum number of computer runs the entire experiment was set up in dimensionless form. The experiment was carried out in two phases as described in subsections 5.2.1 and 5.2.2 which follow.

5.2.1 Phase I Numerical Experiments

Considerable effort was devoted to devising a series of dimensionless runs involving variation of the primary dimensionless groups discussed in Section 3.2. With five independent parameters a complete investigation would entail a

Table 5-4

Phase Angles Used in Test Cases #6 - #11

Test Case #	θ_1	θ_2	θ_3
6	0	$2\pi/3$	$-2\pi/3$
7	0	$2\pi/3$	$-2\pi/3$
8	0	$2\pi/3$	$-2\pi/3$
9	$\pi/2$	$\pi/2+2\pi/3$	$\pi/2-2\pi/3$
10	π	$\pi+2\pi/3$	$\pi-2\pi/3$
11	$3\pi/2$	$3\pi/2+2\pi/3$	$3\pi/2-2\pi/3$

very large number of runs. Accordingly in Phase I the decision was made to hold the variables L_3, L_5 and $\bar{u}_1$ constant with the values given in Table 5-5 while systematically varying $\tilde{k}$ and $\tilde{\omega}$ over the ranges indicated in the same table. The individual runs were visualized as elements in a matrix, as shown in Figure 5-1. The values of $\tilde{k}$ and $\tilde{\omega}$ for each run were assigned according to the position of the element in the matrix. The matrix was designed such that along the main diagonal

$$\tilde{\omega} = \tilde{k}\,\tilde{\bar{u}}_1$$

which satisfies Taylor's Hypothesis.

The dimensionless form of the input variables correspond to a large number of different physical situations. In this form, however, it is difficult to visualize the type of physical situation represented. Actually in Phase I the dimensionless parameters were computed from "typical" dimensional values of the physical parameters. The dimensional values used are presented in Table 5-6. It is important to note that in certain portions of the report dimensional results are presented in lieu of dimensionless values. In these cases the corresponding dimensional inputs are those presented in Table 5-6.

5.2.1.1 Phase I - Original 16 Runs

For the sixteen runs shown in Figure 5-1 a quantitative analysis of the numerical results is presented in Appendix O. A qualitative view of the results of these experiments is provided by means of Figures 5-2 through 5-6. These figures depict the transverse and vertical position of the balloon and the velocities in all three directions as functions of time for each test case within the matrix. In each figure, the sixteen plots are arranged in order of test case number so as to correspond to the elements in the test case matrix. Note that the scales differ from plot to plot within these figures. The scales were selected to provide a maximum of 10 complete oscillations of the forcing function. Also note that the equilibrium point is represented by a darkened line and that the balloon velocity may exceed the upper or lower limits of the graphs over certain intervals. In such situations portions of

Table 5-5

Values of Dimensionless Parameters for Phase I

Parameter	Definition	Value
L_3	$\frac{12\ \nu_o}{AD}$	3.5914×10^{-4}
L_5	$\frac{2}{3}\ \frac{g\ (g/R - \gamma D^2}{A^2 T_o}$	1.7317×10^{-3}
$\tilde{\bar{u}}_1$	$\bar{u}_1/A$	10
$\tilde{k}$	kD	8.168×10^{-4} to 8.168×10^{-1}
$\tilde{\omega}$	$\frac{\omega D}{A}$	8.168×10^{-3} to 8.168

$\tilde{\omega}$ \ $\tilde{k}$	8.168×10^{-4}	8.168×10^{-3}	8.168×10^{-2}	8.168×10^{-1}
8.168×10^{-3}	A_{11}	A_{12}	A_{13}	A_{14}
8.168×10^{-2}	A_{21}	A_{22}	A_{23}	A_{24}
8.168×10^{-1}	A_{31}	A_{32}	A_{33}	A_{34}
8.168	A_{41}	A_{42}	A_{43}	A_{44}

Figure 5-1. Basic Matrix A_{ij} for Cases in Phase I

Table 5-6

Typical Dimensional Values for Phase I

Physical Parameter	Value
T_o	218^o K
R	2.870224×10^6 cm^2/sec^2 ^oK
γ	0.0 $^oK/cm$
g	980.6 cm/sec
μ_o	1.40646×10^{-4} g/cm sec
A	100.0 cm/sec
D	130.0 cm
$\bar{u}_1$	1000.0 cm/sec
σ	3.61494×10^{-4} g/cm^3
ρ_o	3.61494×10^{-4} g/cm^3
k	6.28×10^{-6} to 6.28×10^{-3} cm^{-1} *
ω	6.28×10^{-3} to 6.28×10^{-1} sec^{-1} *

*Such ranges of k and ω correspond to spatial wave lengths from 10 m to 10 km and time periods of 1 sec to 1000 sec.

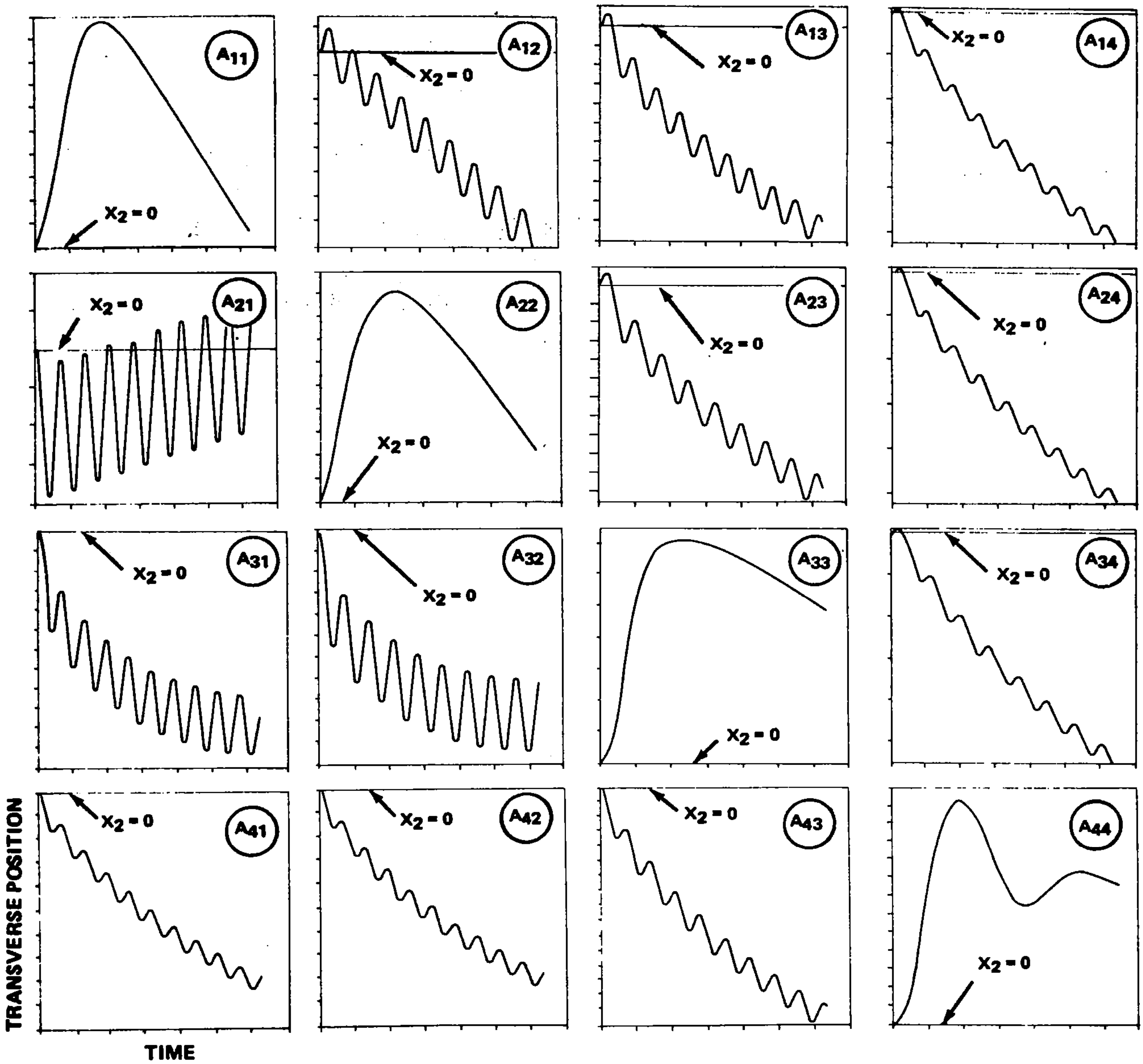

Figure 5-2. x_2-Coordinates of Balloon Position (Phase I)

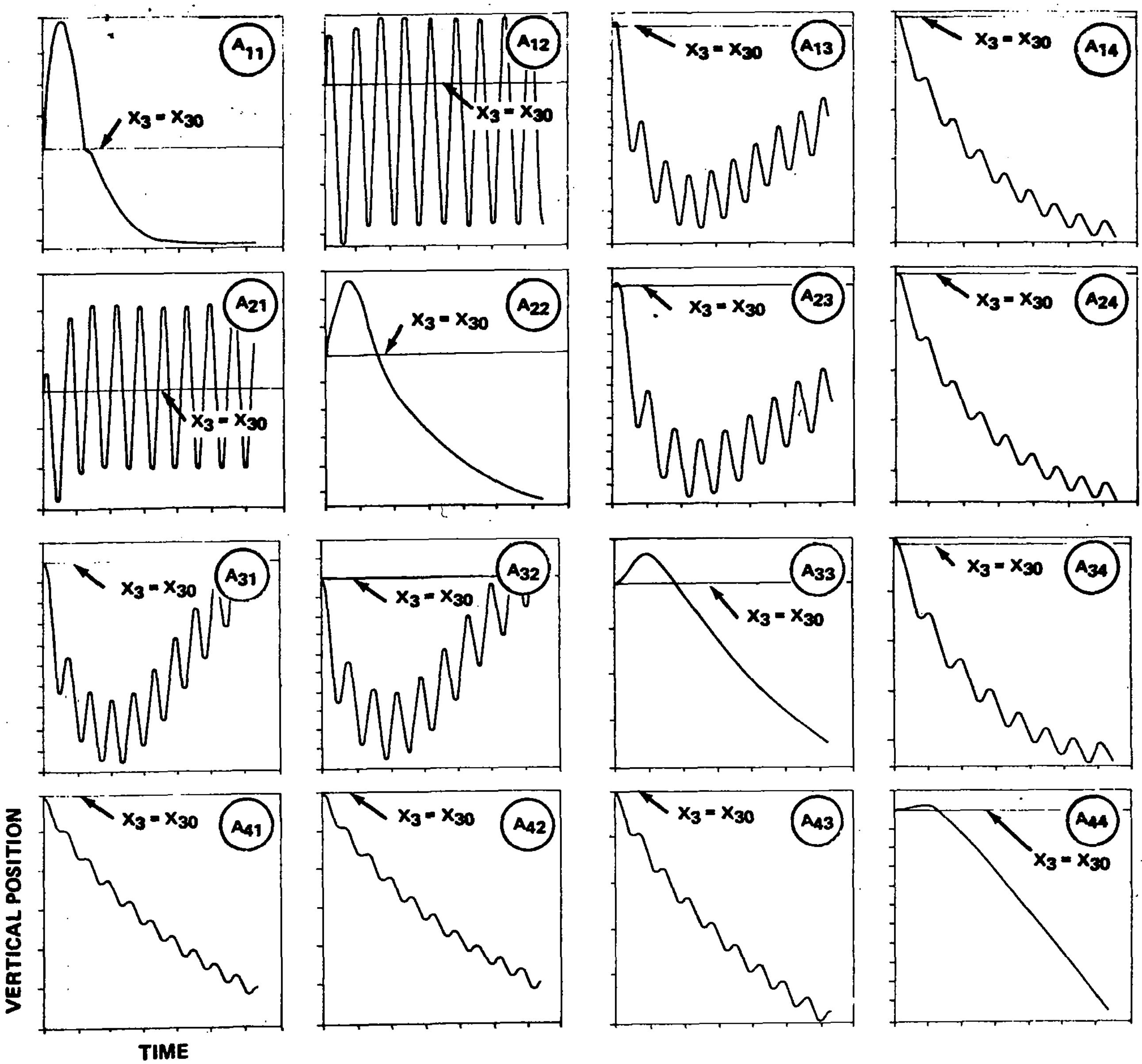

Figure 5-3. x_3-Coordinates of Balloon Position (Phase I)

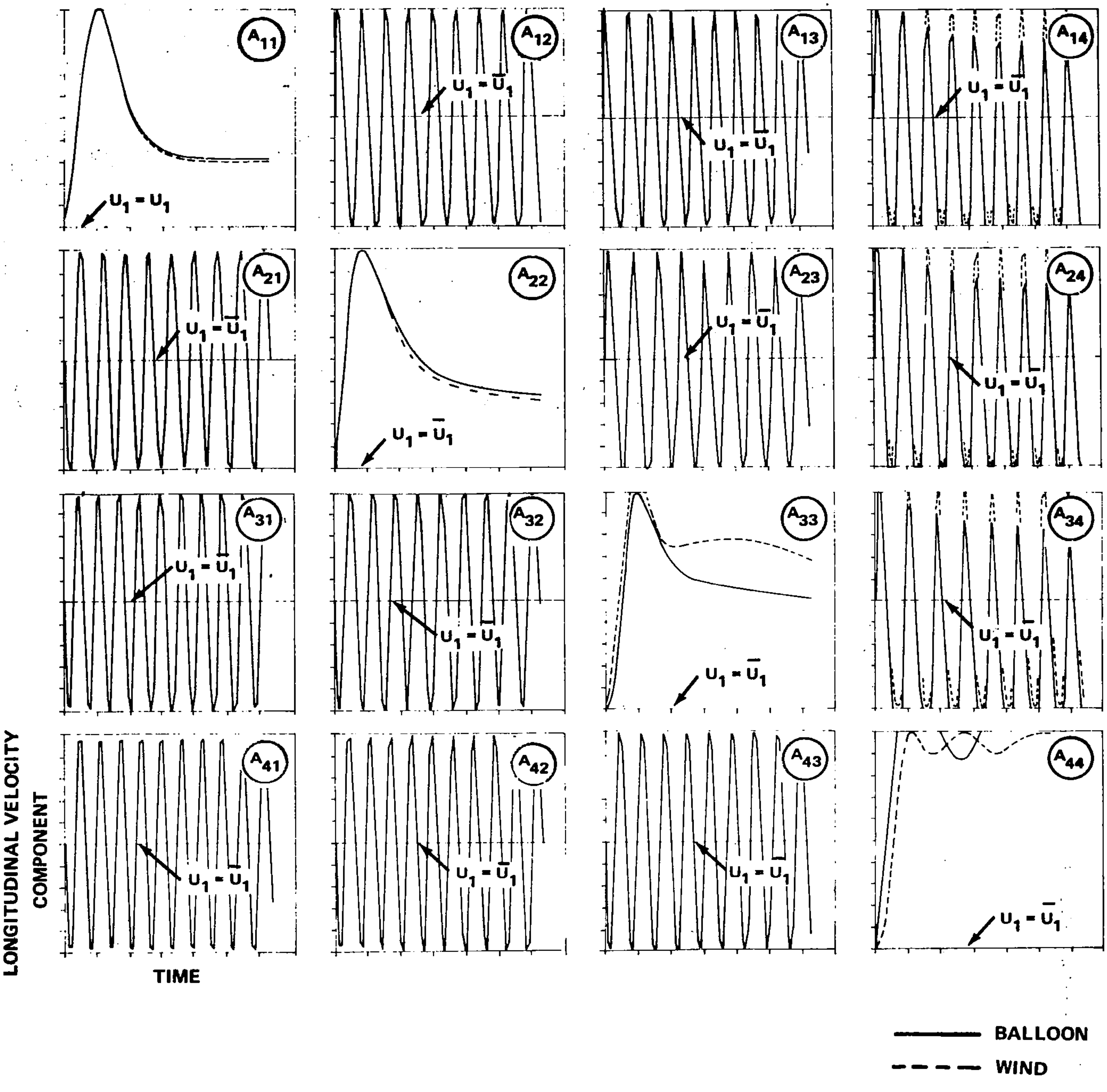

Figure 5-4. x_1-Component of Velocity (Balloon and Wind Phase I)

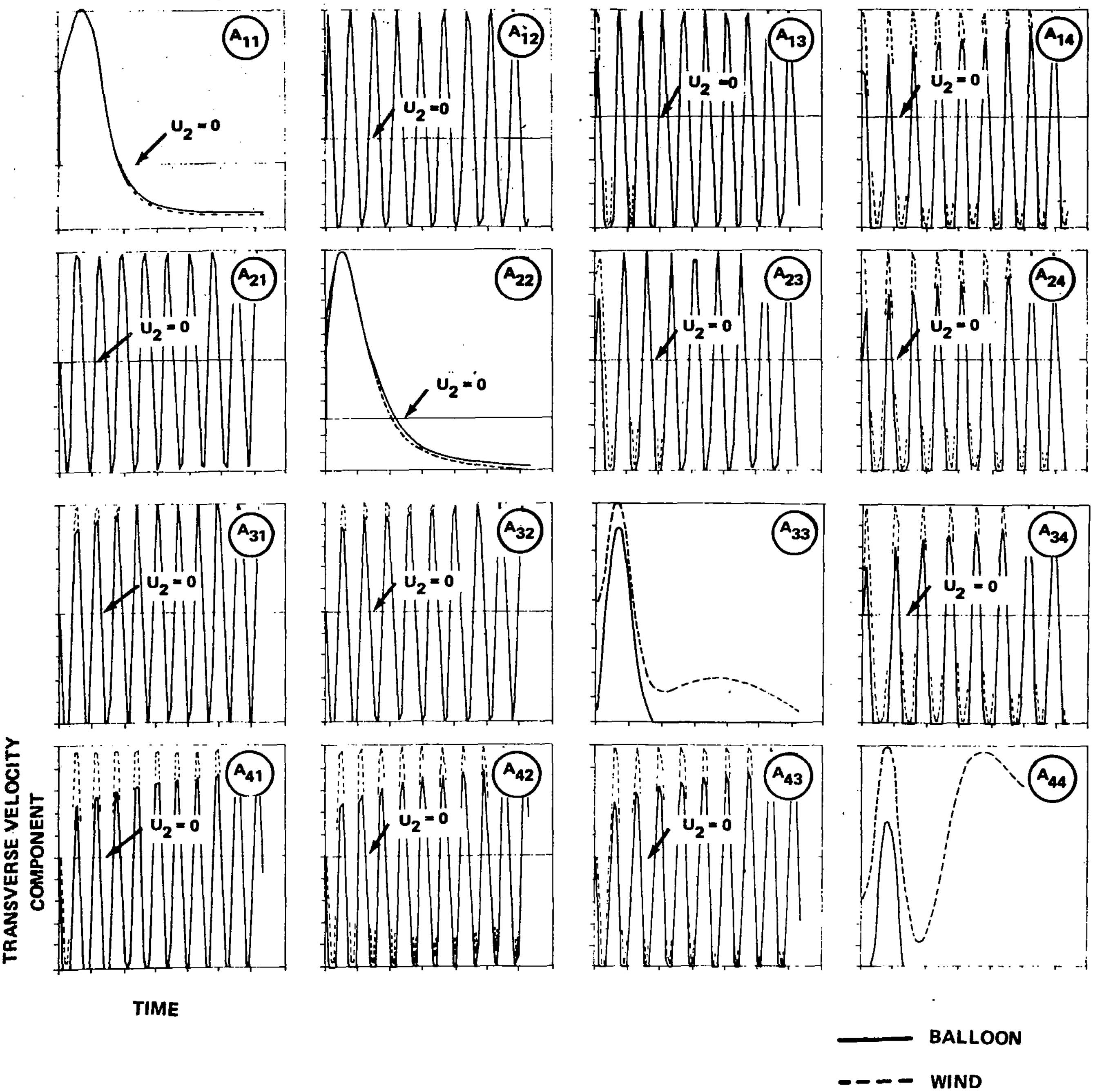

Figure 5-5. x_2-Component of Velocity (Balloon and Wind Phase I)

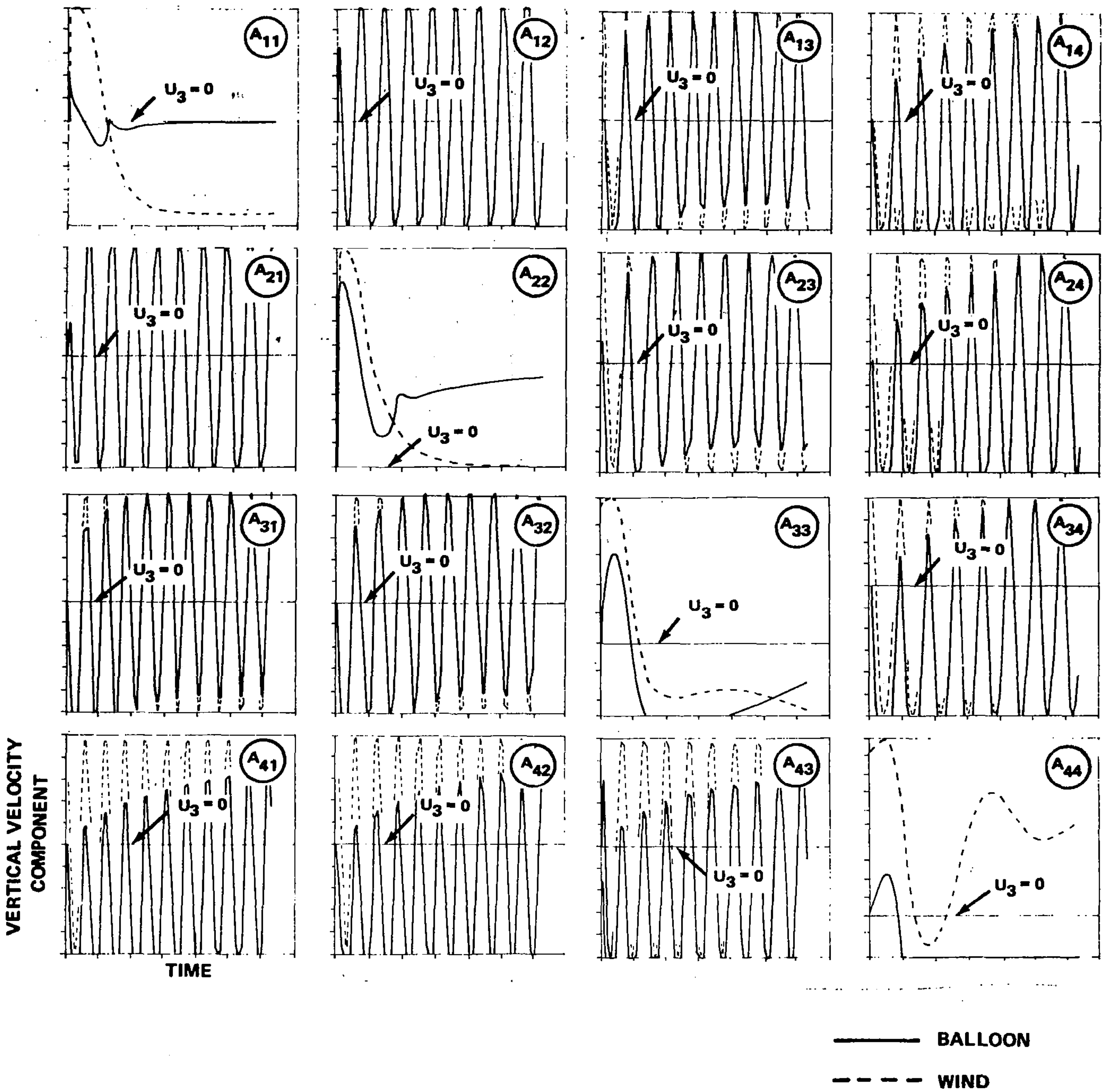

Figure 5-6. x_3-Component of Velocity (Balloon and Wind Phase I)

velocity plots are "chopped off". Examination of Figures 5-2 through 5-6 reveals that all runs, which are off of the main diagonal, display a periodic motion which is in good agreement with first-order theory. As shown in Appendix O, the period of oscillation according to first-order theory is given by

$$\tilde{\tau} = \frac{2\pi}{\tilde{k}|\tilde{\tilde{u}}_1 - \tilde{c}|} \tag{5-1}$$

where

$$\tilde{c} = \frac{\tilde{\omega}}{\tilde{k}} \tag{5-2}$$

Along the main diagonal where Taylor's Hypothesis is satisfied, no long-term periodic motion is observed. The balloon experiences one or two oscillations after which the velocity components appear to reach steady-state values. It is important to note, however, that under such steady-state conditions the balloon drifts laterally (perpendicular to the mean wind direction) and generally remains below its equilibrium altitude.

5.2.1.2 Phase I-Intermediate Runs in Cruciform Arrangement

The marked difference between on-diagonal and off-diagonal runs suggested the need for runs at intermediate values of wave number and frequency in the vicinity of the main diagonal. Accordingly two sets of runs in cruciform arrangements, C_{22} and C_{33}, about elements A_{22} and A_{33}, as shown in Figure 5-7, were carried out. A quantitative description of the results of these runs is presented in Appendix P. The basic trend observed in both sets of runs was one of increasing disagreement between first-order theory and observation, as conditions satisfying Taylor's hypothesis were approached along any branch of either cruciform. This trend indicates that nonlinear effects become significant under conditions which (nearly) satisfy Taylor's Hypothesis. It was also observed that the bounds of the region in which such nonlinear effects occurred were related to the magnitude of the product of the dimensionless period of oscillation, as computed by Equation (5-1) according to first-order theory, and the dimensionless wave number.

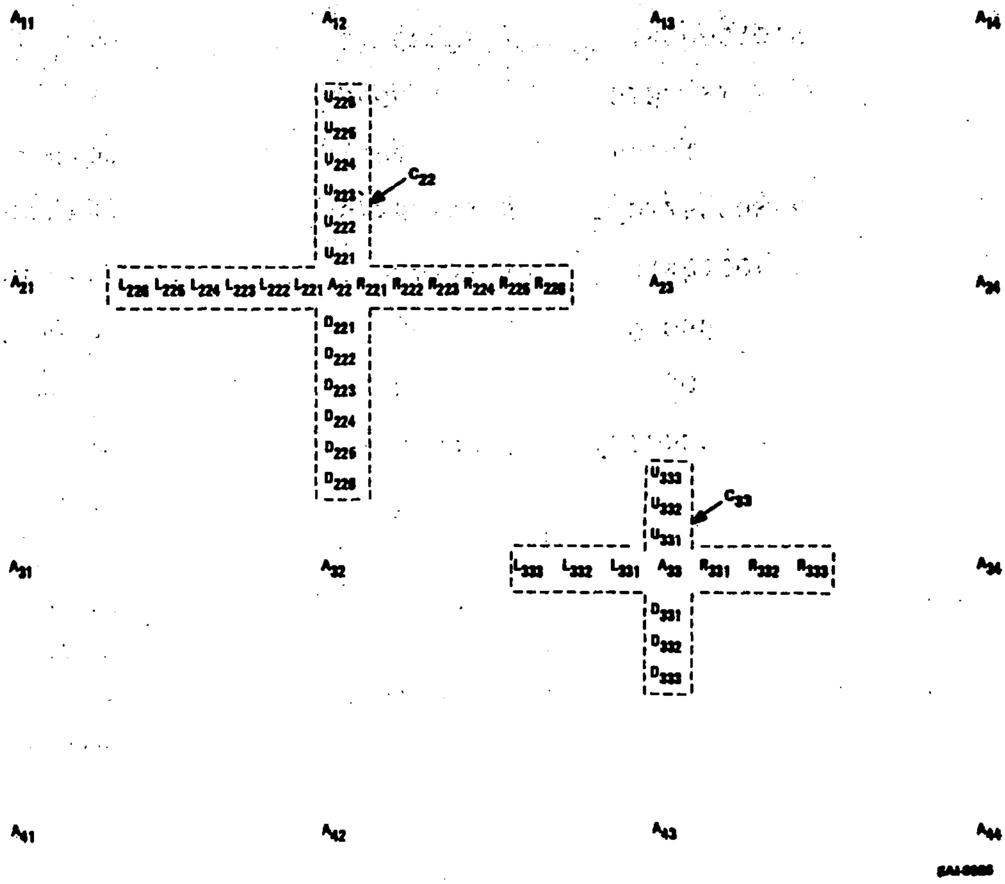

Figure 5-7. Relative Position of Runs in Cruciform Arrangements C_{22} and C_{33}

5.2.1.3 Phase I-Special Runs Concerning Lateral Drift

In all cases of balloon motion studied during Phase I, a lateral(x_2-direction) drift was noted. That is, the balloon appeared to be subject to a mean lateral velocity. This drift was observed for the 16 cases comprising the original experiment matrix as shown in Figure 5-2. An example of this drift is shown in Figures 5-8 and 5-9. Figure 5-8 represents a case off the principal diagonal of the experiment matrix and shows the superposition of the oscillation due to the fluid oscillations and mean drift. Figure 5-9 represents a case on the principal diagonal and shows an initial or transient displacement of the balloon (a feature found in many of the cases examined both on and off the principal diagonal) followed by a final mean drift in the opposite direction.

In examining long periods of balloon motion, it was found that the final direction of the lateral balloon motion depended on which side of the principle diagonal of the experiment matrix the experiment occurred. Thus, the final direction of drift appeared to depend in general on the sign of the quantity ($\bar{u}$ - c), where $\bar{u}$ is the mean wind velocity and c is the phase velocity. When c >$\bar{u}$, a positive lateral drift was observed for the flow field under examination and when c <$\bar{u}$, a negative lateral drift was observed. Examination of the flow field model confirmed in general that with such inequalities, the balloon would be subject to lateral forces consistent with the drift observed. However, since a negative lateral final drift was observed when $\bar{u}$ = c (as shown in Figure 5-9), this rule was not considered sufficient and further tests were necessary.

Several runs were prepared to examine the effects of modifications in the flow field on the balloon drift. These cases consisted of (1) varying the initialization of the balloon motion, (2) modifying the initial phase relationships among the velocity perturbations, and (3) setting $\bar{u}$ = 0. These tests were carried out for the two matrix points, A_{11} and A_{31}, as indicated in Figure 5-7.

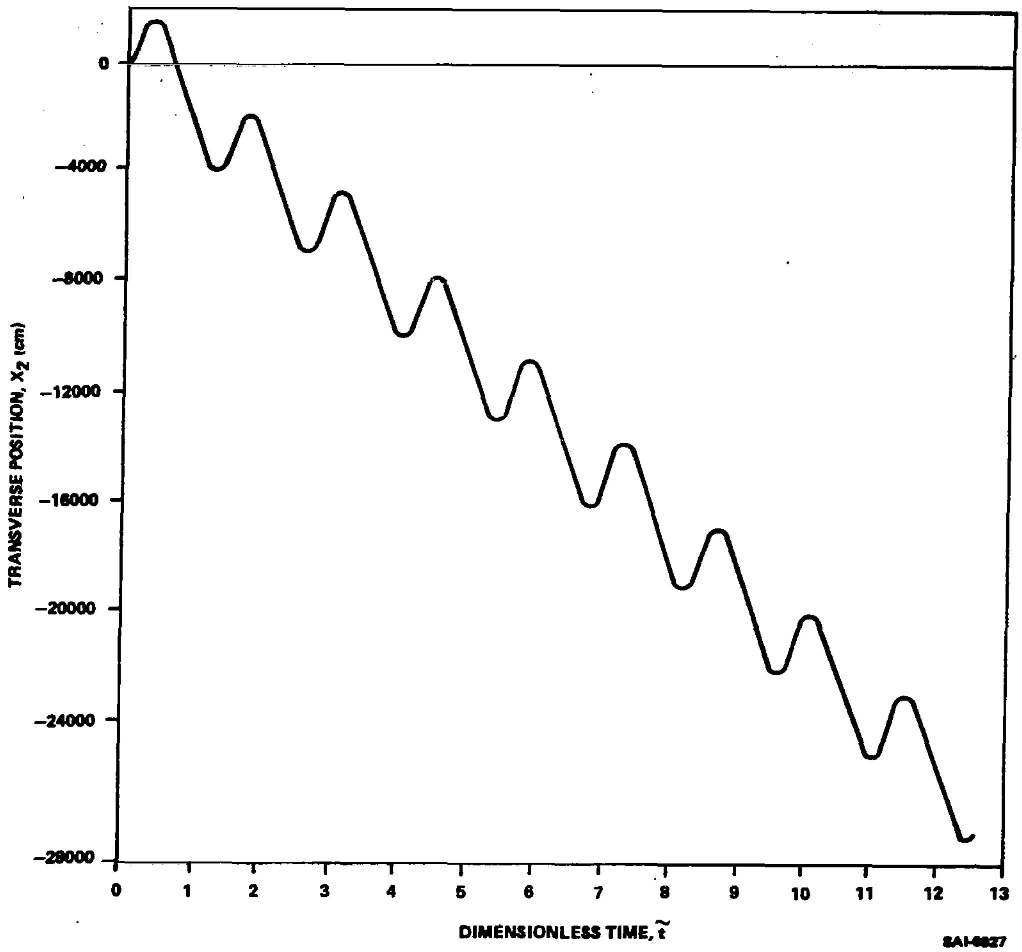

Figure 5-8. Transverse Balloon Drift ($\bar{u} > c$)

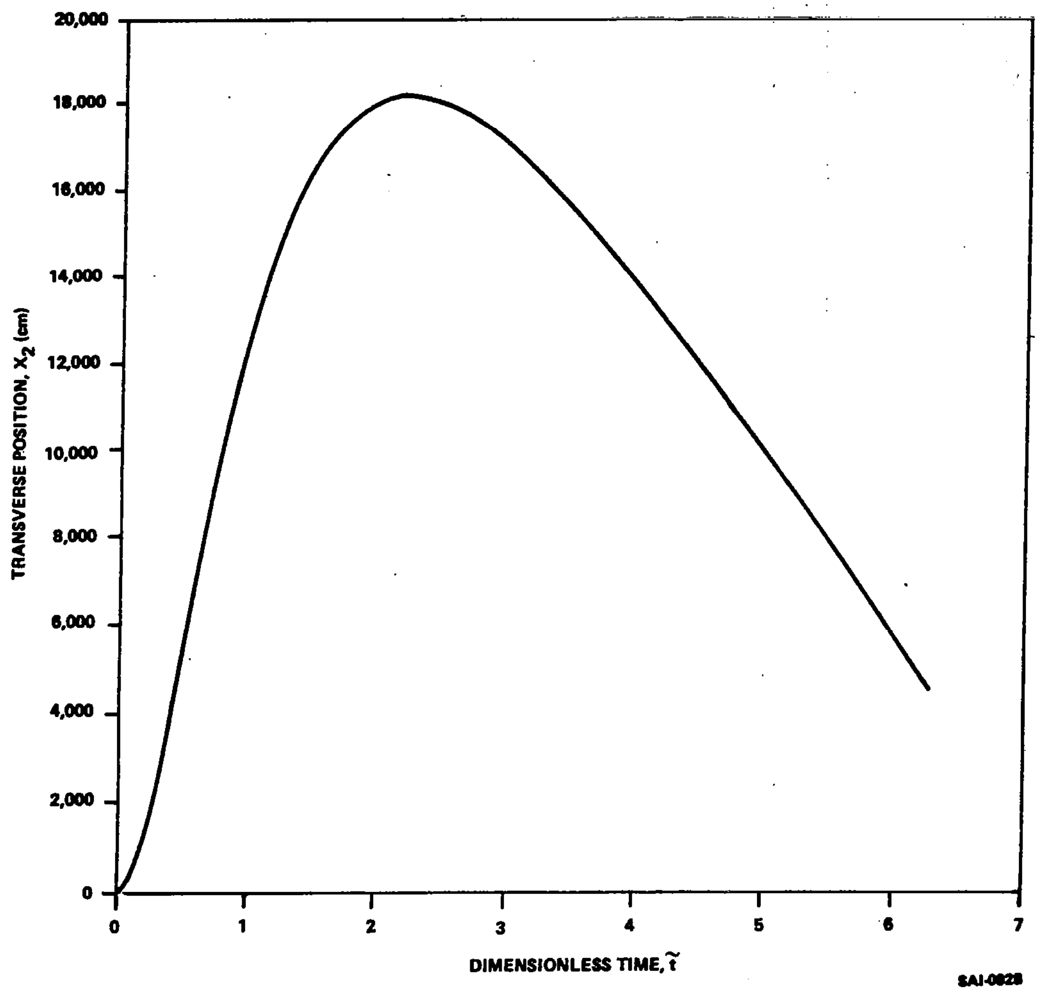

Figure 5-9. Transverse Balloon Drift ($\bar{u}$ = c)

For both cases the first two procedures produced results which generally resembled those of the original experiment. Neither altering the initialization by setting

$$\vec{v} = \vec{u} \tag{5-3}$$

rather than

$$\vec{v} = u\,\hat{i} \tag{5-4}$$

nor changing the phase angles of the y and z perturbations,

$$\Theta_2 \longleftrightarrow \Theta_3 \tag{5-5}$$

quantitatively affected the direction of the drift. Setting $\bar{u} = 0$ alters the original experiment such that $c > \bar{u}$ at all times. With this point in mind, the results, which showed the balloon drifting off in the positive x_2-direction, were consistent with the earlier experiments.

The preceding results indicated that there was no special bias in the model which caused the lateral drift along the main diagonal where Taylor's Hypothesis for the fluid was satisfied. Further study revealed that the mean balloon velocity, $\bar{v}$, (instead of the mean wind velocity, $\bar{u}$,) was the appropriate variable to be compared with the phase velocity, c. Thus the dividing line for lateral drift corresponds to

$$\bar{v} = c \tag{5-6}$$

representing Taylor's Hypothesis for a finite parcel. This relationship is satisfied slightly to the left ($c > \bar{u}$) of the principal diagonal of the original matrix. Three test cases were performed to confirm this relationship. The first, designated T_1, corresponded to $\bar{v} < c$; the second, T_2, represented $\bar{v} = c$; and the third, T_3, $\bar{v} > c$. Figures 5-10 through 5-12 illustrate how the lateral velocity v_2 asymptotically reaches a constant value in accordance with

$$v_2 \begin{cases} >0 & (\bar{v} < c) \\ =0 & (\bar{v} = c) \\ <0 & (\bar{v} > c) \end{cases} \tag{5-7}$$

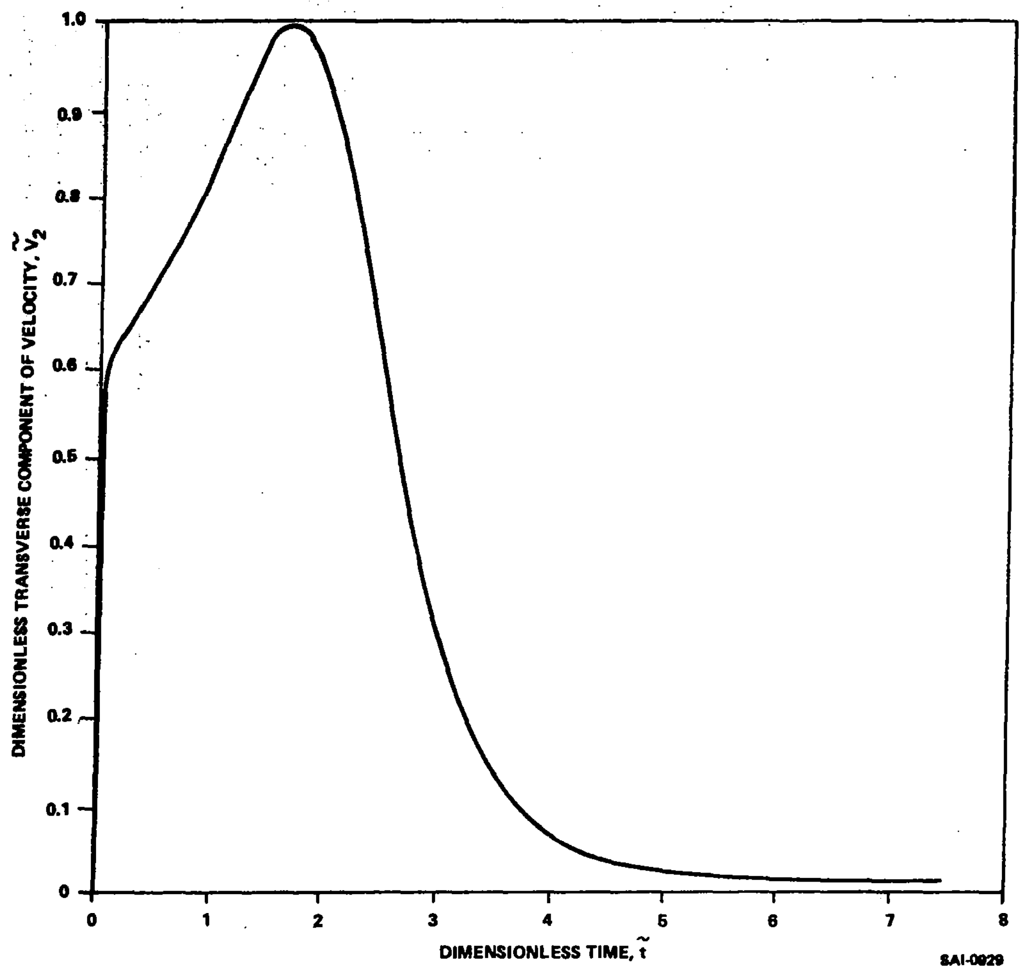

Figure 5-10. Transverse Balloon Velocity for Case T_1 ($\bar{v} < c$)

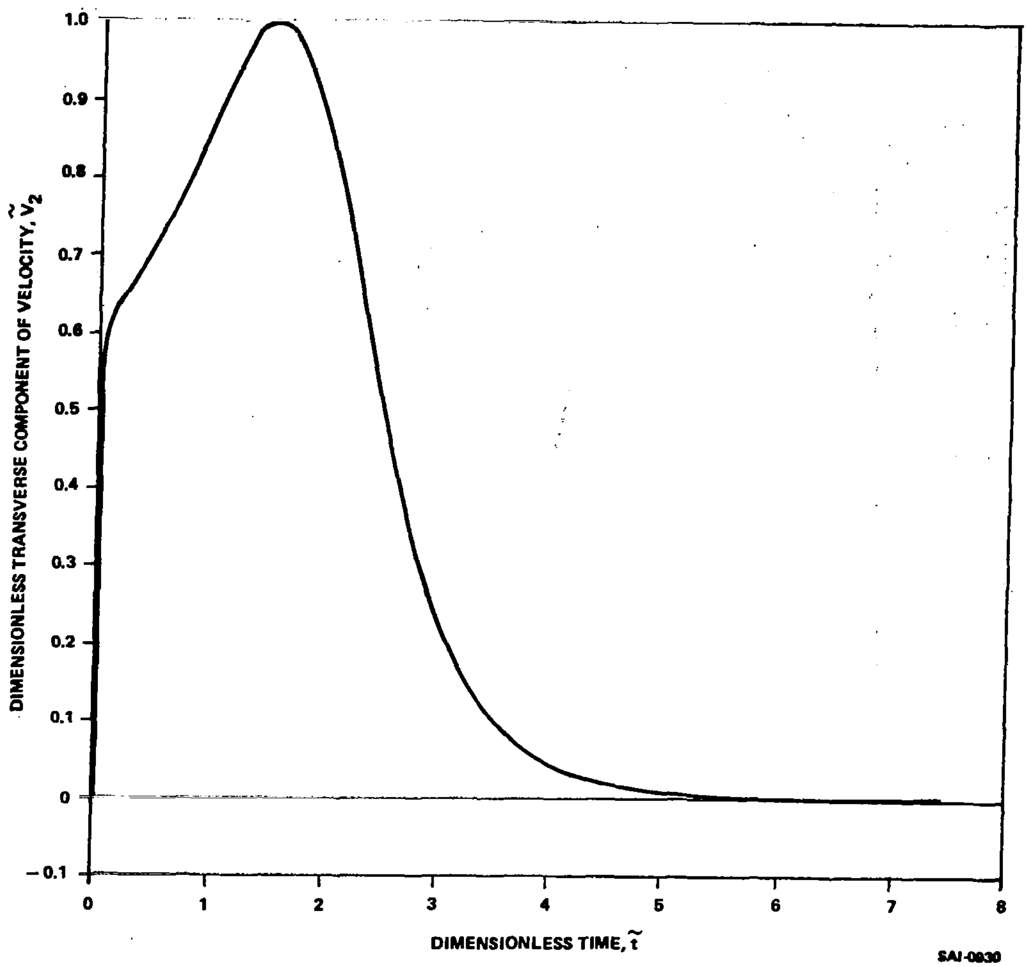

Figure 5-11. Transverse Balloon Velocity for Case T_2 ($\bar{v}$ = c)

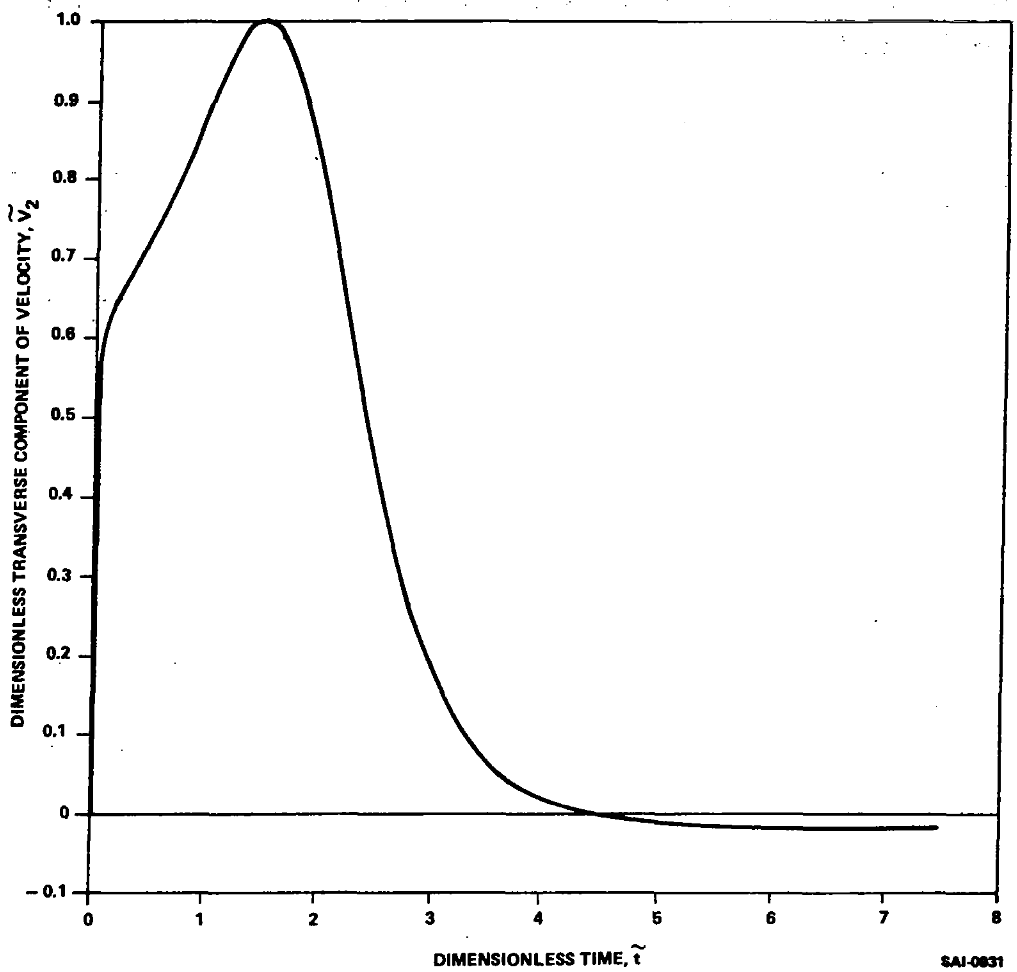

Figure 5-12. Transverse Balloon Velocity for Case T_3 ($\bar{v} > c$)

Similarly, Figures 5-13 through 5-15 show the lateral drift changing direction.*

Thus the question of lateral drift was resolved and the distinction between Taylor's Hypothesis for the fluid ($\bar{u} = c$) and Taylor's Hypothesis for the parcel ($\bar{v} = c$) was clearly established.

5.2.2 Phase II-Numerical Experiments

As noted in subsection 5.2.1.3 the results of Phase I revealed the distinction between Taylor's Hypothesis for the fluid (THF) and Taylor's Hypothesis for a finite parcel (THP). In addition, there was some indication that nonlinear effects became significant when the product of the dimensionless wave number and the dimensionless period of oscillation, according to first-order theory, exceeded some limiting value. For these reasons a second experiment matrix $B_{\ell k}$ was designed. The relation between the original matrix A_{ij} and the second matrix is depicted in Figure 5-16. In the matrix $B_{\ell k}$ along each row the product of $\tilde{k} \cdot \tilde{\omega}$ was held constant while along each column the ratio of $\tilde{\omega}/\tilde{k}$ remained constant. The arrangement of the matrix, along with the value of $\tilde{k}$ and $\tilde{\omega}$ for each element is shown in Figure 5-17. The values of all other parameters are the same as for the first matrix.

Also included in the figure is the product of the dimensionless wave number and the dimensionless period of oscillation (according to first-order theory) for each element of the matrix. It is important to note that along each column this product remains constant, with THF being represented by the fourth column. Because the mean balloon velocity is a dependent variable, it is not possible to satisfy THP exactly along any column of the matrix. Based on analysis of the special runs of Phase I, however, the third column was empirically designed to

---

* Notice should be taken that the direction of lateral drift when $\bar{v} \neq c$ depends upon the flow field model. Thus the inequalities presented in Equation (5-7) might be reversed in some cases.

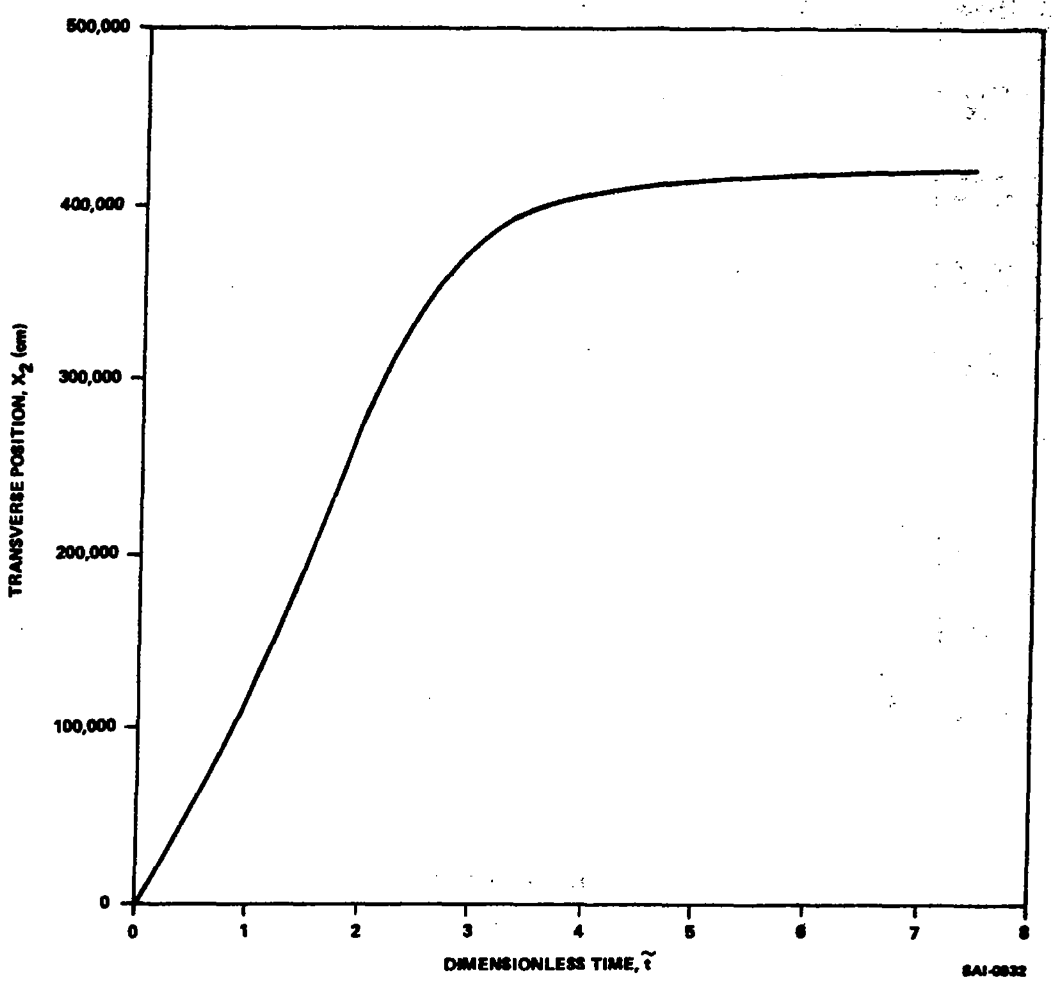

Figure 5-13. Transverse Position of Balloon for Case T_1 (v < c)

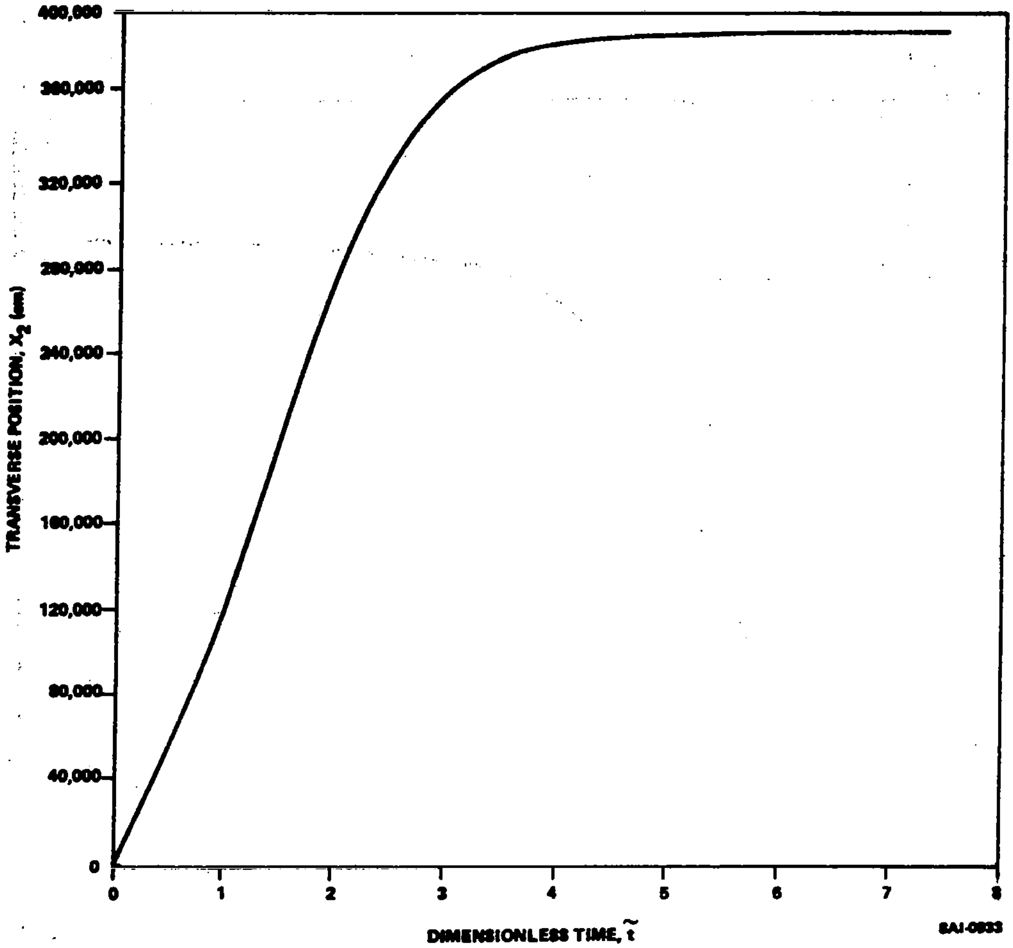

Figure 5-14. Transverse Position of Balloon for Case T_2 ($\bar{v} = c$)

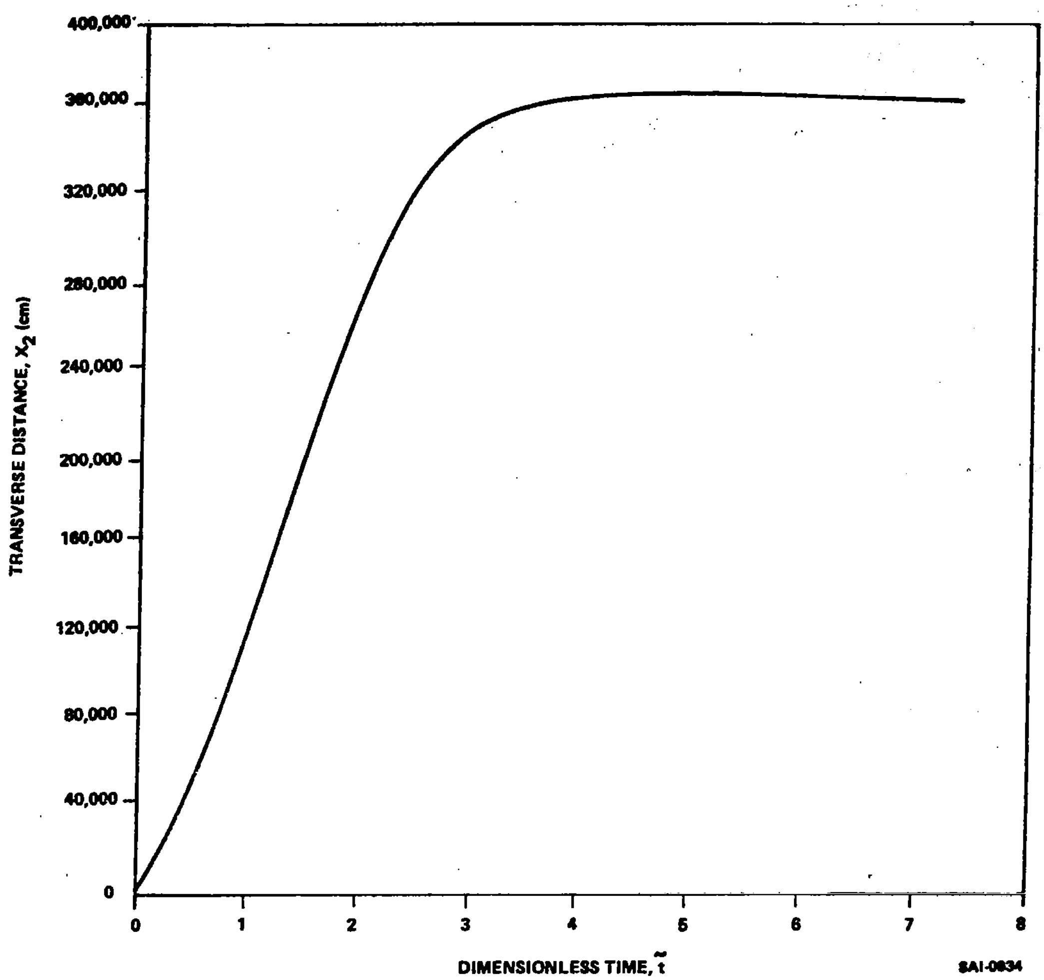

Figure 5-15. Transverse Position of Balloon for Case T_3 ($\bar{v} > c$)

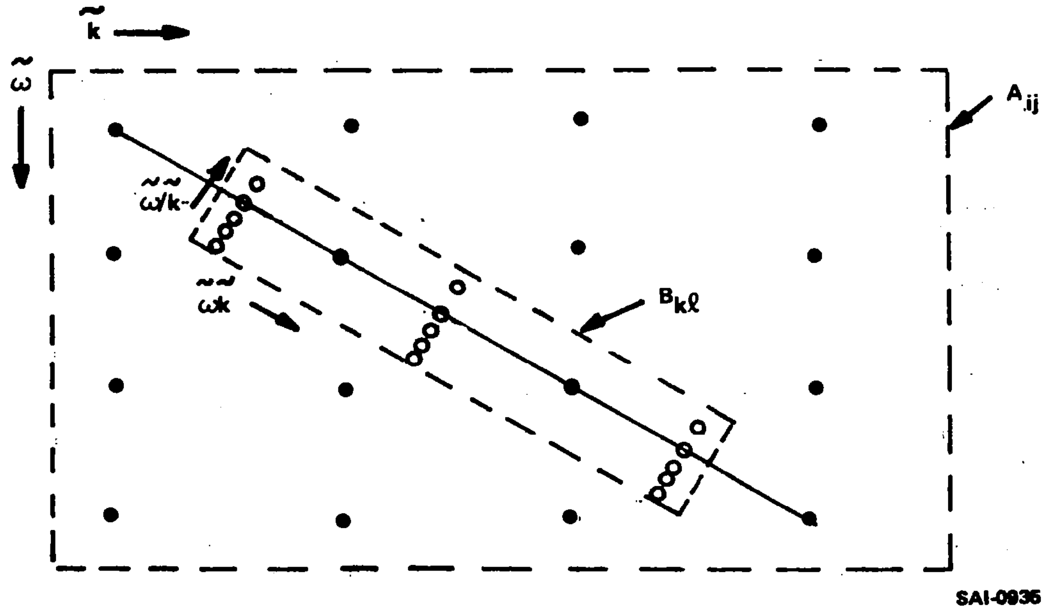

Figure 5-16. Relation Between Experiment Matrix A_{ij} of Phase I and $B_{k\ell}$ of Phase II

$\tilde{\omega}/\tilde{k}$	14.644	11.161	10.580	10.000	6.164
$\lvert\tilde{\tau}\tilde{k}\rvert$ / $\tilde{\omega}\ \tilde{k}$	1.353	5.413	10.825	∞	1.804
2.0182×10^{-4}	B_{11} 3.7124×10^{-3} 5.4361×10^{-2}	B_{12} 4.2529×10^{-3} 4.7466×10^{-2}	B_{13} 4.3674×10^{-3} 4.6209×10^{-2}	B_{14} 4.4924×10^{-3} 4.4924×10^{-2}	B_{15} 5.5651×10^{-3} 3.6265×10^{-2}
2.0182×10^{-2}	B_{21} 3.7124×10^{-2} 5.4361×10^{-1}	B_{22} 4.2529×10^{-2} 4.7466×10^{-1}	B_{23} 4.3674×10^{-2} 4.6209×10^{-1}	B_{24} 4.4924×10^{-2} 4.4924×10^{-1}	B_{25} 5.5651×10^{-2} 3.6265×10^{-1}
2.0182	B_{31} 3.7124×10^{-1} 5.4361	B_{32} 4.2529×10^{-1} 4.7466	B_{33} 4.3674×10^{-1} 4.6209	B_{34} 4.4924×10^{-1} 4.4924	B_{35} 5.5651×10^{-1} 3.6265

Note: Beneath each matrix element there are two numbers. The upper is $\tilde{k}$ and the lower is $\tilde{\omega}$.

Figure 5-17. Matrix $B_{k\ell}$ for Phase II approximately satisfy this hypothesis based on the value of the product, $\tilde{\tau}\tilde{k}$.

A complete set of detailed plots from Phase II is provided in a separate document [1]. Qualitative results are given graphically in Figures 5-18, 5-19 and 5-20. The period of observation is the same for each column but none of the other coordinates necessarly coincide. Figure 5-18 presents the vertical velocity of the balloon and the wind at the balloon's position as a function of time. These results are similar to those found in previous cases. The vertical position of the balloon, shown in Figure 5-19, is seen to correspond to the vertical velocities. Away from THP corresponding to column 3, the balloon is seen to oscillate regularly. Close to THP the balloon is seen to reach equilibrium at progressively lower altitudes to the right (along the rows), or toward the bottom (along the columns), of the figure. Along the bottom row, it can be seen that the balloon does not reach equilibrium within the time period shown, although the balloon velocities are approaching zero. Also in the last case shown along the third row the oscillation is not found.

Figure 5-20 shows the lateral position of the balloon as a function of time. The results are very similar to those discussed in subsection 5.2.1. When the phase velocity exceeds the mean balloon velocity ($c > \bar{v}$), corresponding to column 4 and 5, the balloon drifts toward the positive y-direction. When $c < \bar{v}$ corresponding to column #1 and #2, the balloon dirfts toward the negative y-direction. It is important to note that along column #3 Taylor's Hypothesis for the parcel is not exactly satisfied. In row #1 of column #3 the balloon drifts toward the positive y-direction in near equilibrium, while in subsequent cases the balloon drifts toward the negative y-direction. Thus, the assumption that THP depends only on the product $\tilde{\tau}\tilde{k}$ is found to be incorrect as it probably also depends on the scale of motion (which may also be responsible for the differences seen in row #3 of Figures 5-18 and 5-19).

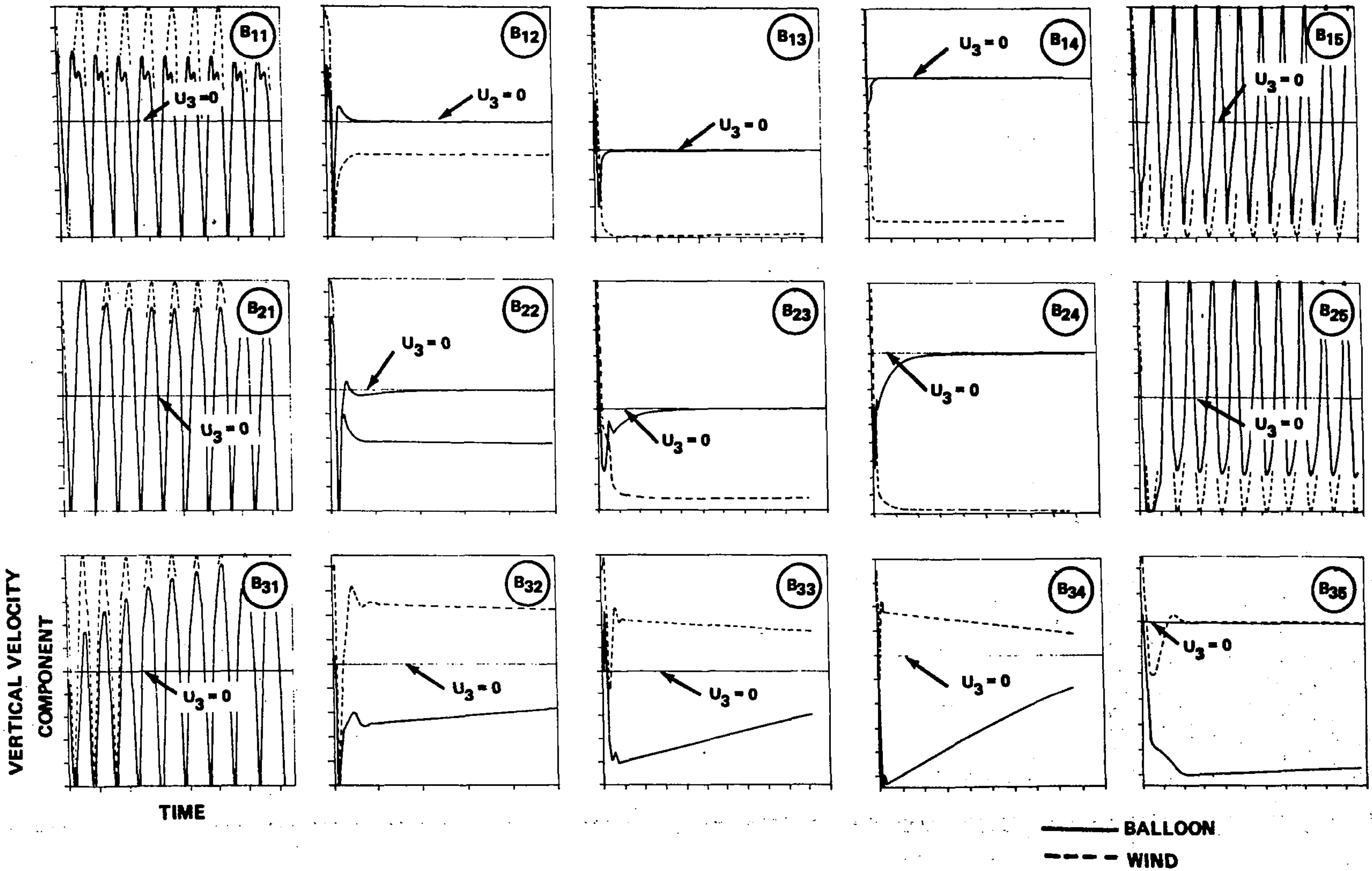

Figure 5-18. Vertical Velocity as a Function of Time (Phase II)

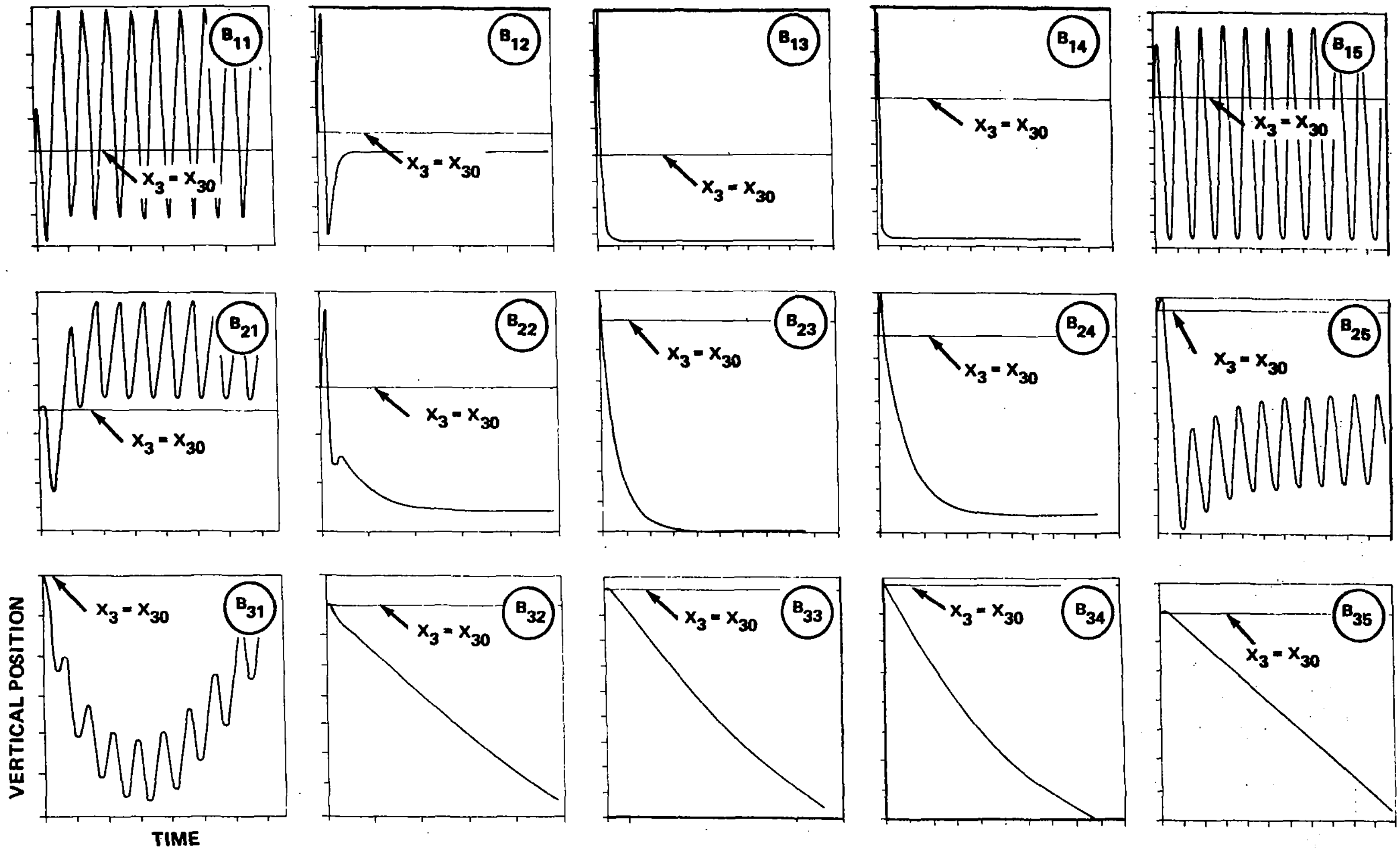

Figure 5-19. Vertical Position of Balloon as a Function of Time (Phase II)

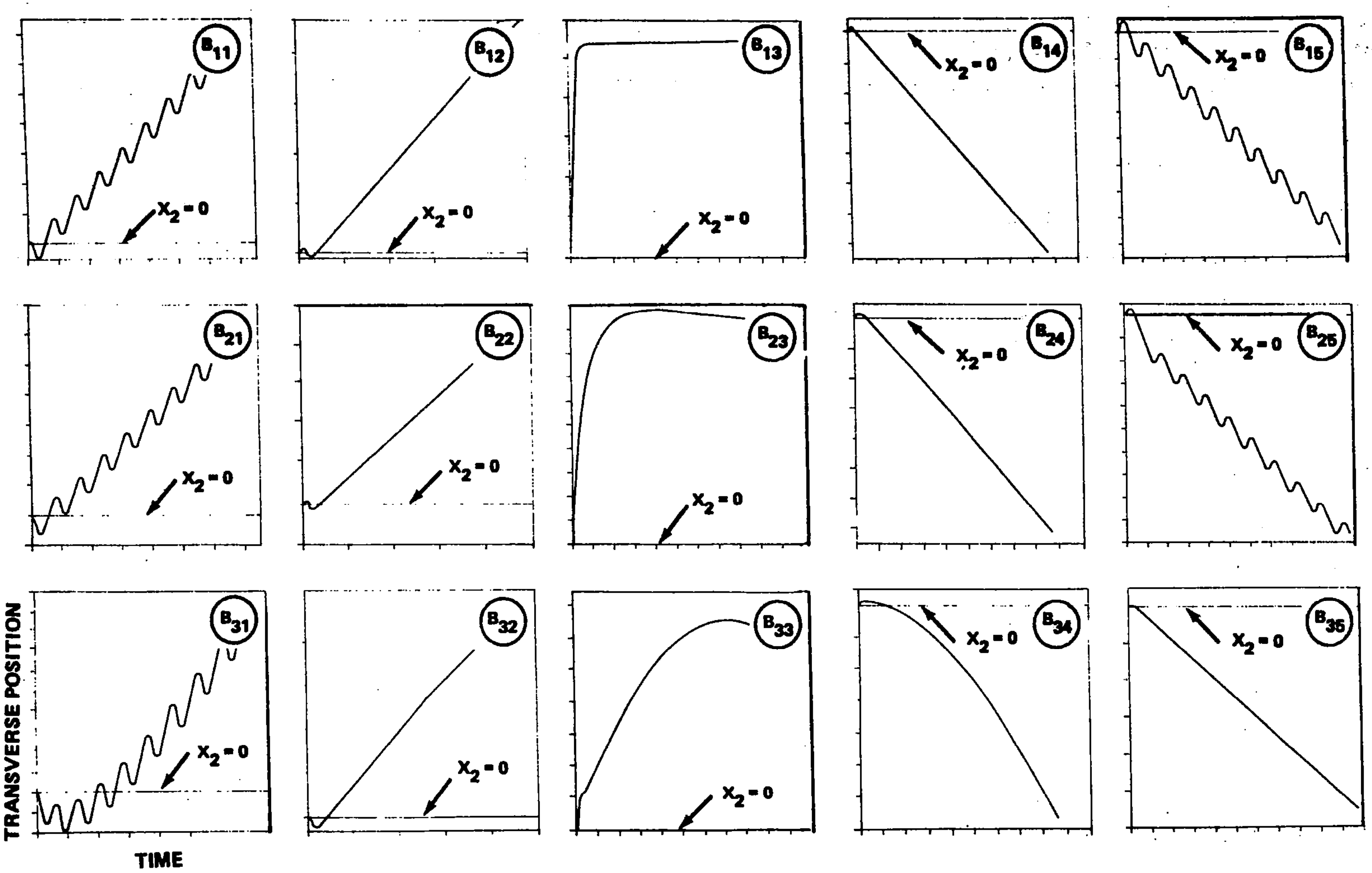

Figure 5-20. Lateral Position of Balloon as a Function of Time (Phase II)

5.3 General Observations Concerning Balloon Response

Examination of the numerical results from Phases I and II of the numerical experiments revealed a number of significant features of the balloon behavior. First of all, the mean motion of the balloon in the horizontal plane did not in general correspond to mean horizontal wind. As already noted the balloon exhibited a lateral drift except when Taylor's Hypothesis (for the parcel) (THP) was satisfied. In addition, when the x_1- component of the mean wind velocity greatly exceeded the phase velocity ($\bar{u}_1 >> c$), the balloon mean x_1- velocity component generally was slightly less than the wind velocity component ($\bar{v}_1 < \bar{u}_1$) as shown in Figure 5-21. However, as c increased relative to $\bar{u}_1$, $\bar{v}_1$ also increased until, as Taylor's Hypothesis (for the fluid) (THF) was approached, $\bar{v}_1$ first equaled and then exceeded $\bar{u}_1$. Subsequently when THF was satisfied, $\bar{v}_1$ exceeded both $\bar{u}_1$ and c. For a value of c slightly greater (~5%) than $\bar{u}_1$, THP was satisfied with c becoming equal to $\bar{v}_1$. Further increases in c resulted in a reduction in $\bar{v}_1$ until, for cases where c was very large compared with $\bar{u}_1$, $\bar{v}_1$ became essentially equal to $\bar{u}_1$.

Comparison of the quasi-Lagrangian frequency of the balloon, Ω_L' with the Eulerian frequency of the wind, ω, also proved of interest. The quasi-Lagrangian frequency was less than the Eulerian frequency for all values of c greater than $\bar{u}_1/2$. For smaller values of c the quasi-Lagrangian frequency exceeded the Eulerian frequency. This variation is shown in Figure 5-22. As indicated in the figure the quasi-Lagrangian frequency is zero when THP is satisfied ($c = \bar{v}_1$). Also the quasi-Lagrangian frequency equals the Eulerian frequency for $c = \bar{u}_1/2$.

As indicated by the figure the numerical results generally agreed with linear theory except in the vicinity of Taylor's Hypothesis where non-linear effects became significant. The relation between the quasi-Lagrangian frequency and the Eulerian frequency was observed to be

$$\Omega_L' = \left| k\, c - k\, \bar{v}_1 \right| \qquad (5\text{-}8)$$

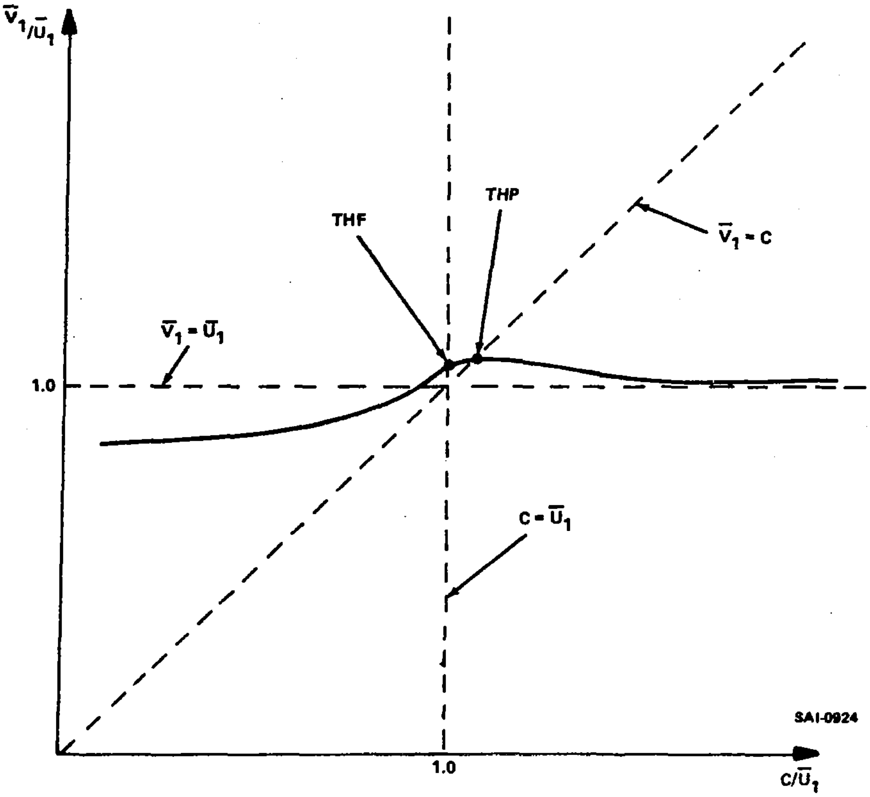

Figure 5-21. General Variation of Mean Balloon Velocity with Phase Velocity Based on Numerical Results

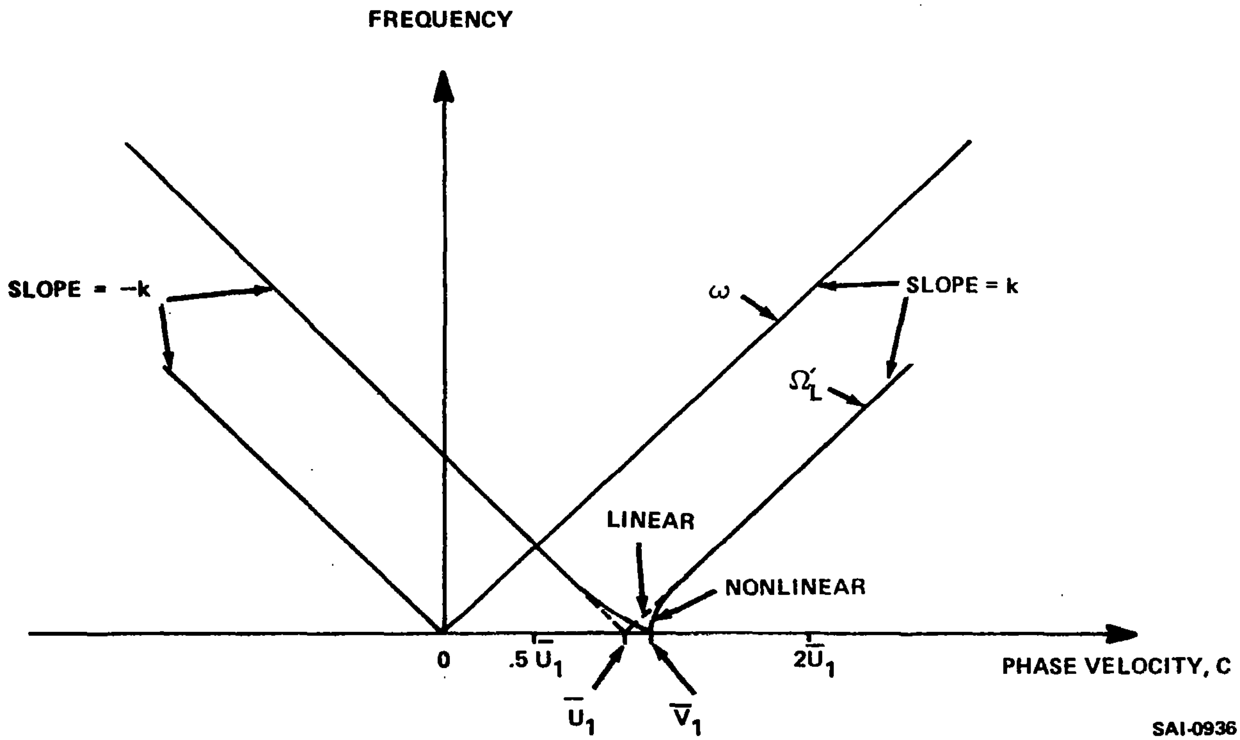

Figure 5-22. General Variation of Quasi-Lagrangian Frequency with Phase Velocity

where

$$\omega = |kc| \tag{5-9}$$

This relation is quite similar to that suggested by Gifford [128] which, as shown in Section 2.3, was of the form

$$\omega = \Omega_L' + k\,\bar{u}_1 \tag{2-1}$$

In Gifford's case the Eulerian frequencies were all larger than the Lagrangian frequencies and thus the absence of the absolute value signs was of no significance. With this fact in mind, combined with the observation that

$$\bar{v}_1 \approx \bar{u}_1 \tag{5-10}$$

it can be seen than the two relations are nearly equivalent. Notice should be taken that the first-order perturbation analysis presented in Appendix H also suggested this same type of relation.

Gifford demonstrated [128] that a relation of the form of Equation (2-1) was sufficient to correlate the measured Lagrangian spectral peak frequencies to the corresponding Eulerian spectral peak frequencies. Three investigations by Angell et.al. [132,137,142] also developed and compared Eulerian and quasi-Lagrangian spectra as discussed in Section 2.3. Unfortunately, in none of these studies were the values of the spatial wave number k determined.* In every case, however, the Lagrangian frequencies were less than the Eulerian and there was a tendency for the ratio, β ($= \omega/\Omega_L'$) to increase as the wind velocity increased. These observations are consistent with the form of Equation (5-8).

In two other studies discussed in Section 2.3, Kao et.al. [133,134] also presented Eulerian and Lagrangian spectra for comparison. In these cases, which involved much higher altitudes and lower frequencies than the studies of Gifford and Angell, the Lagrangian peak spectral frequencies were larger than the Eulerian.

* It is not sufficient to calculate k according to the relation, $k = \omega/c$, because this relation is based on the assumption that THF holds.

Based on Equation (5-8) and Figure 5-18, it would appear that the phase velocities encountered by Gifford and Angell exceeded $\bar{u}_1/2$, while the phase velocities involved in Kao's investigation were less than this value. This result is generally similar to the observations of Mizuno and Panofsky [180] in the atmospheric surface layer. However, because of the fact that both Gifford's and Angell's data involved measurement of small-scale vertical fluctuations at low altitudes (300-4200 feet) while Kao's data involved measurement of large-scale horizontal fluctuations at higher altitudes (18000 to 30000 feet), a certain degree of caution must be exercised before drawing any final conclusions concerning the relative magnitude of phase velocities and mean wind velocities.

Many of the investigations discussed in Section 2.3 involved measurement of the ratio of the Eulerian frequency to the quasi-Lagrangian frequency β. It is important to note that

$$\begin{aligned} \beta &\equiv \omega/\Omega_L' \\ &= |kc|/\Omega_L' \end{aligned} \tag{5-11}$$

A combination of Equations (5-8) and (5-11) yields

$$\begin{aligned} \beta &= \frac{|kc|}{|kc - k\bar{v}_1|} \\ &= \left|\frac{c}{c - \bar{v}_1}\right| \\ &= \left|1 + \frac{\bar{v}_1}{c - \bar{v}_1}\right| \end{aligned} \tag{5-12}$$

Except in the immediate vicinity of Taylor's Hypothesis, Equation (5-12) can be approximated as

$$\beta \approx \left| 1 + \frac{\bar{u}_1}{c - \bar{u}_1} \right| \tag{5-13}$$

6. CONCLUSIONS AND RECOMMENDATIONS

Clearly the response of a constant-volume balloon to atmospheric turbulence is a complex problem. The current investigation has utilized a more rigorous mathematical model than previously employed, but even so, certain simplifications were made to keep the problem tractable. Representing the flow field as a periodic function, as opposed to a random variable, is of special significance. Some of the responses of the balloon to the periodic function may not occur in the presence of the real random process. Thus, caution must be exercised in reaching general conclusions. At the same time, the numerical results obtained are in general agreement with observations, and a number of points are worthy of note. These matters are presented in subsection 6.1. In the course of the study a number of questions arose for which no answers could be obtained due to time and funding limitations. Certain recommendations aimed at answering such questions are provided in subsection 6.2.

6.1 Conclusions

First, the distinction between Taylor's Hypothesis (for the fluid) and Taylor's Hypothesis (for the parcel) is of considerable interest because this distinction sheds light on a number of characteristics of the balloon motion. The balloon does not move with the same mean velocity as the wind and thus when THF is satisfied the balloon does not "lock in" with the wind velocity. When THP is satisfied, however, the balloon does match the mean wind direction (but not its speed). Under such conditions the balloon displays no oscillation or lateral drift.

Except in the vicinity of Taylor's Hypothesis the quasi-Lagrangian frequency of the balloon could be related to the Eulerian frequency of the wind by means of a Doppler shift law, in accordance with first-order theory. In the vicinity of Taylor's Hypothesis first-order theory was not sufficient to relate the Lagrangian and Eulerian frequencies. When THP was exactly satisfied, the Lagrangian frequency was, of course, zero.

Based on available measured data, it would appear that constant-volume balloons generally display some oscillatory motion and thus THP is not being satisfied. Because THP is generally close to THF, this suggests that the latter is also not being satisfied.

An examination of the available Eulerian and Lagrangian turbulence spectra obtained from earlier studies indicates that a simple Doppler shift relation such as that suggested by first-order theory is possibly sufficient for correlation. Unfortunately such an approach requires values of the spatial wave number (based on direct measurement as opposed to calculation based on Taylor's Hypothesis) and these values are not generally available.

Although the balloon did not respond exactly to either the mean wind velocity or the periodic velocity fluctuations, the wind velocity served as a forcing function. The natural oscillatory frequency of the balloon was only observed during the initial phase following the start of a test case.

Casting the problem in dimensionless form and providing a dimensionless numerical solution are also significant. Unfortunately a complete evaluation of the relative importance of the pertinent dimensionless groups was not accomplished and it is not clear whether or not a more "universal" solution can be obtained.

6.2 Recommendations

The most important recommendation would be to replace the current periodic model for the flow field with a random model. The resulting balloon motion could then be subjected to Fourier analysis and realistic Eulerian and Lagrangian spectra could be generated and compared.

Further analysis of the existing numerical data should be made to provide better understanding of the relationship between the various parameters. Such analysis might lead to a more precise relationship between Taylor's Hypothesis (for the fluid) and Taylor's Hypothesis (for the parcel).

The dimensionless groups associated with the dimensionless form of the equation should be varied over a wider range of values to establish their relative importance. A more general solution should be obtained if possible.

Further study should be made of existing Eulerian-Lagrangian turbulence spectra to provide more conclusive proof of the Doppler shift relation between these two types of systems. Methods for calculating the spatial wave number as a function of altitude, without use of Taylor's Hypothesis, should be investigated.

Further investigation should be made into the question of the difference between the mean direction and speed of the balloon motion and that of the wind. Conditions under which such differences are significant in the atmosphere should be defined if possible.

7. REFERENCES CITED

1. Tatom, F. B. and King, R. L.: "Computer Plots of the Motion of Constant-Volume Balloons", SAI-77-   -HU, Science Applications, Inc., May 1976.

2. Ley, Captain C. H.: "Report on Balloon Experiments at Blackpool," Quarterly Journal of the Royal Meteorological Society, Vol. 37, 1911, pp. 33-58.

3. Ley, Captain C. H.: "An Automatic Valve for Pilot Balloons" Quarterly Journal of the Royal Meteorological Society, Vol. 37, 1911, pp. 247-250.

4. Akerman, J. D., Piccard, J. F.: "Upper Air Study by Means of Balloons and the Radio Meteorograph", Journal of the Aeronautical Sciences, Vol. 4, pp. 332-337, 1937.

5. Spilhaus, A. F., Schneider, C. S., Moore, C. B.: "Controlled Altitude Free Balloons", Journal of Meteorology Vol. 5, pp. 130-137, Aug. 1948.

6. Murray, W. D., Schneider, C. S. and Smith, J. R.: "Development and Utilization of Constant-Level Balloons" Transactions, American Geophysical Union, Vol. 31, No. 6 pp. 843-849 December 1950.

7. Hopper, V. D., Wilson, A. R. W.: "A Method for Obtaining Long Exposures at High Altitudes Using Rubber Balloons", Journal of Scientific Instruments, Vol. 30, pp. 211-212, June, 1953.

8. Herz, A. J., Tennent, R. M.: "Ballooning for Research" Science News, Vol. 27, 1953, pp. 46-58.

9. Masterbrook, H. D., Anderson, A. D.: "The Transosonde" Weatherwise, Vol. 7, pp. 79-81, Aug. 1954.

10. Haig, Major T. O.: "Plastic Balloons for High Altitude Research", Journal of Aviation Medicine, Vol. 25, pp. 351-353, 1954.

11. Anderson, A. D., Mastenbrook, A. J.: "A New Upper Air Data System - The Transosonde", Bulletin American Meteorological Society, Vol. 37, pp. 342-350, 1956.

12. Durst, C. S.: "Constant Level Ballooning", Journal of the Institute of Navigation, Vol. 10, pp. 70-77, 1957.

13. Laby, J. E., Lim, Y. K., Hopper, V. D.: "Level Flights with Expansible Balloons" Il Nerovo Aimento Series V; Vol. 5, pp. 249-259, 1957.

14. Haig, T. O., Lally, V. E.: "Meteorological Sounding Systems" Bulletin of the American Meteorological Society Vol. 39, pp. 401-409, 1958.

15. Angell, J. K.: "The Use of Transosonde Data as an Aid to Analysis and Forecasting During the Winter of 1958-1959" Journal of Geophysical Research, Vol. 64, pp. 1845-1853 1959.

16. Lally, V. E.: "Satellite Satellites: A Conjecture on Future Atmospheric-Sounding Systems" Bulletin American Meteorological Society, Vol. 41. pp. 429-432, 1960.

17. Hopper, V. D., Laby, J. E.: "Importance of Global Wind Study in the 30 km Region" Symposium on Antarctic Meteorology, 1959, pp. 466-480, published 1960.

18. Angell, J. K.: "Use of Constant Level Balloons in Meteorology", Advances in Geophysics, Vol. 8, 1961 pp. 137-219.

19. Young, Murray J.: "Comparison of Methods for Determining Probable Impact Areas in Planning Short Range Instrumented Balloon Flights", Journal of Applied Meteorology, Vol. 1 December 1962, pp. 531-535.

20. Angell, J. K.: "Meteorological Applications of Constant-Volume Balloons", The Meteorological Magazine, Vol. 92, No. 1087, pp. 37-48 February 1963.

21. Giles, K. C., Angell, J. K.: "A Southern Hemisphere Horizontal Sounding System: A Preliminary Study", Bulletin of the American Meteorological Society, Vol. 44. pp. 687-696, 1963.

22. Booker, D. R., Cooper, L. W.: "Superpressure Balloons for Weather Research", Journal of Applied Meteorology, Vol. 4 Feb. 1965, pp. 122-129.

23. Calder, Nigel: "Ten Thousand Balloons", New Scientist, Vol. 26, pp. 494-496, 1965.

24. Gildenberg, B. D.: "Meteorological Aspects of Constant-Level Balloon Operations in the Southwestern United States" AFCRL-66-706, October 1966.

25. Reynolds, A. D., Lamberth, R. L.: "Ambient Temperature Measurements from Radiosondes Flown on Constant-Level Balloons" Journal of Applied Meteorology, Vol. 5, June 1966, pp. 304-307.

26. Lichfield, G. W., Frykman, R. W.: "Ghost Balloons Riding The Skies Will Report the World's Weather", Electronics Vol. 39, pp. 98-106, Nov. 1966.

27. Lally, V. E., Lichfield, E. W., Solot, S. B.: "The Southern Hemisphere Ghost Experiment" World Meteorological Organization Bulletin, Vol. 15, pp. 124-128, 1966.

28. Blamont, J. E., "The EOLE Experiment", Spaceflight, Vol. 8, pp. 139-140, 1966.

29. Lally, Vincent: "Trial Balloons in the Southern Hemisphere", Science, Vol. 155, pp. 456-459, Jan. 1967.

30. Lichfield, E. W., Frykman, R. W.: "Electronics for Around-the-World GHOST Balloon Flights", Proceedings, Fourth AFCRL Scientific Balloon Symposium, Jan. 1967, pp. 59-67.

31. Lally, V. E.: "The Use of Satellites to Track Ghost Balloons", American Astronautical Society 13th Annual Meeting, Dallas, Texas, May 1967.

32. Booker, D. R., Cooper, L. W., Hart, H. E.: "Updraft and Air Flux Studies Utilizing Instrumented Aircraft and Super-Pressure Balloon-Transponder Systems", Weather Science, Inc. Norman, Okla., Contract E22-79-67 (N) Final Report, Nov. 1967.

33. Franch, K. E.: "Ascent Trajectory of a Superpressure Balloon", Journal of Spacecraft and Rockets, Vol. 4 (11), pp. 1557-1559, 1967.

34. Morel, P.: "Preliminary Flights of EOLE Balloons", Space Research VIII - North Holland Publishing Company, Amsterdam, pp. 1005, 1011. 1967.

35. Morel, P., Fourrier, J., Freif, M., Sitbon, P.: "Eole-Pacific IV Field Exercises", U. S. National Aeronautics and Space Administration, Technical Translation of "Campagne Eole-Pacifique IV, Premiere Partie", March, 1968, 34 pages.

36. Lally, V. E.: "Comments on "The Occurrence of Icing on Constant Level Balloons", Journal of Applied Meteorology, Vol. 7, April, 1968, p. 958.

37. Mason, Earl S.: "Building and Tracking of Mylar Constant Density Balloons at Low Cost", Journal of Applied Meteorology, Vol. 7, June, 1968, pp. 512-513.

38. Morel, P., Fourrier, J., and Sitbon, P.: "The Occurrence of Icing on Constant Level Balloons", Journal of Applied Meteorology, Vol. 7, pp. 626-634 August, 1968.

39. Ginsburg, Th.: "DAS GHOST-Projekt", Waltraumfehrt, Sept./ Oct. 1968, pp. 133-140.

40. Tefft, J. D.: "Joint NCAR-GSFC Meteorological Experiment Employing NIMBUS-D/IRLS, U.S. Air Force, Cambridge Research Labs., Bedford, Mass., Special Reports. No. 85, Dec. 1968.

41. Jessup, E. A.: "Application of Constant-Volume Balloons for Determining Air Divergence and Trajectories", U.S. National Severe Storms Lab., Norman, Okla., Technical Circular No. 7, Dec. 1968.

42. Alexander, H.: "Flight Analysis of a Constant Level Expendable-Type Balloon", Proceedings, Fifth AFCRL Scientific Balloon Symposium, Dec. 1968, pp. 19-31.

43. Lally, V. E.: "Southern Hemisphere Ghost Flight Program; the First Year", Space Research, Amsterdam, Vol. 8, 1968, pp. 1002-1004.

44. Morel, P.: "Preliminary Flights of EOLE Balloons", Space Research, Amsterdam, Vol. 8, 1968, pp. 1005-1011.

45. Nolan, George F.: "Meteorological Considerations for Tethered and Hovering Free Balloons", Earth Observations from Balloons Sponsored by the American Society of Photogrammetry, Feb. 1969.

46. Booker, D. R.: "Evidence of Severe Storm Rotational Characteristics Obtained from Superpressure Balloons Trajectories", Conference on Severe Local Storms, 6th, Chicago, April 1-10, 1969 (Preprints of papers presented at the Conference, 1969, p. 32-37.

47. Hard, H. D., Hall, D. C., Sutherland, J. L.: "Superpressure Balloon-Transponder Systems: A summary of three years use in thunderstorm research", Weather Service, Inc., Norman, Okla., WR 903, Contract E22-65-69 (N), June 15,1969.

48. Allen, P.W., White, R. E.: "Method of obtaining long-range air trajectories at low altitudes using constant-volume balloons", Upper-Air Instruments and Observations: Proceeding of the World Meteorological Organization Technical Conference, Sept. 8-12, 1969, pp. 285-296.

49. Fourrier, J.: "Possibility of Measuring Humidity using Constant Level Balloons," Upper-Air Instruments and Observations: Proceedings of the World Meteorological Organization Technical Conference, Sept. 8-12, 1969, pp. 313-327.

50. Lally, V. E., Lichfield, E. W.: "Summary of Status and Plans for the GHOST Balloon Project", Upper-Air Instruments and Observations: Proceedings of the World Meteorological Organization Technical Conference, Sept. 8-12, 1969, pp. 297-312.

51. Anonymous: "Nimbus Balloons from Ascension Island", Facilities for Atmospheric Research, No. 10, Sept. 1969.

52. Anonymous: "Balloons, Buoys, and Satellites", NCAR Quarterly, Boulder, Colo., No. 25, Nov. 1969, pp. 8-11.

53. Lally, V. E., Lichfield, E. W.: "Summary of Status and Plans for the GHOST Balloon Project", American Meterological Society, Bulletin, Nov. 1969, pp. 867-874.

54. Morel, Pierre: "Eole Constant Level Balloon Flights in the Troposphere", Space Research, Vol. 9, 1969, pp. 586-589.

55. Fourier, J., Morel, P. and Sitbon, P.: "Ambient Temperature Measurements from Constant-Level Balloons", Journal of Applied Meteorology, Vol. 9, pp. 154-157, February 1970.

56. Ohta, S., Ito, T.: "Superpressure Balloon and Precise Radio-Sonde System for the Research of Vertical Air-Motion", Papers in Meteorology and Geophysics, April, 1970, pp.45-72.

57. Spier, J. L.: "Balloons above the Southern Hemisphere", Hemel en Dampkring, The Hague, Vol. 68, April, 1970, pp. 84-86.

58. Lally, V. E.: "Constant-Level Balloons for Sounding Systems", Meteorological Monographs, Vol. 11, No. 33, pp. 392-396, Oct. 1970.

59. Ballard, H. N., Beyers, N. J., Izquierdo, M.: "A Constant-Altitude Balloon Experiment at 48 Kilometers", Sixth AFCRL Scientific Balloon Symposium, June 1970.

60. Blamont, J. E., Heinsheimer, T. F., Pommeraen, J. P.: "Position Determination Methods Used to Track Superpressure Balloons", Monthly Weather Review, Vol. 98, pp. 756-764, 1970.

61. Kulinchenko, T. M.: "Primenenie Aerostatov V Issledovanii Svobodnoi Atmosfery", Tsentral' Naia Aerologicheskaia Observatoriia, Trudy, 100, 1970, pp. 147-155.

62. Muller, J.: "Le Programme Eole", La Recherche Spatiale, Paris, Vol. 10, Aug., 1971.

63. Pinglier, A.: "Le Programme Franco-Americain Tiros N.", La Recherche Spatiale, Paris, 10, August 1971.

64. Cherry, N. J.: "Characteristics and Performance of Three Low-Cost Superpressure Balloon (Tetroon) Systems", Journal of Applied Meteorology, Vol. 10, Oct., 1971, pp. 982-990.

65. Sofiyev, Ye. I.: "Methods of Calculating the Ballest Weight for Compensated, Nonexpandable Balloons at a Given Altitude", Tashkeont, Sredneaziatskiy Nauchno-Issledovatel' skiy Gidrometeorologicheskiy Institut, Trudy. 53, 1971.

66. World Meteorological Organization: "Present Status of Constant-Level Balloon Programmes", World Weather Watch Planning Report No. 33, 1971.

67. France, Météorologie Nationale, Paris: "EOLE, 1971-1972", Met-Mar Bulletin No. 76, July 1972, pp. 25-30.

68. Morel, P.: "The Eole Experiment", Proceedings of the World Meteorological Organization Technical Conference, Toyko, Japan, Oct. 2, 1972.

69. Garger, Ye. K., Pis'menskiy, V. F.: "Kotsenke Kharakteristik Ballonov Postoyannogo Ob" Yema (Tetronov)", Leningrad. Institut Eksperimental' noy Meteorologii. Trudy, Vol. 2, pp. 141-151, 1972.

70. Mezeix, J. F., Isaka, H., Soulage, R. G.: "Etude De La Retention D'Eau Par Des Corps Plastiques: Application Amx Ballons Meteorologiques Plafonnants", Journal de Recherches Atmospheriques, Vol. 8, pp. 91-98, April/June, 1973.

71. Hoecker, W. H.: "Tetroon Drag Coefficients from Experimental Free-Flight Data", Journal of Applied Meteorology, Volume 12, pp 1062-1065, September 1973.

72. Levanon, N. et.al.: "On the Behavior of Superpressure Balloons at 150 mb", Journal of Applied Meteorology, Volume 13, pp. 494-504, June 1974.

73. Carten, A. S., Jr.: "An Investigation of the Applicability of High Altitude, Lighter-Than-Air (LTA) Vehicles to the Tactical Communications Relay Problem", Report #AFCRL-TR-74-0399, August, 1974.

74. Cadet, D., Ovarlez, H., Ovarlez, J.: "Superpressure Balloon Flights in the Tropical Boundary Layer", Journal of Applied Meteorology, Vol. 14, Dec. 1975, pp. 1478, 1484.

75. Durst, C. S. and Gilbert, G. H.: "Constant-Height Balloons-Calculation of Geostrophic Departures", Quarterly Journal of Royal Meteorological Society, Vol. 76, pp. 75-86, 195.

76. Murray, W. D., Schneider, C. S., and Smith, J. R.: "Development and Utilization of Constant-Level Balloons", Transactions, American Geophysical Union, Vol. 31. No. 6 pp. 843-849, December 1950.

77. Berry, F. A.: "Constant-Level-Balloon and Meteorological Trajectory Studies at Project AROWA", Transactions American Geophysical Union, Vol. 35, Section of Meteorology, Paper #4, May 1954, p.368.

78. Ohnsorg, F., Mantis, H. T.: "The Structure of Upper Winds as Determined by Constant-Altitude Balloons", Transactions American Geophysical Union, Vol. 35, Section of Meteorology, Paper #5, May, 1954, p. 368.

79. Moore, C. B., Smith, J. R., and Gaalswyk, A.: "On the Use of Constant-Level Balloons to Measure Horizontal Motions in the Atmosphere" Journal of Meteorology, Vol. 11, No. 3, pp. 167-172, June 1954.

80. Arakawa, H.: "Basic Principles of the Balloon Bomb", Papers in Meteorology and Geophysics, Vol. 6, pp. 239-243, 1956.

81. Neiburger, M., Angell, J. K.: "Meteorological Applications of Constant-Pressure Balloon Trajectories", Journal of Meteorology, Vol. 13, pp. 166-194, April, 1956.

82. Holzworth, G. C., Kauper, E. K. and Smith, T. B.: "Some Observed Low-Level Air Trajectories over Los Angeles, California", Monthly Weather Review, pp. 387-392, August 1963.

83. Pack, D. H., Angell, J. K.: "A Preliminary Study of Air Trajectories in the Los Angeles Basin as Derived from Tetroon Flights", Monthly Weather Review, Vol. 9, pp. 583-604, Dec. 1963.

84. Angell, J. K., Pack, D. H., Holzworth, G. C., Dickson, C.R.: "Tetroon Trajectories in an Urban Atmosphere", Journal of Applied Meteorology, Vol. 5, pp. 565-572, 1966.

85. Angell, J. K., Hass, W. A.: "Effect of Clustering Upon a 500-mb Horizontal Sounding System", Monthly Weather Review, Vol. 94, pp. 151-165, 1966.

86. Lund, I. A.: "Fifty Millibar Balloon Trajectories" Proceedings, Fourth AFCRL Scientific Balloon Symposium, Jan. 1967, pp. 215-232.

87. Solot, S. B.: "Some Meteorological Results of the Southern Hemisphere GHOST Experiment", Proceedings, Fourth AFCRL Scientific Balloon Symposium, Jan. 1967, p. 297.

88. Allen, P. W., Jessup, E. A., White, R. E.: "Long Range Trajectories", Proceedings of the USAEC Meteorological Information meeting, Chalk River Nuclear Labs, Sept 11-14, 1967, pp. 176-190.

89. Solot, S. B.: Ghost Balloon Data, Vol. II: Balloon 28X, Jan. 1968, NCAR-TN-34.

90. Solot, S. B.: Ghost Balloon Data, Vol. III: Balloon 34J, Jan. 1968, NCAR-TN-34.

91. Solot, S. B.: Ghost Balloon Data, Vol X: Balloon Data 79R, Jan. 1968, NCAR-TN-34.

92. Ahrens, D., Miller, A.: Air Trajectories in the San Francisco Bay Area, Report No. 5, San Jose State College Meteorology Department, Sept. 1968.

93. Hall, D. R., Hall, D. C., Hart, H. E.: "Balloon Transponsder Studies of Severe Storm Systems", Weather Science, Inc., Norman, Okla., Final Report, Oct. 1968, 34 pages.

94. Solot, S. B.: "Ghost Balloons are Solving the Riddle of The Southern Hemisphere Circulation", Proceedings, Fifth AFCRL Scientific Balloon Symposium, Dec. 1968, p. 223.

95. Lally, V. E., Carlson, N., Frykman, R. W., Lichfield, E. W., Rickel, A. B., Verstraete, M.: "Superpressure Balloon Flights from Christchurch, New Zealand, August 1967 - June 1968", National Center for Atmospheric Research, Boulder, Colo., NCAR Technical Notes, Feb. 1969, 74 pages.

96. Lally, V., Schumann, A., Reed, R.: "Superpressure Balloon Flights in the Tropical Stratosphere", Science, Vol. 166 (3906), pp. 738-739, Nov. 1969.

97. Hoecker, W. H., Angell, J. K.: "Effect of a Sudden Change in Terrain Height on the Three-Dimensional Low-Level Air Flow, as Estimated from Tetroon Flights", Monthly Weather Review, Dec. 1969, pp. 845-849.

98. Mesinger, F., Mintz, Y.: "Numerical Simulation of the 1970-71 Eole Experiment", L.A. Dept. of Meteorology, Numerical Simulation of Weather and Climate Technical Report No. 4, Jan, 1970, 51 pages.

99. Mesinger, F., Mintz, Y.: "Numerical Simulation of the Clustering of Constant-Volume Balloons in the Global Domain", L.A. Dept. of Meteorology, Numerical Simulation of Weather and Climate Technical Report No. 5, Feb. 1970 35 pages.

100. Lally, V. E., Rickel, A. B., Verstraete, M.: Superpressure Balloon Flights from Christchurch, New Zealand, July 1968 - December 1969", National Center for Atmospheric Research, Boulder, Colorado, NCAR Technical Notes TN-48, May 1970, 104 pages.

101. Pack, D. H.: "Tetroon Flights in Los Angeles, Calif., 1969" U. S. Air Resources Lab, Silver Spring, Md., Technical Memorandum C-RLTM-ARL 19, June 1970.

102. Morel, Pierre: "Large Scale Dispersion of Constant-Level Balloons in the Southern General Circulation", Annales de Geophysique, Vol. 26 (4), pp. 815-828, 1970.

103. Angell, J. K.: "Helical Circulations in the Planetary Boundary Layer", Journal of the Atmospheric Sciences, Vol. 28, Jan. 1971 pp. 135-138.

104. Angell, J. K., Allen, P. W., and Jessup, E. A.: "Mesoscale Relative Diffusion Estimates from Tetroon Flights", Journal of Applied Meteorology, Vol. 10, pp. 43-46 February 1971.

105. Angell, J. K., Pack, D. H., Dickson, C. R., Hoecker, W. H.: "Urban Influence on Nighttime Airflow Estimated from Tetroon Flights", Journal of Applied Meteorology, April, 1971, pp. 194, 204, Vol. 10.

106. Angell, J. K., Pack, D. H., Machta, L., Proulx, R., Dickson, C. R.: "Mesoscale Trajectories, Helicopter Oxidant Measurements and Surface Wind Fields", Conference on Air Pollution Meteorology, April 5-19, 1971, Preprints of Papers, pp. 119-120.

107. Blamont, J. E., Heinsheimer, T. F., Pommereau, J. P.: "An Experimental Demonstration of the Isentropic Nature of the Motion of Stratospheric Air Masses", Journal of the Atmospheric Sciences, Boston, Vol. 28, No. 6, Sept. 1971. pp. 1015-1020.

108. Ballard, H. N., Beyers, N. J., Miers, B. T.,Izquierdo, M., Whitacre, J.: "Atmospheric Tidal Measurements at 50km from a Constant-Altitude Balloon", U. S. Army Electronics Command Research and Development Technical Report ECOM-5417, December 1971.

109. Angell, J. K., Pack, D. H., Machta, L., Dickson, C. R., Hoecker, W. H.: "Three-Dimensional Air Trajectories Determined from Tetroon Flights in the Planetary Boundary Layer of the Los Angeles Basin", Journal of Applied Meteorology, April 1972, Vol. 11, pp. 451-471.

110. Angell, J. K.: "Comparison of Circulations in Transverse and Longitudinal Planes in an Unstable Planetary Boundary Layer", Journal of the Atmospheric Sciences, Vol. 29, pp. 1252-1261, Oct. 1972.

111. Webster, P. J., Curtin, D. G.: "Interpretations of the EOLE Experiment I. Temperal Variation of Eulerian Quantities", Journal of the Atmospheric Sciences, Vol. 31., pp. 1860-1875, Oct. 1974.

112. Morel, P., Bandeen, W.: "The EOLE Experiment: Early Results and Current Objectives", American Meteorological Society Bulletin, Vol. 54, April 1973, pp. 298-306.

113. Levine, J., Garstang, M. LaSear, N. E.: "A Measurement of the Velocity Field of a Cumulus Cloud", Journal of Applied Meteorology, Volume 12, pp. 841-846, August 1973.

114. Angell, J. K., Hoecker, W. H., Dickson, C. R., and Pack, D. H.: "Urban Influence on a Strong Daytime Air Flow as Determined from Tetroon Flights" Journal of Applied Meteorology, Volume 12, pp. 924-936, September 1973.

115. Leahey, D. M., Hicklin, H. S.: "Tetroon Studies of Diffusion Potential in the Airshed Surrounding the Crowsnest Pass Area", Atmosphere, (Toronto, Canada), Vol. 11, pp. 77-87, 1973.

116. Morel, P., Desbois, M.: "Mean 200-mb Circulation in the Southern Hemisphere Deduced from EOLE Balloon Flights". Journal of the Atmospheric Sciences, Vol. 31, pp. 394-407 March, 1974.

117. Angell, J. K.: "Mean Meridional Winds Estimated from Constant Level Balloon Flights in Southern Hemisphere Temperate Latitudes", Royal Meteorological Society, Bracknell, Eng., Quarterly Journal, Vol. 100, pp. 212-220, April 1974.

118. Giles, K. C., Peterson, R. E.: "A Study of Wind Velocities Measured from Constant-Pressure Balloons", Journal of Meteorology, Vol. 14, pp. 569-572, Dec. 1957.

119. Wilkins, Eugene, M.: "observations on the Separation of Pairs of Neutral Balloons and Applications to Atmospheric Diffusion Theory", Journal of Meteorology, Vol. 15, pp. 324-327, June 1958.

120. Laby, J. E., and Sparrow, J. G.: "Wind Studies Using Level Balloons" Journal of Applied Meteorology, Vol. 4, pp. 585-589, October 1965.

121. Angell, J. K., Pack, D. H.: "Mesoscale Diffusion Derived from Tetroon Flights", Proceedings of the USAEC Meteorlogical Information Meeting, Chalk River Nuclear Labs, Sept. 11-14, 1967, pp. 241-251.

122. Reynolds, R. D., Lamberth, R. L.: "Investigation of a Complex Mountain Wave Situation", Journal of Applied Meteorology, Vol. 7, June 1968, pp. 353-358.

123. Dickson, C. R. and Angell, J. K.: "Eddy Velocities in the Planetary Boundary Layer as Obtained from Tetroon Flights at Idaho Falls", Journal of Applied Meteorology, Vol. 7 Dec. 1968, pp. 986-993.

124. Vergenier, J., Lilly, D. K.: "The Dynamic Structure of Lee Wave Flow as Obtained from Balloon and Airplane Observations" Monthly Weather Review, Vol. 98, March 1970, pp. 220-232.

125. Lile, R. C.: "Tetroon-Derived Eddy Viscosity in the Region of the Elevated West Coast Temperature Inversion", Scientific Report No. 1, July, 1970.

126. Reynolds, R. D. "Superpressure Balloons as Isentropic/Isopynic Tracers" Journal of Applied Meteorology, Volume 12, pp. 369-373, March 1973.

127. Emmons, G., Haurwitz, B., Spilhaus, A. F.: "Oscillations in the Stratosphere & High Troposphere", Bulletin American Meteorological Society, Vol. 31, No. 4, April 1950, pp. 135-138.

128. Gifford, Frank, Jr.: "A Simultaneous Lagrangian-Eulerian Turbulence Experiment" Monthly Weather Review, Vol. 83, No. 12, December 1955, pp.293-301.

129. Angell, J.K., Pack, D. H.: "Analysis of some Preliminary Low-Level Constant Level Balloon (Tetroon) Flights", Monthly Weather Review, Vol. 88, No. 7, pp. 235-248, July, 1960.

130. Angell, J. K. "An Analysis of Operational 300 MB Transonde Flights from Japan in 1957-58", Journal of Meteorology, Vol. 17, pp. 20-35, 1960

131. Angell, J. K., Pack, D. H.: "Analysis of Low-Level Constant Volume Balloon (Tetroon) Flights from Wallops Island" Journal of the Atmospheric Sciences, Vol. 19, pp. 87-98 1962.

132. Angell, J. K.: "Measurements of Lagrangian and Eulerian Properties of Turbulence at a Height of 2500 Feet" Quarterly Journal of the Royal Meteorological Society, 90 (383) pp. 57-71, 1964.

133. Kao, S. K. and Bullock, W. S.: "Lagrangian and Eulerian Correlations and Energy Spectra of Geostrophic Velocities" Quarterly Journal of the Royal Meteorological Society, Vol. 90, No. 384, pp. 166-174, 1964.

134. Kao, S. K.: "Some Aspects of the Large-Scale Turbulence and Diffusion in the Atmosphere" Quarterly Journal of the Royal Meteorological Society, Vol. 91, No. 387 pp. 10-17 1965.

135. Kao, S. K.: "Some Characteristics of Relative Particle Dispersion in the Atmosphere's Boundary Layer", Proceedings of the USAEC Meteorological Information Meeting, Chalk River Nuclear Labs, Sept. 11-14, 1967, pp. 437-452.

136. Angell, J. K., Pack D. H., Delver, N.: "Brant-Vaisala Oscillations in the Planetary Boundary Layer", Journal of the Atmospheric Sciences, Vol.26, Nov. 1969, pp. 1245-1252.

137. Angell, J. K., Pack, D. H., Hoecker, W. H., Delver, N.: "Lagrangian-Eulerian Time-Scale Ratios Estimated from Constant-Volume Balloon Flights Past a Tall Tower", Royal Meteorological Society, Quarterly Journal, Jan. 1971 pp.87-92.

138. Garger, Ye. K. et.al.: "Razraketka i Naturnyye Ispytaniya Ballonov Postoyannogo Ob" Yema (Tetronov)", Leningrad, Institut Eksperimental' noy Meteorologii, Trndy, Vol. 2, pp. 125-140.

139. Morel, P., Necco, G.: "Scale Dependence of the 200-mb Divergence Inferred from EOLE Data", Journal of the Atmospheric Sciences, Vol. 30, July 1973, pp. 909-921.

140. Desbois, M.: "Tranferts Macroturbulents a 200 mb d'apris les donnees de l'experience EOLE dand l' hemisphere Sud", Annales de Geophysique, Vol. 29, pp. 252-537, Oct/Dec, 1973.

141. Gascard, J. C. "Vertical Motions in a Region of Deep-Water Formation", Deep-Sea Research, Vol. 20, pp. 1011-1027, 1973.

142. Angell, J. K.: "Lagrangian-Eulerian Time-Scale Relationship Estimated from Constant Volume Balloon Flights Past a Tall Tower", Turbulent Diffusion in Environmental Pollution, Advances in Geophysics, Vol. 18B, pp. 419-431 Academic Press, 1974.

143. Desbois, M.: "Ondes Stationnaires et progressives de la Circulation Atmospherique a 200 mb dans l' Hemisphere Sud e'tudiees a' l'aide de l'experience EOLE", Annuals of Geophysical Transactions, Vol. 30, 1974, pp. 459-471.

144. Basset, A. B.: A Treatise on Hydrodynamics, Vol. 2, Chapter 5, Deighton, Bell and Co., Cambridge, 1888

145. Tchen, C. M.: "Mean Value and Correlation Problems Connected with the Motion of Small Particles Suspended in a Turbulent Fluid", Ph.D. Dissertation Delft, Martinus Nijhoff, the Hague, 1947.

146. Corrsin, S., and Tumler, J.: "On the Equation of Motion for a Particle in Turbulent Fluid", Applied Scientific Research, Section A, Vol. 6, pp. 114-116, 1953.

147. Lumley, J. L.: "Some Problems Connected with the Motion of Small Particles in Turbulent Fluid, Ph.D. Dissertation, John Hopkins University, 1957.

148. Hinze, J. O.: Turbulence, McGraw-Hill Book Co., N.Y. 1959.

149. Choo, B. T.: "Turbulent Transport Behavior of Small Particles in Dilute Suspension" Osterichisches Ingenieur-Archiv. Sonderabdruck aus Bd., XVIII, Heft 1 and 2, 1964.

150. Hjelmfelt, A. T. Jr. and Mockros, L. F.: "Motion of Discrete Particles in a Turbulent Fluid", Applied Scientific Research, Vol. 16, pp. 149-161, 1966.

151. Shirazi, M. A.: "On the Motion of Small Particles in a Turbulent Fluid Field", Ph.D. Dissertation, University of Illinois, 1967.

152. Gorbis, Z. R. and Spokinyi, F. E.: "Pulsating Motions of a Solid Particle in Turbulent Flow", Mekhanika Zhidkosti i Gaza, Vol. 4, No. 1, pp. 137-141, 1969.

153. Hill, M. K. and Zukoski, E. E., "Behavior of Spherical Particles at Low Reynolds Numbers in a Fluctuating Translational Flow - Preliminary Experiments", Aerospace Research Laboratories 72-0017, 1972.

154. Morsi, S. A. and Alexander, A. J.: "An Investigation of Particle Trajectories in Two-Phase Flow Systems", Journal of Fluid Mechanics, Vol. 55, Part 2, pp. 193-208, 1972

155. Contaxes, N. A. and Tatom, F. B.: "The Motion of a Void in a Highly Viscous Rotating, Accelerating Flow", Nortronics-Huntsville Internal Note, No. 76, 1968

156. Calton, I. and Schwartz, .. H.: "Motion of Bubbles in a Rotating Container", Journal of Spacecraft, Vol. 9, No. 6, pp. 468-471, 1972.

157. Brunt, D.: "The Period of Simple Vertical Oscillations in the Atmosphere", Quarterly Journal Meteorological Society, Vol. 53, pp. 30-31, 1927.

158. Larsen, L. H.: "Oscillations of a Neutrally Buoyant Sphere in a Stratified Fluid", Deep-Sea Research, Vol. 16, pp. 587-603, April 1969.

159. Kao, S. K.: "An Analysis of the Trajectory of a Constant-Pressure Balloon wn a Long Atmospheric Wave in Comparison with the Nonlinear Theory", Journal of Meteorology, Vol. 18, pp. 251-256, 1961.

160. Reed, W. H. III,: "Dynamic Response of Rising and Falling Balloon Wind Sensors with Application to Estimates of Wind Loads on Launch Vehicles", NASA Technical Note D-1821, October 1963.

161. Hirsch, J. H., Booker, D. R.: "Response of Superpressure Balloons to Vertical Air Motions", Journal of Applied Meteorology, Vol. 5, pp. 226-229, April, 1966

162. Scoggins, J. R.: "Spherical Behavior and the Measurement of Wind Profiles" NASA TN D-3994, June, 1967.

163. Hanna, S. R. and Hoecker, W. H.: "The Response of Constant-Density Balloons to Sinusoidal Variations of Vertical Wind Speeds", Journal of Applied Meteorology, Vol. 10, pp. 601-604, June 1971.

164. Grant, F. C.: "Proposed Technique for Launching Instrumented Balloons into Tornadoes", NASA TN D-6503, Langley Research Center, Nov. 1971.

165. Fichtl, G. H. "Aerodynamic Properties of Spherical Balloon Wind Sensors", Journal of Applied Meteorology, Vol. 11, No. 3, pp. 472-481, April 1972.

166. Fichtl, G. H.: "Spherical Balloon Response to Three-Dimensional Time-Dependent Flows", NASA TN D-6829, July, 1972.

167. Fichtl, G. H.: "Behavior of Spherical Balloons in Wind Shear Layers", Journal of Geophysical Research, Vol. 77, No. 21, pp. 3931-3935, July 20, 1972.

168. Ohnsorg, F.: "Error Lstimates for Constant-Level Balloon Tracking" Journal of Meteorology, Vol. 14, pp. 81-83 February 1937.

169. Mesinger, Fedor: "Behavior of a Very Large Number of Constant-Volume Trajectories", Journal of the Atmospheric Sciences, Vol. 22, pp. 479-492, 1965.

170. Nolan, G. F. (Editor A. O. Korn): "The Constancy of Winds in the Lower Stratosphere and Constant-Level Balloon Planning", Proceedings, AFCRL Scientific Balloon Workshop 1965, (AFCRL-66-309), May, 1966 p.9.

171. Etkin, B.: Dynamics of Flight, John Wiley & Sons, Inc.1959.

172. Wandel, C. F. and Kofoed, Hansen, O: "On the Eulerian-Lagrantian Transform in the Statistical Theory of Turbulence" Journal of Geophysical Research, Vol. 67, No.8 pp. 3089-3092, July 1962.

173. Panofsky, H. A.: "Scale Analysis of Atmospheric Turbulence at 2m", Quarterly Journal of the Royal Meteorologica. Society, Vol. 88, pp. 57-69, 1962.

174. Corrsin, S.: "Estimate of the Relation Between Eulerian and Lagrangian Scales in Large Reynolds Number Turbulence" Journal of Atmospheric Sciences, Vol. 20 pp. 115-119, 1963.

175. Lumley, J. L. and Panofsky, H. A.: The Structure of Atmospheric Turbulence, Interscience Publishers, 1964.

176. Slade, D. H. (Ed.): Meteorology and Atomic Energy 1968, U. S. Atomic Energy Commission, Office of Information Services, July 1968.

177. Priestley, M. B.: "Time Dependent Spectral Analysis and its Application in Prediction and Control", Journal of Sound and Vibration, May 1971, Vol. 17 (4), pp. 517-534.

178. Panchev, S.: Random Functions and Turbulence, Pergamon Press, 1971.

179. Etkin, B.: "Flight in a Turbulent Atmosphere", Dynamics of Atmospheric Flight, John Wiley & Sons, Inc., 1972, pp. 529-563.

180. Mizuno, T. and Panofsky, H. A.: "The Validity of Taylor's Hypothesis in the Atmospheric Surface Layer" Boundary-Layer Meteorology, pp. 375-380, D. Reidel Publishing Co. 1975.

181. Hess, S. L.: Introduction to Theoretical Meteorology Holt, Rinehart and Winston, New York, 1959.

APPENDIX A

Balloon Terminology

During the past 65 years a number of different terms have been used to describe that class of balloons which are designed for horizontal flight with a constant volume at essentially a constant altitude. The definitions which follow are designed to aid the reader in understanding the similarities and differences between the types of balloons to which the terms apply. For convenience the definitions are arranged in alphabetical order.

CONSTANT ALTITUDE BALLOON - A helium-filled, zero-pressure balloon made of polyethelene for high altitude research.

CONSTANT DENSITY BALLOON - A pillow-shaped balloon made of Mylar.

CONSTANT-LEVEL BALLOON - A balloon which by means of ballast or superpressure is designed to operate at essentially a constant altitude.

CONSTANT-PRESSURE BALLOON - A balloon of the type used in the transosonde system.

CONSTANT-VOLUME BALLOON - A balloon whose volume remains essentially constant during flight. This condition is usually achieved by inflating the balloon to a pressure which is considerably greater than the ambient air pressure at the equilibrium altitude.

CONTROLLED ALTITUDE FREE BALLOON - A balloon made of polyethelene with a control device to maintain constant altitude.

HORIZONTAL SOUNDING BALLOON - A superpressure balloon made of Mylar designed for level flight for periods in excess of 60 days.

LEVEL BALLOON - An expansible balloon made of rubber or Neoprene equipped with a valve in the neck to maintain constant levels at high altitudes.

NEUTRAL BALLOON - A balloon with zero lift.

PILOT BALLOON - A balloon made of rubber or Neoprene used for observing winds aloft.

SUPERPRESSURE BALLOON - A balloon made of nonstretchable material (normally Mylar) so that its volume is essentially constant with excess internal pressure.

TETROON - A one-cubic-meter constant-volume balloon of tetrahedronal shape constructed of Mylar.

TRANSOSONDE - A constant-level balloon equipped with meteorological sensing instruments, a radio transmitter, and a power supply.

APPENDIX B

Equation of Motion for Immersed Bodies

The governing equation for the motion of a body submerged in a turbulent fluid consists of the equation for the conservation of momentum of the body coupled with the equation for conservation of momentum of the fluid. The governing equation has been developed in various forms 141,144-156,161,163,165,166 with various simplifying assumptions for a number of different applications, but there is not total agreement as to the validity or equivalence of all such forms. The development which follows is relatively general and the result is an equation which is representative of the type encountered in the analysis of the motion of bodies immersed in a turbulent flow.

Consider first the conservation of momentum for a spherical body of density σ, diameter D, and mass m, slowly moving (Re<0.1)* with a velocity v_i in an otherwise stationary fluid in the presence of a gravitational field, as originally developed by Basset 144 . This equation can be written in the form

$$m \frac{dv_i}{dt} + m_a \frac{dv_i}{dt} = (F_D)_i + (F_p)_i + (F_g)_i + (F_B)_i \qquad \text{(B-1)}$$

where

$$m_a = \frac{1}{2} m \, \rho/\sigma \qquad \text{(apparent mass)} \qquad \text{(B-2)}$$

$$(F_D)_i = -3\pi D \mu v_i \qquad \text{(drag force)} \qquad \text{(B-3)}$$

$$(F_p)_i = -m/\sigma \, \partial p/\partial x_i \qquad \text{(pressure force)} \qquad \text{(B-4)}$$

$$(F_g)_i = m g_i \qquad \text{(gravitational force)} \qquad \text{(B-5)}$$

$$(F_B)_i = 3/_2 \, \rho D^2 \sqrt{\pi \nu} \int_o^t \frac{dv_i(t')/dt'}{\sqrt{t - t'}} dt' \qquad \text{(Basset term)} \qquad \text{(B-6)}$$

* This condition is not necessarily satisfied with a CVB

Before proceeding further it is important to note that the apparent mass term, $m_a dv_i/dt'$, can be derived from inviscid flow theory and has the same value for both viscous and inviscid flow. The apparent mass term represents the time-rate-of-change of fluid momentum due to inviscid effects. The Basset term is produced by viscous effects and thus can be interpreted as the time-rate-of-change of momentum of the fluid due to viscous effects. Together the apparent mass and Basset terms produce an additional drag on the body which is a function of the time-rate-of-change of the relative velocity of the fluid with respect to the body.

The next step in the development involves considering the case of a body slowly moving in a fluid with non-uniform velocity $u_i\ (t,x_i)$. The non-uniform velocity $u_i\ (t,x_i)$ represents a turbulent flow process with the following assumptions [148].

1. The turbulence is steady and homogeneous.
2. The domain of turbulence is infinite in extent.
3. The body is spherical with a motion relative to the fluid which is characterized by a Reynolds number less than 0.1.*
4. The body is small relative to the smallest turbulence wavelength present.
5. While the body is in motion the fluid immediately surrounding it will be composed of the same fluid particles.
6. The only external force acting on the body is produced by a gravitational field (or other potential field).

The conservation of momentum equation for this case can be written:

$$m \frac{dv_i}{dt} + m_a \frac{d(v_i - u_i)}{dt} = (F_D)_i + (F_p)_i + (F_g)_i + (F_B)_i \qquad \text{(B-7)}$$

where

$$(F_D)_i = -3\pi D\mu(v_i - u_i) \qquad \text{(B-8)}$$

$$(F_p)_i = -m/\sigma\ \partial p/\partial x_i \qquad \text{(B-9)}$$

---

* The condition of small Re (0.1) is not necessarily satisfied with a CVB.

$$(F_g)_i = mg_i \tag{B-10}$$

$$(F_B)_i = -\frac{3}{2}\rho D^2\sqrt{\pi\nu}\int_0^t \frac{d\left[v_i(t') - u_i(t')\right]/dt'}{\sqrt{t - t'}}\,dt' \tag{B-11}$$

Notice should be taken that in apparent mass term, the drag term, and the Basset term the body velocity v_i has been replaced by the relative velocity $(v_i - u_i)$, because in each case the resistance is a function of the relative velocity between the body and the fluid.

The next step in the development of the body momentum equation consists of expressing the pressure force term as a function of the fluid velocity. For the case of an incompressible fluid with a velocity $u_i(t)$ which is a function of time but is spatially uniform, conservation of fluid momentum can be expressed as

$$\rho\,\frac{Du_i}{Dt} = -\partial p/\partial x_i + \rho g_i \tag{B-12}$$

For the case of the non-uniform fluid velocity $u_i(t,x_i)$ the instantaneous equation for the conservation of fluid momentum can be written for the incompressible case as:

$$\rho\,\frac{Du_i}{Dt} = -\partial p/\partial x_i + \mu\,\frac{\partial^2 u_i}{\partial x_j \partial x_j} + \rho g_i \tag{B-13}$$

Notice should be taken that in equation (B-13) the instantaneous fluid properties are represented and not the time-averaged. Thus, although the flow may be turbulent, no turbulent or Reynolds stresses appear in the equation for momentum conservation.

In his original development Tchen [145] neglected the viscous stress terms and effectively equated the follow-the-fluid particle derivative, Du_i/Dt, to the follow-the-solid body derivative, du_i/dt. Such a process corresponds to the simplifying assumption:

$$-\frac{\partial p}{\partial x_i} \approx \frac{du_i}{dt} - \rho g_i \tag{B-14}$$

Tchen used this relation to replace the pressure force term in equation (B-1). Corrsin and Lumley [146] first noted the inexactness of this approximation while Hinze [148] indicated that such an approach was valid if:

$$\frac{D^2}{\nu}\ \frac{\partial u}{\partial x} << 1 \qquad \text{(B-15)}$$

and

$$\frac{v}{D^2(\partial^2 u/\partial x^2)} >>> 1 \qquad \text{(B-16)}$$

Hinze's development of Equations (B-15) and (B-16) is not altogether rigorous as indicated by the absence of subscripts. More precisely the two conditions are:

$$\frac{D^2}{18\nu} \left| (u_k - v_k)\left(\frac{\partial u_i}{\partial x_k}\right) / (u_i - v_i) \right| << 1 \qquad \text{(B-17)}$$

and

$$\frac{v_k\ (\partial u_i/\partial x_k)}{2/3\ \nu(\partial^2 u_i/\partial x_j\ \partial x_j)} >> 1 \qquad \text{(B-18)}$$

If the flow is near isotropic it is reasonable to assume:

$$u_1 - v_1 \approx u_2 - v_2 \approx u_3 - v_3 \qquad \text{(B-19)}$$

$$v_1 \approx v_2 \approx v_3 \qquad \text{(B-20)}$$

$$\frac{\partial u_i}{\partial x_1} \approx \frac{\partial u_i}{\partial x_2} \approx \frac{\partial u_i}{\partial x_3} \qquad \text{(B-21)}$$

and

$$\frac{\partial^2 u_i}{\partial x_1{}^2} \approx \frac{\partial^2 u_i}{\partial x_2{}^2} \approx \frac{\partial^2 u_i}{\partial x_3{}^2} \qquad \text{(B-22)}$$

With these assumptions equations (B-17) and (B-18) reduce to

$$\frac{D^2}{6\nu} \left| \partial u_i/\partial x_j \right| << 1 \qquad \text{(B-23)}$$

and

$$\frac{9}{D^2} \left| \frac{v_i}{\partial^2 u_j / \partial x_k^2} \right| >> 1 \qquad \text{(B-24)}$$

Equations (B-23) and (B-24) are seen to agree with equations (B-15) and (B-16) except for the subscripts, the numerical constants, and the use of absolute values, all of which Hinze omitted.

Because the spatial derivatives of the fluid velocity represent instantaneous values as opposed to time-averaged values, for the case of homogeneous turbulent flow, the order of magnitude of such derivatives can be expressed in terms of the scale and intensity of the turbulence as follows:

$$| \partial u_i / \partial x_j | \simeq \sqrt{\overline{u_i'^2}} \; / \lambda_j \qquad \text{(B-25)}$$

$$| \partial^2 u_i / \partial x_j^2 | \simeq \sqrt{\overline{u_i'^2}} \; / \lambda_j^2 \qquad \text{(B-26)}$$

where

λ_j = micro-scale of turbulence.

A combination of equations (B-23) and (B-25) yields:

$$\frac{D^2}{6\nu} \sqrt{\overline{u_i'^2}} \; / \lambda_j \qquad << 1 \qquad \text{(B-27)}$$

while combining equations (B-24) and (B-26) produces:

$$\frac{9}{D^2} \frac{| v_i | \lambda_j^2}{\sqrt{\overline{u_i'^2}}} >>> 1 \qquad \text{(B-28)}$$

Now

$$v_i \sim \bar{u}_i + \sqrt{\overline{u_i'^2}} \qquad \text{(B-29)}$$

Thus equation (B-28) can be reduced to

$$\frac{9\left(\bar{u}_i/\sqrt{\overline{u_i'^2}} + 1\right)\lambda_j^2}{D^2} \ggg 1 \qquad \text{(B-30)}$$

For a turbulent flow field with known values of kinematic viscosity, turbulence intensity, turbulence micro-scale, and mean fluid velocity, equations (B-27) and B-30) provide a means of quantitatively determining the maximum size bodies for which Tchen's approximation of the pressure force is valid.

For spherical bodies which satisfy the preceding restrictions the particle momentum equation can be written

$$m\frac{dv_i}{dt} + m_a\frac{d(v_i-u_i)}{dt} = -3\pi D\mu(v_i - u_i) + m\rho/\sigma\,\frac{du_i}{dt} + mg_i - m\rho g_i/\sigma - \frac{3}{2}D^2\sqrt{\pi\rho\mu}\int_o^t \frac{d\,[v_i(t')-u_i(t')]/dt'}{\sqrt{t-t'}}\,dt' \qquad \text{(B-31)}$$

Now

$$m = \frac{\pi}{6}\,D^3\sigma \qquad \text{(B-32)}$$

and

$$m_a = \frac{\pi}{12}\,D^3\rho \qquad \text{(B-33)}$$

Introduction of the two preceding relations into equation (B-31) produces

$$\frac{dv_i}{dt} + a\,v_i = a\,u_i + b\,\frac{du_i}{dt} + c\int_o^t \frac{d\,[u_i(t')-v_i(t')]/dt'}{\sqrt{t-t'}}\,dt' + d\,g_i \qquad \text{(B-34)}$$

where

$$a = \frac{36\mu}{(2\sigma+\rho)\,D^2} \qquad \text{(B-35)}$$

$$b = \frac{3\rho}{2\sigma+\rho} \qquad \text{(B-36)}$$

$$c = \frac{18}{(2\sigma + \rho)\,D} \sqrt{\frac{\rho\mu}{\pi}} \tag{B-37}$$

$$d = \frac{2\,(\sigma - \rho)}{2\,\sigma + \rho} \tag{B-38}$$

Equation (B-34) is the most familiar form of the immersed body momentum equation. It should be realized, however, that in this form the application of the equation is generally limited by the original assumptions, as well as the restrictions imposed by equations (B-27) and (B-30).

APPENDIX C

Derivation of Dimensionless Equations for Conservation of Balloon Momentum

As developed in Section 3.1.1 the equations for conservation of balloon momentum in dimensionless form can be written

$$\frac{d\tilde{v}_i}{d\tilde{t}} = 36\left(\frac{\tilde{\rho}}{2+\tilde{\rho}}\right)\tilde{\nu}\ (\tilde{u}_i - \tilde{v}_i) + \frac{3}{2}\left(\frac{\tilde{\rho}}{2+\tilde{\rho}}\right)C_{D\ell}\ (\tilde{u}_i - \tilde{v}_i)\left|\ \vec{\tilde{u}} - \vec{\tilde{v}}\ \right|$$

$$+ 3\left(\frac{\tilde{\rho}}{2+\tilde{\rho}}\right)\frac{D\tilde{u}_i}{D\tilde{t}} + \left(\frac{\tilde{\rho}}{2+\tilde{\rho}}\right)(\tilde{v}_j - \tilde{u}_j)\ \frac{\partial\tilde{u}}{\partial\tilde{x}_j} - \frac{2\ (1-\tilde{\rho})}{2+\tilde{\rho}}\ \tilde{g}\ \delta_{i3}$$

$$- 18\left(\frac{\tilde{\rho}}{2+\tilde{\rho}}\right)\sqrt{\frac{\tilde{\nu}}{\pi}}\int_0^{\tilde{t}} \frac{\frac{d(\tilde{v}_i - \tilde{u}_i)}{d\tilde{t}'}\,d\tilde{t}'}{\sqrt{\tilde{t} - \tilde{t}'}} \qquad \text{(C-1)}$$

Now the density ρ is not a constant but varies with altitude, x_3. For an ideal gas

$$\rho = \frac{p}{RT} \qquad \text{(C-2)}$$

For the case of a constant temperature lapse rate, γ, in a hydrostatic atmosphere,

$$p = p_o\ \left(\frac{T}{T_o}\right)^{\frac{g}{R\gamma}} \qquad \text{(C-3)}$$

A combination of Equations (C-2) and (C-3) produces

$$\rho = \frac{p_o}{RT}\ \left(\frac{T}{T_o}\right)^{\frac{g}{R\gamma}}$$

$$= \frac{p_o}{RT_o}\ \left(\frac{T}{T_o}\right)^{\frac{g}{R\gamma}}$$

$$= \rho_o\left[1 - \frac{\gamma}{T_o}\ \ (x_3 - x_{30})\right]^{\frac{g}{R\gamma}-1} \qquad \text{(C-4)}$$

where x_{30} is the equilibrium altitude at which $\sigma = \rho_o$. If Equation (C-4) is divided by σ the result is

$$\tilde{\rho} = \frac{\rho_o}{\sigma}\left[1 - \frac{\gamma}{T_o}(x_3 - x_{30})\right]^{\frac{g}{R\gamma}-1}$$

$$= \left[1 - \tilde{a}\,\Delta\,\tilde{x}_3\right]^{\tilde{b}-1} \qquad \text{(C-5)}$$

where

$$\tilde{a} = \frac{\gamma D}{T_o}\ . \qquad \text{(C-6)}$$

$$\Delta\tilde{x}_3 = x_3/D - x_{30}/D \qquad \text{(C-7)}$$

$$\tilde{b} = g/(R\gamma) \qquad \text{(C-8)}$$

Now Equation (C-5) can be substituted into Equation (C-1) but the result is quite cumbersome. A term by term examination of the R. H. S. of Equation (C-1) reveals that only in the numerator of the fifth term, representing buoyancy, does the variation of $\tilde{\rho}$ appear significant. If Equation (C-5) is substituted into only this term in Equation (C-1), the result is still awkward because of the nonlinear form of Equation (C-5). To avoid this difficulty, by means of series expansions,

$$(1 - \tilde{a}\ \Delta\tilde{x}_3)^{b-1} = 1 - (\tilde{b} - 1)\ \tilde{a}\ \ \Delta\tilde{x}_3 + O\,(\Delta^2\tilde{x}_3) \qquad \text{(C-9)}$$

Neglecting second order terms,

$$\rho \simeq 1 - (\tilde{b} - 1)\ \tilde{a}\ \Delta\tilde{x}_3 \qquad \text{(C-10)}$$

If Equation (C-10) is substituted into the numerator of the fifth term of the R. H. S. of Equation (C-1), the result is

$$\frac{d\tilde{v}_i}{d\tilde{t}} = 36\left(\frac{\tilde{\rho}}{2+\tilde{\rho}}\right)\tilde{\nu}\;(\tilde{u}_i - \tilde{v}_i) + \frac{3}{2}\left(\frac{\tilde{\rho}}{2+\tilde{\rho}}\right)C_{D\ell}\;(\tilde{u}_i - \tilde{v}_i)\;|\vec{\tilde{u}} - \vec{\tilde{v}}|$$

$$+ 3\left(\frac{\tilde{\rho}}{2+\tilde{\rho}}\right)\frac{D\tilde{u}_i}{D\tilde{t}} + \left(\frac{\tilde{\rho}}{2+\tilde{\rho}}\right)(\tilde{v}_j - \tilde{u}_j)\frac{\partial\tilde{u}_i}{\partial\tilde{x}_j}$$

$$- \frac{2(\tilde{b}-1)\tilde{a}}{2+\tilde{\rho}}\;\Delta\tilde{x}_3\;\tilde{g}\;\delta_{i3} - 18\left(\frac{\tilde{\rho}}{2+\tilde{\rho}}\right)\sqrt{\frac{\tilde{\nu}}{\pi}}\int_o^{\tilde{t}}\frac{\frac{d(\tilde{v}_i - \tilde{u}_i)}{d\tilde{t}'}\,d\tilde{t}'}{\sqrt{\tilde{t} - \tilde{t}'}} \qquad \text{(C-11)}$$

Equation (C-11) represents a dimensionless form of the balloon equations from which certain dimensionless parameters can be obtained. A term by term inspection of the R. H. S. of Equation (C-11) results in the following dimensionless groups:

$$L_1 = \frac{\rho}{2\sigma + \rho} \qquad \text{(C-12)}$$

$$L_2 = \frac{\sigma}{2\sigma + \rho} \qquad \text{(C-13)}$$

$$L_3 = \frac{12\nu}{A\ D} \qquad \text{(C-14)}$$

$$L_4 = \frac{1}{2}\ C_{D\ell} \qquad \text{(C-15)}$$

$$L_5 = \frac{2}{3}\ \frac{g\ (g/R - \gamma\ )\ D^2}{A^2\ T_o} \qquad \text{(C-16)}$$

$$L_6 = 6\ \sqrt{\frac{\nu}{AD}} \qquad \text{(C-17)}$$

In terms of the six preceding dimensionless groups, Equation (C-11) can be written

$$\frac{d\tilde{v}_i}{d\tilde{t}} = 3L_1L_3\ (\tilde{u}_i-\tilde{v}_i) + 3L_1L_4\ (\tilde{u}_i-\tilde{v}_i)|\vec{\tilde{u}}-\vec{\tilde{v}}|$$

$$+ 3L_1 \frac{\mathrm{Đ}\tilde{u}_i}{D\tilde{t}} + L_1(\tilde{v}_j-\tilde{u}_j)\frac{\partial\tilde{u}_i}{\partial x_j} - 3L_2L_5\ \Delta x_3\delta_{i3}$$

$$- 3L_1L_6\int_o^{\tilde{t}} \frac{\frac{d(\tilde{v}_1-\tilde{u}_j)}{d\tilde{t}'}}{\sqrt{\tilde{t}\quad\tilde{t}'}}\ d\tilde{t}' \qquad \text{(C-18)}$$

APPENDIX D

Dimensional Inviscid Flow Field Development

The velocity components are assumed to be of the form

$$u_1 = \bar{u}_1 + A \sin (k_1 x_1 + k_2 x_2 + k_3 x_3 - \omega t + \Theta_1) \quad \text{(D-1)}$$

$$u_2 = B \sin (k_1 x_1 + k_2 x_2 + k_3 x_3 - \omega t + \Theta_2) \quad \text{(D-2)}$$

$$u_3 = C \sin (k_1 x_1 + k_2 x_2 + k_3 x_3 - \omega t + \Theta_3) \quad \text{(D-3)}$$

For brevity let

$$\xi = k_1 x + k_2 y + k_3 z \quad \text{(D-4)}$$

Then

$$\frac{\partial u_1}{\partial x_1} = Ak_1 \cos (\xi - \omega t + \Theta_1) \quad \text{(D-5)}$$

$$\frac{\partial u_2}{\partial x_2} = Bk_2 \cos (\xi - \omega t + \Theta_2) \quad \text{(D-6)}$$

$$\frac{\partial u_3}{\partial x_3} = Ck_3 \cos (\xi - \omega t + \Theta_3) \quad \text{(D-7)}$$

For mass conservation,

$$\frac{\partial u_1}{\partial x_1} + \frac{\partial u_2}{\partial x_2} + \frac{\partial u_3}{\partial x_3} = 0 \quad \text{(D-8)}$$

Thus

$$Ak_1 \cos (\xi - \omega t + \Theta_1) + Bk_2 \cos (\xi - \omega t + \Theta_2) + Ck_3 \cos (\xi - \omega t + \Theta_3) = 0 \quad \text{(D-9)}$$

or

$$Ak_1 \{\cos (\xi - \omega t) \cos \Theta_1 - \sin (\xi - \omega t) \sin \Theta_1\} + Bk_2 \{\cos (\xi - \omega t) \cos \Theta_2 - \sin (\xi - \omega t) \sin \Theta_2\} + Ck_3 \{\cos (\xi - \omega t) \cos \Theta_3 - \sin (\xi - \omega t) \sin \Theta_3\} = 0 \quad \text{(D-10)}$$

To satisfy Equation (D-10), it is necessary for

$$(Ak_1 \cos \Theta_1 + Bk_2 \cos \Theta_2 + Ck_3 \cos \Theta_3) \cos (\xi - \omega t) = 0 \quad \text{(D-11)}$$

and

$$(Ak_1 \sin \Theta_1 + Bk_2 \sin \Theta_2 + Ck_3 \sin \Theta_3) \sin (\xi - \omega t) = 0 \qquad \text{(D-12)}$$

This in turn requires

$$Ak_1 \cos \Theta_1 + Bk_2 \cos \Theta_2 + Ck_3 \cos \Theta_3 = 0 \qquad \text{(D-13)}$$

and

$$Ak_1 \sin \Theta_1 + Bk_2 \sin \Theta_2 + Ck_3 \sin \Theta_3 = 0 \qquad \text{(D-14)}$$

Equation (D-13) can be multiplied by tan Θ_1 to obtain

$$Ak_1 \sin \Theta_1 + Bk_2 \cos \Theta_2 \tan \Theta_1 + Ck_3 \cos \Theta_3 \tan \Theta_1 = 0 \qquad \text{(D-15)}$$

Subtracting (D-15) from (D-14) yields

$$Bk_2 (\sin \Theta_2 - \cos \Theta_2 \tan \Theta_1) + Ck_3 (\sin \Theta_3 - \cos \Theta_3 \tan \Theta_1) = 0 \qquad \text{(D-16)}$$

Solving for B,

$$B = - \frac{Ck_3}{k_2} \frac{(\sin \Theta_3 - \cos \Theta_3 \tan \Theta_1)}{(\sin \Theta_2 - \cos \Theta_2 \tan \Theta_1)} \qquad \text{(D-17)}$$

Next Equation (D-13) can be multiplied by tan Θ_2 to obtain

$$Ak_1 \cos \Theta_1 \tan \Theta_2 + Bk_2 \sin \Theta_2 + Ck_3 \cos \Theta_3 \tan \Theta_2 = 0 \qquad \text{(D-18)}$$

Subtracting (D-18) from (D-14) yields

$$Ak_1 (\sin \Theta_1 - \cos \Theta_1 \tan \Theta_2 + Ck_3 (\sin \Theta_3 - \cos \Theta_3 \tan \Theta_2) = 0 \qquad \text{(D-19)}$$

Solving for A,

$$A = - \frac{Ck_3}{k_1} \frac{(\sin \Theta_3 - \cos \Theta_3 \tan \Theta_2)}{(\sin \Theta_1 - \cos \Theta_1 \tan \Theta_2)} \qquad \text{(D-20)}$$

Thus if Equation (D-17) and (D-20) are satisfied, the inviscid flow field model described in Equations (D-1) through (D-3) satisfies the continuity equation.

Certain other partial derivatives of velocity with respect to space and time can be derived from the model as follows:

$$\frac{\partial u_1}{\partial x_2} = Ak_2 \cos (\xi - \omega t + \Theta_1) \qquad \text{(D-21)}$$

$$\frac{\partial u_1}{\partial x_3} = Ak_3 \cos (\xi - \omega t + \Theta_1) \tag{D-22}$$

$$\frac{\partial u_2}{\partial x_1} = Bk_1 \cos (\xi - \omega t + \Theta_2) \tag{D-23}$$

$$\frac{\partial u_2}{\partial x_3} = Bk_3 \cos (\xi - \omega t + \Theta_2) \tag{D-24}$$

$$\frac{\partial u_3}{\partial x_1} = Ck_1 \cos (\xi - \omega t + \Theta_3) \tag{D-25}$$

$$\frac{\partial u_3}{\partial x_2} = Ck_2 \cos (\xi - \omega t + \Theta_3) \tag{D-26}$$

$$\frac{\partial u_1}{\partial t} = -A\omega \cos (\xi - \omega t + \Theta_1) \tag{D-27}$$

$$\frac{\partial u_2}{\partial t} = -B\omega \cos (\xi - \omega t + \Theta_2) \tag{D-28}$$

$$\frac{\partial u_3}{\partial t} = -C\omega \cos (\xi - \omega t + \Theta_3) \tag{D-29}$$

As formulated the model contains a total of eleven different parameters ($\bar{u}_1$, A, B, C, k_1, k_2, k_3, ω, Θ_1, Θ_2, and Θ_3). As given by Equations (D-17) and (D-20) for conservation of mass, two of the three amplitudes (A, B, and C) must be functions of the third. Thus there are nine independent parameters in Equations (D-1) through (D-3). In the current study, it was not feasible to consider all possible combinations of these nine parameters. The following simplifications were made: First, all wave numbers (k_1, k_2 and k_3) were taken to be equal,

$$k_1 = k_2 = k_3 = k \tag{D-30}$$

Second, by proper choice of the phase angles (Θ_1, Θ_2, and Θ_3) the amplitudes were taken to be equal.

$$A = B = C \tag{D-31}$$

It can be readily shown by means of Equations (D-17) and (D-20) that the phase angles,

$$\Theta_1 = 0 \tag{D-32}$$

$$\Theta_2 = 2\pi/3 \tag{D-33}$$

$$\Theta_3 = -2\pi/3 \tag{D-34}$$

or any similar combination of phase angles set 120° apart, satisfy Equation (D-31).

Based on the simplifications noted, the fluid velocity components can be written as

$$u_i = \bar{u}_1\, \delta_{i1} + A \sin\,(\zeta - \omega t + \Theta_i) \tag{D-35}$$

where

$$\zeta = k\,(x_1 + x_2 + x_3) \tag{D-36}$$

$$\Theta_1 = 0 \tag{D-37}$$

$$\Theta_2 = 2\pi/3 \tag{D-38}$$

$$\Theta_3 = -2\pi/3 \tag{D-39}$$

APPENDIX E

Dimensionless Inviscid Flow Field Development

As developed in Appendix D, the wind velocity components can be expressed as:

$$u_i = \bar{u}_1 \delta_{i1} + A \sin (\zeta - \omega t + \Theta_i) \qquad \text{(E-1)}$$

where

$$\zeta = k (x_1 + x_2 + x_3) \qquad \text{(E-2)}$$

$$\Theta_1 = 0 \qquad \text{(E-3)}$$

$$\Theta_2 = 2\pi/3 \qquad \text{(E-4)}$$

$$\Theta_3 = -2\pi/3 \qquad \text{(E-5)}$$

Based on the nondimensional procedure followed in Appendix C, Equation (E-1) can be written in the following dimensionless form:

$$\tilde{u}_i = \tilde{\bar{u}}_1 \delta_{i1} + \sin (\zeta - \tilde{\omega}\tilde{t} + \Theta_i) \qquad \text{(E-6)}$$

where

$$\tilde{u}_i = u_i/A \qquad \text{(E-7)}$$

$$\tilde{\bar{u}}_1 = \bar{u}_1/A \qquad \text{(E-8)}$$

$$\zeta = \tilde{k} (\tilde{x}_1 + \tilde{x}_2 + \tilde{x}_3) \qquad \text{(E-9)}$$

$$\tilde{\omega} = \omega D/A \qquad \text{(E-10)}$$

$$\tilde{t} = At/D \qquad \text{(E-11)}$$

$$\tilde{k} = kD \qquad \text{(E-12)}$$

$$\tilde{x}_i = x_i/D \qquad \text{(E-13)}$$

Equation (E-6) represents the dimensionless form of the inviscid flow field. Notice should be taken that in dimensionless form the flow field can be described in terms of three dimensionless groups, $\tilde{\tilde{u}}_1$, $\tilde{k}$, and $\tilde{\omega}$. The dimensionless variables $\tilde{x}_i$ and $\tilde{t}$ are not necessary for characterizing the flow field because they represent the coordinates of the balloon in space and time (to be obtained from the solution of the differential equation governing the balloon motion).

APPENDIX F

Reynolds Number Relation to Dimensionless Groups

The Reynolds number for flow past the balloon is defined as:

$$Re = \frac{\rho \, |\vec{u}-\vec{v}| D}{\mu} \tag{F-1}$$

Now, the maximum difference between the wind velocity and the balloon velocity must be roughly equal to the amplitude A in the inviscid flow field model. Thus,

$$\left| \vec{u} - \vec{v} \right| \approx A \tag{F-2}$$

Therefore,

$$Re \approx \frac{\rho \, AD}{\mu} \tag{F-3}$$

An examination of the first dimensionless groups given in Appendix C reveals that to first-order accuracy,

$$Re \approx 12/L_3 \tag{F-4}$$

where

$$L_3 = \frac{12\nu}{AD} \tag{F-5}$$

APPENDIX G

Dimensional Analysis

Dimensional analysis is a standard technique for reducing the number of variables in a problem and for identifying the important parameters associated with the problem. This is particularly useful when one has a physical problem the variables of which are well known but for which no analytic relationship is known. But, it is also useful for determining the necessary nondimensional groups for a given set of analytic relationships describing a physical process.

For the analysis of a balloon in a realistic atmosphere, this analysis is presented as an extension of the development of the nondimensional equations discussed in Appendices C and E. The pertinent variables for the analysis are:

v_i	balloon velocity
x_i	balloon position
u_i	ambient wind velocity
t	elapsed time
ρ	ambient density
μ	dynamic viscosity
g	gravitational acceleration
σ	density of the balloon
D	diameter of the balloon
$C_{D\ell}$	drag coefficient ($10^3 < Re < 10^5$)

The first two variables, v_i and x_i represent the unknown properties of the balloon. These two variables are not independent of each other since v_i is simply the time deviative of x_i. The variable u_i, representing the ambient wind velocity can be expressed as

$$u_i = u_i\ (\bar{u}_1, A, k, \omega) \qquad \text{(G-1)}$$

The ambient density, ρ, can likewise be expressed as

$$\rho = \rho(\rho_o, \gamma, T_o, g, R, x_3) \tag{G-2}$$

The viscosity, μ, can also be expressed as

$$\mu = \mu(\mu_o, \gamma, T_o, x_3) \tag{G-3}$$

Thus there are 16 variables $(v_i, x_i, \bar{u}_1, A, k, \omega, t, \rho_o, \gamma, T_o, R, \mu_o, g, \sigma, D, C_{D\ell})$ involved in the dimensional analysis. The primary dimensions involved are mass (M), length (ℓ), time (t) and temperature (T). The dimensional matrix for this case is as follows:

	v_i	x_i	$\bar{u}_1$	A	k	ω	t	ρ_o	γ	T_o	R	μ_o	g	σ	D	$C_{D\ell}$
M	0	0	0	0	0	0	0	1	0	0	0	1	0	1	0	0
ℓ	1	1	1	1	-1	0	0	-3	-1	0	2	-1	1	-3	1	0
t	-1	0	-1	-1	0	-1	1	0	0	0	-2	-1	-2	0	0	0
T	0	0	0	0	0	0	0	0	1	1	-1	0	0	0	0	0

According to the Buckingham Π theorem, with 16 variables and 4 primary dimensions, there will be a maximum of 12 dimensionless groups. The 12 dimensionless groups take on a variety of forms depending on the choice of primary variables. If A, ρ_o, D and T_o are chosen as the primary variables, then the following dimensionless groups result:

$$\Pi_1 = v_i/A \tag{G-4}$$

$$\Pi_2 = x_i/D \tag{G-5}$$

$$\Pi_3 = \bar{u}_1/A \tag{G-6}$$

$$\Pi_4 = \omega D/A \tag{G-7}$$

$$\Pi_5 = At/D \tag{G-8}$$

$$\Pi_6 = \gamma D/T_o \tag{G-9}$$

$$\Pi_7 = RT_o/A^2 \tag{G-10}$$

$$\Pi_8 = \mu_o/(A\rho_o D) \tag{G-11}$$

$$\Pi_9 = gD/A^2 \tag{G-12}$$

$$\Pi_{10} = \sigma/\rho_o \tag{G-13}$$

$$\Pi_{11} = kD \tag{G-14}$$

$$\Pi_{12} = C_{D\ell} \tag{G-15}$$

Some of the preceding dimensionless groups are identical to or closely resemble the dimensionless groups derived in Appendices C and E of this report. Others, however, are not so easily identified. The relationships between the two sets of dimensionless groups can be developed as follows:

$$\tilde{v}_i = \Pi_1 \text{ (balloon velocity)} \tag{G-16}$$

$$\tilde{x}_i = \Pi_2 \text{ (balloon position)} \tag{G-17}$$

$$\tilde{t} = \Pi_5 \text{ (elapsed time)} \tag{G-18}$$

$$L_1 \cong \frac{1}{2\Pi_{10} + 1} \tag{G-19}$$

$$L_2 \cong \frac{\Pi_{10}}{2\Pi_{10} + 1} \tag{G-20}$$

$$L_3 \cong 12\ \Pi_8 \tag{G-21}$$

$$L_4 \cong \frac{1}{2}\ \Pi_{12} \tag{G-22}$$

$$L_5 \cong \frac{2}{3}\ \Pi_9 \left(\frac{\Pi_9}{\Pi_7} - \Pi_6 \right) \tag{G-23}$$

$$L_6 \cong 6\ \sqrt{\Pi_{8/\pi}} \tag{G-24}$$

$$\tilde{k} = \Pi_{11} \tag{G-25}$$

$$\tilde{\omega} = \Pi_4 \tag{G-26}$$

$$\tilde{\tilde{u}}_1 = \Pi_3 \tag{G-27}$$

The use of the approximate equalities in Equations (G-19) through (G-22) and in Equation (G-24) reflects the fact that L_1 through L_4 and L_6 contain the variables ρ and μ while Π_8, Π_{10} and Π_{11} contain their equilibrium counterparts ρ_o and μ_o. An examination of Equations (G-16) through (G-27) reveals that all 12 dimensionless groups (Π_1 through Π_{12}) appear in the definitions of the dimensionless terms which arise in the dimensionless differential equation for balloon motion and the dimensionless inviscid flow field model. Furthermore, as previously noted, $\tilde{v}_i$ and $\tilde{x}_i$ (Π_1 and Π_2) are not independent of each other but represent the solution of the differential equation for the balloon equation. The variable $\tilde{t}$ (Π_5) is obviously dimensionless time, with respect to which both $\tilde{x}_i$ and $\tilde{v}_i$ can be expressed. The remaining eight dimensionless groups can be reduced to five if the ratio ρ/σ is taken as unity and if C_D is taken as constant.* Thus, with this simplification the entire problem can be characterized in terms of five dimensionless groups:

$$\frac{12\nu}{AD},\ \frac{2\ g(g/R-\gamma)D^2}{3A^2\ T_o},\ kD,\ \frac{\omega D}{A}\ ,\ \text{and}\ \ \frac{\bar{u}_1}{A}\ .$$

The solution in terms of dimensionless balloon position (x_i/D) and velocity (v_i/A) as functions dimensionless time (At/D) should remain unchanged (to first-order accuracy) provided these five groups remain constant.

---

* This reduction from eight to five dimensionless groups is possible in part, because of the manner in which Π_6, Π_7, Π_8, Π_9, and Π_{11} occur in the governing equations.

APPENDIX H

First Order Perturbation Analysis of Constant-Volume Balloon Motion in Turbulent Flow

The problem under consideration is a constant-volume balloon floating in a two-dimensional turbulent flow field with stationary turbulence which is homogeneous in the x-direction. The coordinate system is shown in Figure H-1.

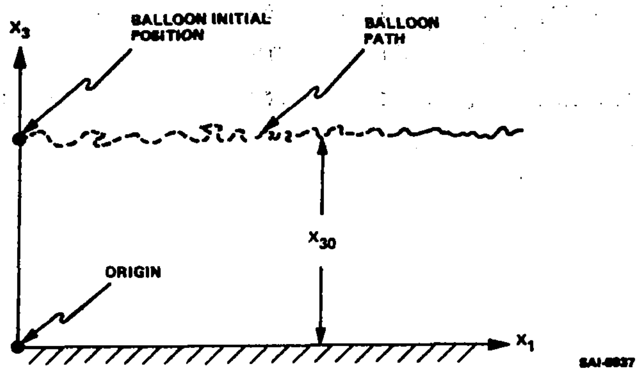

Figure H-1. Coordinate System for First-Order Perturbation Analysis

The longitudinal component of the wind velocity can be expressed as

$$u_1\ (x_1,t,x_3) = u_1\ (x_3) + u_1'\ (x_1,t,x_3) \tag{H-1}$$

The fluctuating portion of the longitudinal component can be expressed in terms of a Fourier integral,

$$u_1'\ (x_1,t,x_3) = \int_{-\infty}^{\infty}\int_{-\infty}^{\infty} B\ (k,\omega;x_3)e^{\ i\ (kx_1-\omega t)}dk\ d\omega \tag{H-2}$$

The coordinates of the CVB are functions of both time and the initial balloon position. Because the turbulence is homogeneous in the x-direction and the mean wind velocity is assumed to be constant with respect to x_1 and t, only the x_3-coordinate of the initial position is significant. Thus

$$(\text{Balloon Coordinates}) = \left[X_1(t,X_{30}),X_3(t,X_{30})\right] \tag{H-3}$$

The horizontal component of the balloon velocity can be written as

$$v_1(t,X_{30}) = \frac{\partial X_1}{\partial t} = u_1\left[X_1(t,X_{30}),t,X_3(t,X_{30})\right] \tag{H-4}$$

Equating the horizontal component of the balloon velocity to the corresponding wind velocity component at the balloon location is based on the assumption that the balloon responds perfectly to the wind velocity in the horizontal direction.

The vertical component of balloon velocity can be written:

$$v_3(t,X_{30}) = \frac{\partial X_3}{\partial t} \tag{H-5}$$

Notice should be taken that v_3 cannot be set equal to vertical component of the wind velocity, u_3, because a constant-volume balloon cannot be perfectly responsive in the vertical direction.

The balloon coordinates can be written as:

$$\begin{aligned} X_1\ (t,X_{30}) &= \int_o^t v_1\ (t,X_{30})\ dt \\ &= \bar{u}_1\ (X_{30})\ t + \int_o^t u_i'\ (X_1,t,X_3)\ dt \\ &= \bar{X}_1\ (X_{30},t) + X_1'(t,X_{30}) \end{aligned} \tag{H-6}$$

and

$$\begin{aligned} X_3\ (t,X_{30}) &= \int_o^t v_3\ (t,X_{30})\ dt + X_{30} \\ &= X_3'\ (t,X_{30}) + X_{30} \end{aligned} \tag{H-7}$$

The fluctuating portion of the longitudinal component of the balloon velocity, v_1', can be expressed in terms of a Fourier integral analogous to that for the wind velocity component, u_1'. Thus:

$$v_1'\ (t,X_{30}) = v_1\ (t,X_{30}) - \bar{u}_1\ (X_3)$$

$$= \int_{-\infty}^{\infty}\int_{-\infty}^{\infty} B\ (k,\omega;X_3)e^{\,i\left[k(\bar{X}_1 + X_1')-\omega t\right]}\,dkd\omega \tag{H-8}$$

Expansion of $B(k,\omega;X_3)$ in a Taylor series about X_{30} yields

$$B(k,\omega;X_3) = B(k,\omega;X_{30}) + \frac{\partial B}{\partial Z}(X_3-X_{30}) + \frac{1}{2}\frac{\partial^2 B}{\partial Z^2}(X_3-X_{30})^2 + \ldots$$

$$= B(k,\omega;X_{30}) + \frac{\partial B}{\partial Z} X_3' + \frac{1}{2}\frac{\partial^2 B}{\partial Z^2}(X_3')^2 + \ldots \qquad \text{(H-9)}$$

Likewise the exponential series for $e^{ikX_1'}$ can be written

$$e^{ikX_1'} = 1 + ik X_1' - \frac{1}{2}(k X_1')^2 + \ldots \qquad \text{(H-10)}$$

A combination of Equations (H-8) through (H-10) yields

$$v_1'(t,X_{30}) = \int_{-\infty}^{\infty}\int_{-\infty}^{\infty}\left[B(k,\omega;X_{30}) + \frac{\partial B}{\partial Z}X_3' + \frac{1}{2}\frac{\partial^2 B}{\partial Z^2}(X_3')^2 + \ldots\right]\left[1 + ikX_1' - \frac{1}{2}(kX_1')^2 + \ldots\right] e^{i(k\bar{X}_1 - \omega t)}\, dk\, d\omega \qquad \text{(H-11)}$$

To first-order accuracy*

$$v_1'(t,X_{30}) = \int_{-\infty}^{\infty}\int_{-\infty}^{\infty} B(k,\omega;X_{30})\, e^{i(k\bar{X}_1-\omega t)} dk\, d\omega \qquad \text{(H-12)}$$

In similar fashion the velocity component $v_1'(t+\tau, X_{30})$ can be expressed to first-order accuracy as

$$v_1'(t+\tau,X_{30}) = \int_{-\infty}^{\infty}\int_{-\infty}^{\infty} B(k,\omega;X_{30})\, e^{i[k(\bar{X}_1+\bar{u}_1\tau) - \omega(t+\tau)]}\, dk\, d\omega \qquad \text{(H-13)}$$

Because v_1' is real, the Fourier integral representation for $v_1'(t+\tau,X_{30})$ can be written as

$$v_1'(t+\tau,X_{30}) = \int_{-\infty}^{\infty}\int_{-\infty}^{\infty} B^*(k,\omega;X_{30})e^{-i[k(\bar{X}_1+\bar{u}_1\tau) - \omega(t+\tau)]} dk\, d\omega \qquad \text{(H-14)}$$

* The first term in the series expansion of $B(k,\omega;Z)$ is first-order because $B(k,\omega;Z)$ itself represents a perturbation and is first-order. Thus the only first-order term in the product, $B(k,\omega;Z)e^{ikX_1'}$ is the product of the first terms of the two series.

The product $v_1'(t,X_{30})\, v_1'(t+\tau,X_{30})$ can be expressed as

$$v_1'(t,X_{30})\, v_1'(t+\tau,X_{30})$$
$$= \int_{-\infty}^{\infty}\int_{-\infty}^{\infty}\int_{-\infty}^{\infty}\int_{-\infty}^{\infty} B(k',\omega';X_{30})\, B^*(k,\omega;X_{30})\, e^{i(k'\bar{X}_1-\omega' t)}$$
$$e^{-i\,[k(\bar{X}_1+\bar{u}_1\,\tau)\,-\,\omega(t+\tau)]}\, dk'd\omega'dk\, d\omega \qquad \text{(H-15)}$$

Equation (H-15) holds for each realization of the ensemble. Thus the ensemble average representing the quasi-Lagrangian time auto-correlation function, can be written as

$$\langle v_1'\,(t,X_{30})\, v_1'\,(t+\tau,X_{30})\rangle$$
$$= \int_{-\infty}^{\infty}\int_{-\infty}^{\infty}\int_{-\infty}^{\infty}\int_{-\infty}^{\infty} \langle B(k',\omega';X_{30})\, B^*\,(k,\omega;X_{30})\rangle$$
$$e^{-i\,[\bar{X}_1(k'-k)-t(\omega'-\omega)]}\, e^{-i(k\,\bar{u}_1\,\tau-\,\omega\tau)}\, dk'd\omega'dk\, d\omega \qquad \text{(H-16)}$$

A more useful form of Equation (H-16) can be obtained by the following change of variables:

$$\left.\begin{aligned} k'' &= k - k' \\ \omega'' &= \omega - \omega' \end{aligned}\right\} \longrightarrow \left\{\begin{aligned} k' &= k - k'' \\ \omega' &= \omega - \omega'' \end{aligned}\right. \qquad \text{(H-17)}$$

Introduction of k'' and ω'' in Equation (H-16) produces

$$v_1'(t,X_{30})\, v_1'\,(t+\tau,X_{30})$$
$$= \int_{-\infty}^{\infty}\int_{-\infty}^{\infty}\int_{-\infty}^{\infty}\int_{-\infty}^{\infty} \langle B(k-k'',\omega-\omega'';X_{30})\, B^*(k,\omega;X_{30})\rangle$$
$$e^{-i(k''\bar{X}_1\,-\,\omega'' t)}\, e^{-i(k\bar{u}_1\,\tau-\omega\tau)}\, dk''d\omega''dk\, d\omega \qquad \text{(H-18)}$$

The general Eulerian space-time power spectrum, $\phi_E(k,\omega,x_1,t;x_3)$, of the horizontal wind velocity $u_1'(x_1,t,x_3)$ by definition is:

$$\phi_E(k,\omega,x_1,t;x_3) = \int_{-\infty}^{\infty}\int_{-\infty}^{\infty} \langle B(k-k'',\omega-\omega'';x_3)\, B^*(k,\omega;x_3)\rangle \, e^{i(k''x_1-\omega''t)}\, dk''d\omega'' \qquad \text{(H-19)}$$

At the balloon coordinates $(\bar{X}_1, X_{30})$ the general power spectrum of the wind velocity component $u_i(\bar{X}_1,t,X_{30})$ would be

$$\phi_E(k,\omega,\bar{X}_1,t;X_{30}) = \int_{-\infty}^{\infty}\int_{-\infty}^{\infty} \langle B(k-k'',\omega-\omega'';X_{30})\, B^*(k,\omega;X_{30})\rangle \, e^{i(k''\bar{X}_1 - \omega''t)}\, dk''d\omega'' \qquad \text{(H-20)}$$

For the case under consideration the turbulence is homogeneous in the x_1-direction and stationary, and thus the corresponding Eulerian space-time power spectrum is not a function of $\bar{X}_1$ or t. For such a case,

$$\phi_E(k,\omega,\bar{X}_1,t;X_{30}) \longrightarrow \phi_E(k,\omega;X_{30}) \qquad \text{(H-21)}$$

A combination of Equations (H-20) and (H-21) produces

$$\phi_E(k,\omega;X_{30}) = \int_{-\infty}^{\infty}\int_{-\infty}^{\infty} \langle B(k-k'',\omega-\omega'';X_{30})\, B^*(k,\omega;X_{30})\rangle \, e^{i(k''\bar{X}_1 - \omega''t)}\, dk''d\omega'' \qquad \text{(H-22)}$$

In order for the RHS of Equation (H-22) to be consistent with the LHS

$$\langle B(k-k'',\omega-\omega'';X_{30})\; B^*(k,\omega;X_{30})\rangle = F(k,\omega;X_{30})\,\delta(k'')\,\delta(\omega'') \qquad \text{(H-23)}$$

where

$$F(k,\omega;X_{30}) \propto \langle B(k,\omega;X_{30})\; B^*(k,\omega;X_{30})\rangle \qquad \text{(H-24)}$$

A combination of Equations (H-22) through (H-24) yields

$$\phi_E (k,\omega;X_{30}) = \int_{-\infty}^{\infty}\int_{-\infty}^{\infty} F (k,\omega;X_{30}) \quad \delta(k'') \; \delta(\omega'') \; e^{\,i(k''\bar{X}_1 - \omega''t)} \; dk''d\omega'' = F (k,\omega; X_{30}) \tag{H-25}$$

and

$$\phi_E (k,\omega;X_{30}) \propto \; < B (k,\omega;X_{30}) \; B^* (k,\omega;X_{30}) > \tag{H-26}$$

The quasi-Lagrangian time auto correlation for stationary turbulence with homogeneity in the x-direction can be developed by a combination of Equations (H-18),(H-23) and (H-25) as follows:

$$< v_1' (t;X_{30}) \; v_1' (t + \tau;X_{30}) > \; = \int_{-\infty}^{\infty}\int_{-\infty}^{\infty} \phi_E (k,\omega;X_{30}) \; e^{-i (k\bar{u}_1 - \omega)\tau} \; dk \; d\omega \tag{H-27}$$

The LHS of Equation (H-27) must be independent of time because, due to stationarity the RHS is not a function of time. Thus,

$$< v_1' (t;X_{30}) \; v_1' \; (t + \tau;X_{30}) > \; \longrightarrow \; H_L (\tau,X_{30}) \tag{H-28}$$

Thus the quasi-Lagrangian time auto correlation function for stationary turbulence, with x_1-direction homogeneity, can be expressed as:

$$H_L (\tau;X_{30}) = \int_{-\infty}^{\infty}\int_{-\infty}^{\infty} \phi_E (k,\omega;X_{30}) \; e^{-i(k\bar{u}_1 - \omega)\tau} \; dk \; d\omega \tag{H-29}$$

Equation (H-29) can be cast in a more convenient form by means of a coordinate transformation where

$$\left.\begin{aligned} K &= k \\ \Omega &= k\bar{u}_1 - \omega \end{aligned}\right\} \tag{H-30}$$

The quantity $(-\Omega)$ is the doppler frequency observed in a coordinate system moving with a velocity $\bar{u}_1$. In K,Ω - space Equation (H-29) becomes

$$H_L(\tau;X_{30}) = \int_{-\infty}^{\infty}\int_{+\infty}^{-\infty} \phi_E(K,K\bar{u}_1 - \Omega;X_{30})\, e^{-i\Omega\tau} \begin{vmatrix} \frac{\partial k}{\partial K} & \frac{\partial k}{\partial \Omega} \\ \frac{\partial \omega}{\partial K} & \frac{\partial \omega}{\partial \Omega} \end{vmatrix} dK\, d\Omega$$

$$= \int_{-\infty}^{\infty}\int_{+\infty}^{-\infty} \phi_E(K, K\bar{u}_1 - \Omega;X_{30})\, e^{-i\Omega\tau} \begin{vmatrix} 1 & 0 \\ \bar{u}_1 & -1 \end{vmatrix} dK\, d\Omega$$

$$= \int_{-\infty}^{\infty}\int_{-\infty}^{\infty} \phi_E(K,K\bar{u}_1 - \Omega;X_{30})\, e^{-i\Omega\tau}\, dK\, d\Omega \qquad \text{(H-31)}$$

At the same time, based on generalized Fourier integral theory,

$$H_L(\tau;X_{30}) = \int_{-\infty}^{\infty} \Psi_L(\Omega;X_{30})\, e^{-i\Omega\tau}\, d\Omega \qquad \text{(H-32)}$$

where $\Psi(\Omega;X_{30})$ is the quasi-Lagrangian time power spectrum. Thus by comparison of Equations (H-31) and (H-32),

$$\Psi_L(\Omega,X_{30}) = \int_{-\infty}^{\infty} \phi_E(K, K\bar{u}_1 - \Omega;X_{30})\, d K \qquad \text{(H-33)}$$

Notice should be taken that Equation (H-31) represents a relationship between the quasi-Lagrangian time auto correlation function and the Eulerian space-time power spectrum for stationary turbulence with x-direction homogeneity, while Equation (H-33) relates the quasi-Lagrangian time power spectrum with the same Eulerian space-time power spectrum. Both relations are based on first-order perturbation theory.

The true significance of Equations (H-31) and (H-33) can be ascertained by applying them to certain situations involving both nondispersive and dispersive media. First, in a nondispersive media Taylor's hypothesis holds and thus,

$$\omega = k \bar{u}_1 \tag{H-34}$$

or

$$\Omega = 0 \tag{H-35}$$

For this case Equation (H-33) becomes

$$\Psi_{L(TAYLOR)}(\Omega, X_{30}) = \int_{-\infty}^{\infty} \Phi_{E(TAYLOR)}(K, K\bar{u}_1 - \Omega; X_{30})\, dK$$

$$= \int_{-\infty}^{\infty} \Phi_{E(TAYLOR)}(K; X_{30})\ \delta(\Omega)\, dK$$

$$= \delta(\Omega) \int_{-\infty}^{\infty} \Phi_{E(TAYLOR)}(K; X_{30})\, dK \tag{H-36}$$

where $\Phi_E\ (K, X_{30})$ is the Eulerian space power spectrum Equation (H-36) indicates that the quasi-Lagrangian time spectrum based on Taylor's hypothesis is simply a spike at $\Omega = 0$. A combination of Equations (H-31) and (H-36) yields

$$H_{L(TAYLOR)}(\tau, X_{30}) = \int_{-\infty}^{\infty} \delta(\Omega) \int_{-\infty}^{\infty} \Phi_{E(TAYLOR)}(K;\ X_{30})\, dK e^{-i\Omega\tau}\, d\Omega$$

$$= \int_{-\infty}^{\infty} \Phi_{E(TAYLOR)}(K_i\ X_{30})\, dK \tag{H-37}$$

Notice should be taken that the RHS of Equation (H-37) is independent of τ. Thus the quasi-Lagrangian time auto correlation function is independent of τ and

$$H_{L(TAYLOR)}(\tau,\ X_{30}) = H_{L(TAYLOR)}(X_{30}) \tag{H-38}$$

Equation (H-38) combined with Equation (H-28) indicates that

$$H_{L(TAYLOR)}(X_{30}) = \langle v_1'\ (X_{30})\ v_1'\ (X_{30}) \rangle$$

$$= \sigma^2_{v_1}\ (X_{30}) \tag{H-39}$$

Based on Equation (H-39) the quasi-Lagrangian time auto correlation function (for the case of Taylor's Hypothesis), for the balloon velocity component $v_1'(t,X_{30})$, equals the variance of the same velocity component. The latter in turn equals the variance of the x_T-component of the wind velocity. These relations are based on the first-order perturbation analysis with the assumption of a perfectly responsive balloon (in the x-direction) with stationary turbulence which is homogeneous in the x-direction.

For the case of a dispersive media, Taylor's hypothesis does not hold. Instead

$$\omega = \bar{u}_1 \, k + F(k) \tag{H-40}$$

or

$$\Omega = -F(K) \tag{H-41}$$

The inverse of Equation (H-41) proves more useful and can be written

$$K = f(\Omega) \tag{H-42}$$

A combination of Equations (H-33) and (H-42) yields

$$\begin{aligned}
\Psi_{L(\text{DISPERSIVE})}(\Omega;X_{30}) &= \int_{-\infty}^{\infty} \Phi_{E(\text{DISPERSIVE})}(K,K\bar{u}_1-\Omega;X_{30})\,dK \\
&= \int_{-\infty}^{\infty} \Phi_{E(\text{DISPERSIVE})}(K;X_{30})\,\delta\left[f(\Omega)-K\right]\,dK \\
&= \Phi_{E(\text{DISPERSIVE})}\left[f(\Omega);X_{30}\right]
\end{aligned} \tag{H-43}$$

Thus in a dispersive media the quasi-Lagrangian time power spectrum can be related to the corresponding Eulerian spatial power spectrum if the function $f(\Omega)$ is known. Furthermore, the quasi-Lagrangian time auto correlation function can be related to the same Eulerian spatial power spectrum by a conbination of Equations (H-32) and (H-43) as follows:

$$H_L(\tau;X_{30}) = \int_{-\infty}^{\infty} \Phi_{E(\text{DISPERSIVE})}\left[f(\Omega);X_{30}\right] e^{-i\Omega\tau}\,d\Omega \tag{H-44}$$

For dispersive Rossby waves the phase velocity c is given by the relation

$$c = \bar{u}_1 - \beta/k^2 \tag{H-45}$$

By definition

$$c = \omega/k \tag{H-46}$$

and thus

$$\omega = \bar{u}_1 k - \beta/k \tag{H-47}$$

or

$$\Omega = \beta/k \tag{H-48}$$

Thus for a Rossby wave, based on Equation (H-42) and (H-48),

$$f_{(ROSSBY)}(\Omega) = \beta/\Omega \tag{H-49}$$

Then

$$\Psi_{L\,(ROSSBY)}(\Omega;X_{30}) = \Phi_{E(ROSSBY)}(\beta/\Omega;X_{30}) \tag{H-50}$$

The relation between $\Phi_{E(ROSSBY)}(K_i\ X_{30})$ and K is known to be of the form

$$\Phi_{E(ROSSBY)}(K;X_{30}) \propto K^{P_1} \tag{H-51}$$

where

$$P_1 < 0$$

Therefore

$$\Psi_{L(ROSSBY)}(\Omega,X_{30}) \propto \Omega^{-P_1} \tag{H-52}$$

For dispersive gravity waves,

$$\omega = \bar{u}_1 k \pm \sqrt{gk} \tag{H-53}$$

or

$$\Omega = \mp \sqrt{gk} \tag{H-54}$$

Thus, based on Equation (H-42) and (H-54),

$$f_{(GRAVITY)}(\Omega) = \Omega^2/g \tag{H-55}$$

In this case

$$\Psi_{L(GRAVITY)}(\Omega;X_{30}) = \Phi_{E(GRAVITY)}(\Omega^2/g,X_{30}) \tag{H-56}$$

The relation between $\Phi_{E(GRAVITY)}(K,X_{30})$ and K is of the form

$$\Phi_{E(GRAVITY)}(K,X_{30}) \propto K^{P_2} \tag{H-57}$$

where

$$P_2 < 0$$

Therefore

$$\Psi_{L(GRAVITY)}(\Omega,X_{30}) \propto \Omega^{2P_2} \tag{H-58}$$

Rossby waves possess long wave lengths and thus small wave numbers while gravity waves have relatively short wave lengths and hence larger wave numbers. A plot of $\Phi_E(K;X_{30})$ for these two types of waves is given in Figure H-2. The corresponding plot of $\Psi_L(\Omega;X_{30})$ is shown in Figure H-3.

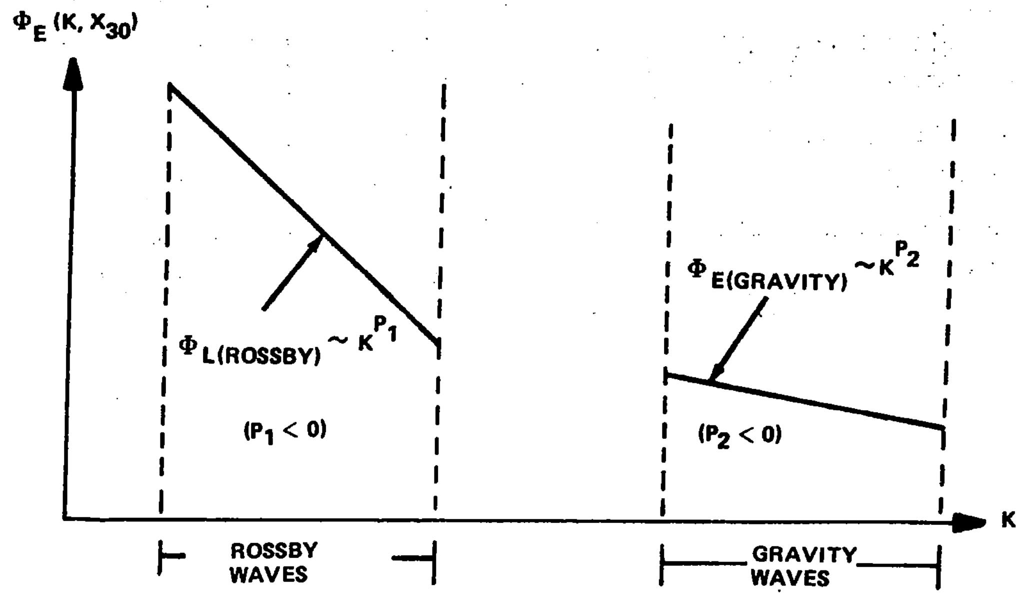

Figure H-2. Eulerian Space Power Spectra for Rossby and Gravity Waves

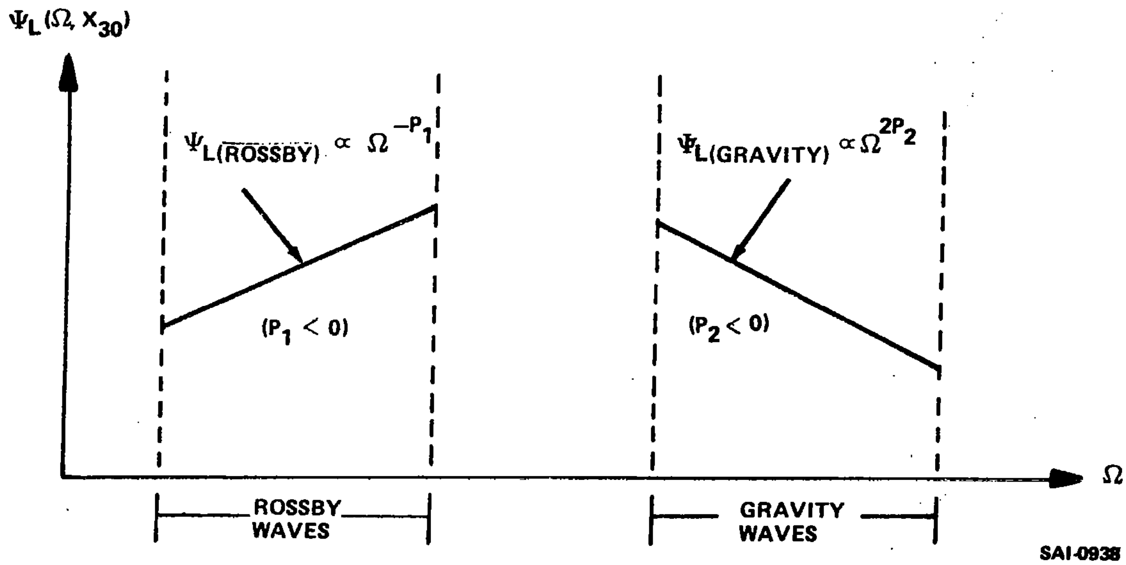

Figure H-3. Lagrangian Time Power Spectra for Rossby and Gravity Waves

APPENDIX I

NOTES ON SPACE-TIME SPECTRUM ϕ_E (k, ω; X_{30})

The function ϕ_E (k, ω; X_{30}) represents the Eulerian Space-time spectral density at altitude X_{30} of turbulent eddy with wave number k and frequency ω. If no relation between k and ω exist, the general variation of ϕ with k and ω might be pictured as shown in Figure I-1.

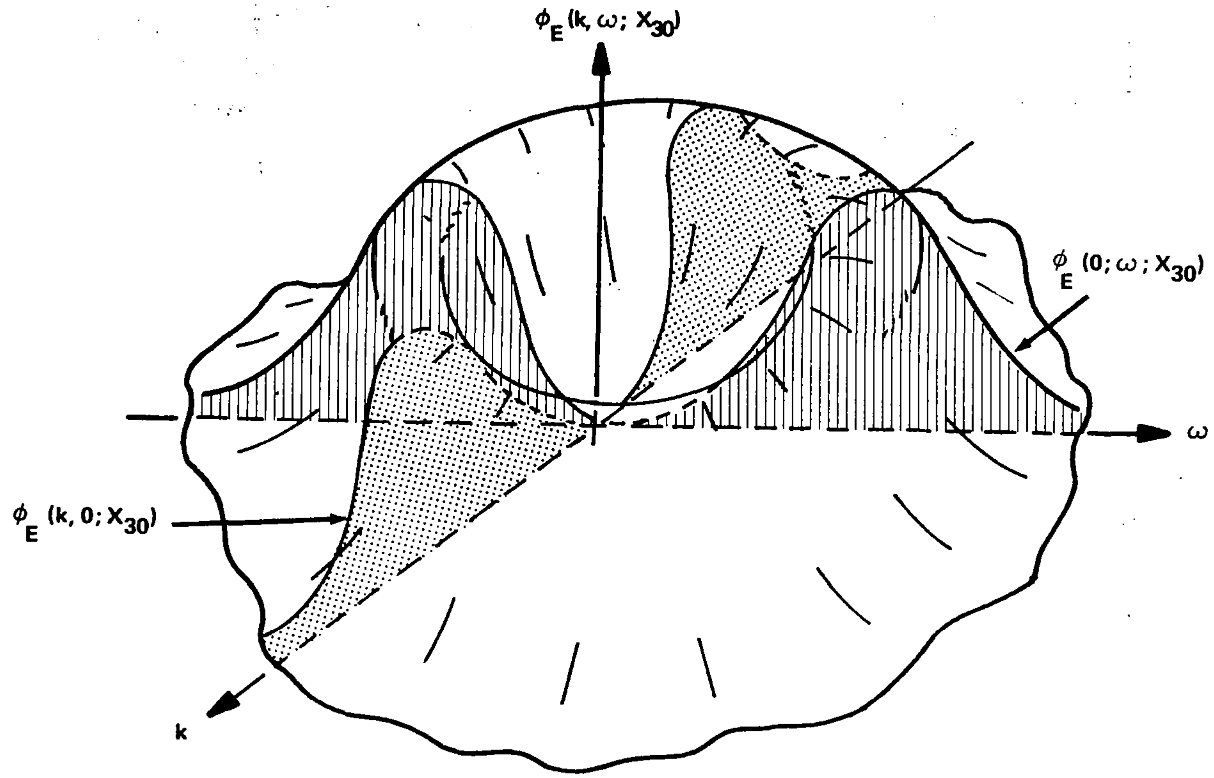

Figure I-1. General Eulerian Space-Time Power Spectrum

If, however, k and ω are related according to Taylor's hypothesis,

$$\omega = k\bar{u}_1 \tag{I-1}$$

$\phi_{E(TAYLOR)}$, as a function of k and ω, appears as shown in Figure I-2.

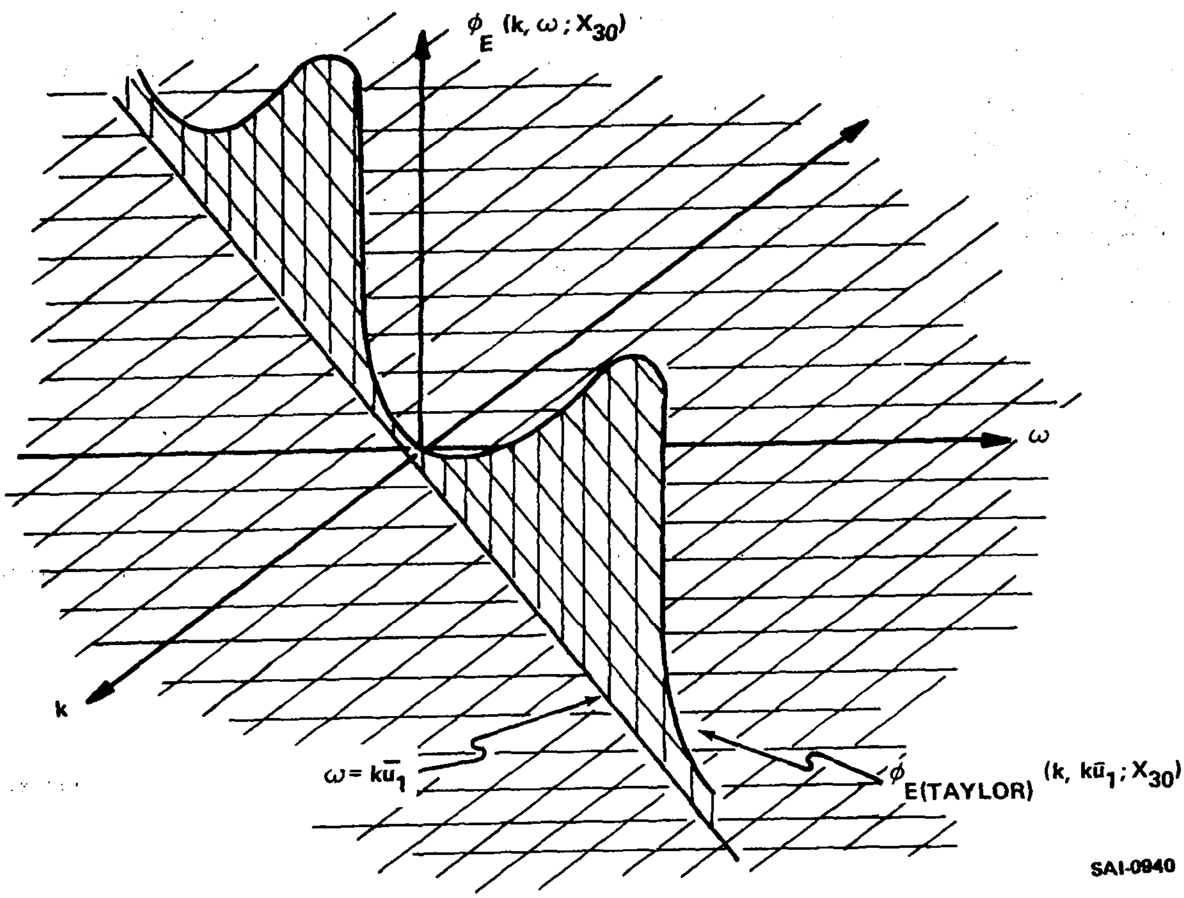

Figure I-2. Eulerian Space-Time Power Spectrum According to Taylor's Hypothesis

Notice should be taken that, with increasing $\bar{u}_1$, the plane containing $\phi_{E(TAYLOR)}(k, k\bar{u}_1; X_{30})$ rotates CCW.

For the case of dispersive media,

$$\omega = k\bar{u}_1 + F(k) \tag{I-2}$$

For this case, ϕ_E as a function of k and ω appears as shown in Figure I-3.

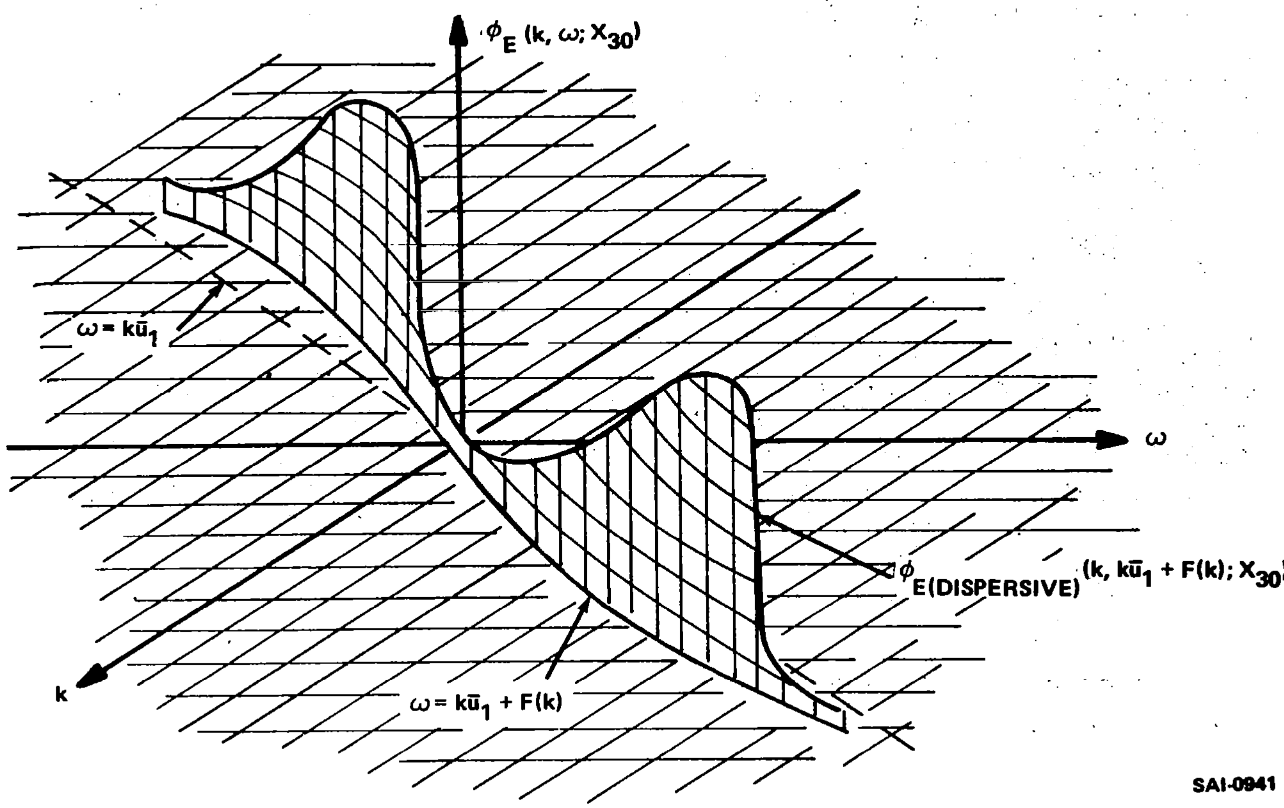

Figure I-3. Eulerian Space-Time Power Spectrum for Dispersive Media

The preceding figure represents the general concept of the spectral density function for a dispersive media. Two specific examples are useful. For a Rossby wave,

$$\omega = k\bar{u}_1 - \frac{\beta}{k} \qquad \text{(I-3)}$$

Although Rossby waves are limited to relatively low frequencies and thus low wave numbers, it is beneficial to picture the variation of $\phi_{E\,(ROSSBY)}$ with k and ω over a wide range of values of k and ω as shown in Figure I-4.

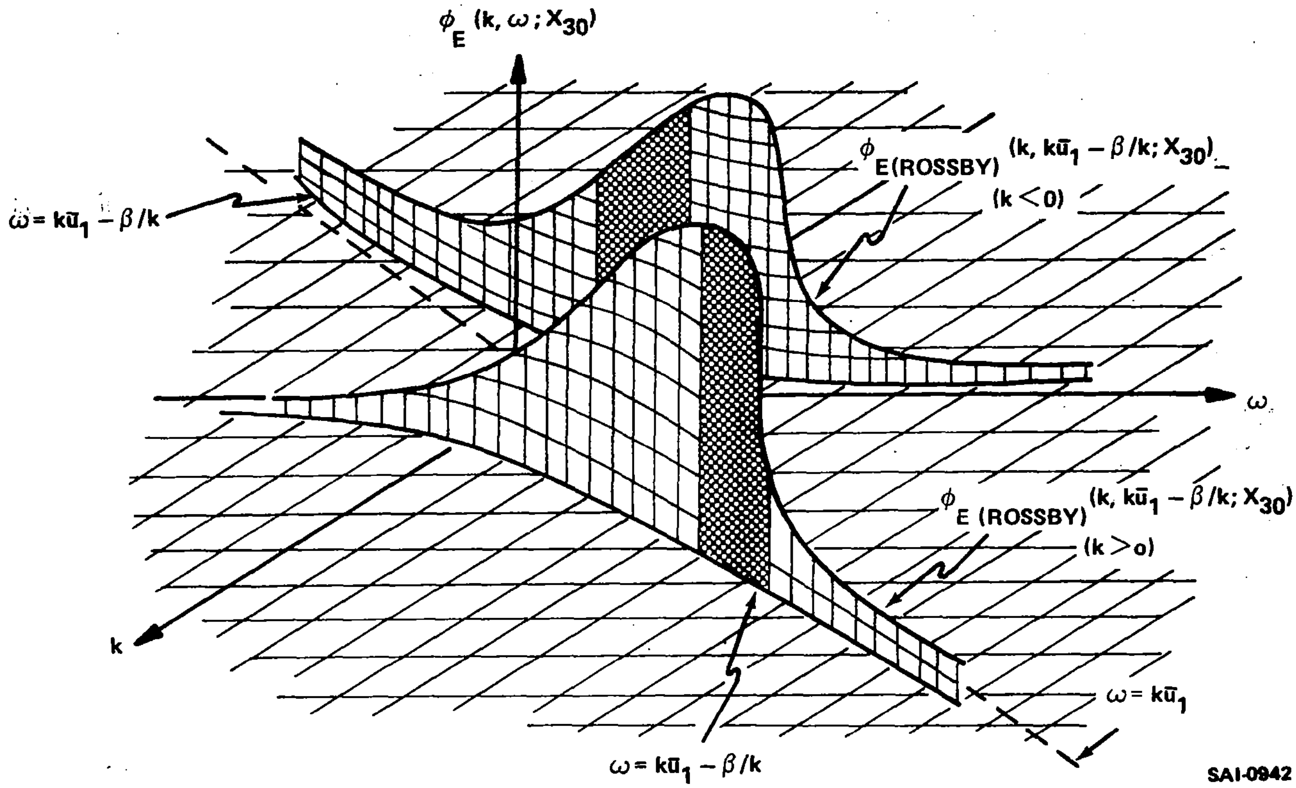

Figure I-4. Eulerian Space-Time Power Spectrum for Rossby Waves

Notice should be taken in the preceding figure that the heavily shaded portion of the plots of $\phi_{E\,(ROSSBY)}(k,\ k\bar{u}_1 - \beta/k;\ X_{30})$ represents the regions where Rossby waves would most likely be present.

For gravity waves

$$\omega = \bar{u}_1 k \pm \sqrt{gk} \tag{I-4}$$

Gravity waves normally occur at relatively high values of k, but as before it is beneficial to plot the curve over a range of values of both k and ω. The result is as shown in Figure I-5.

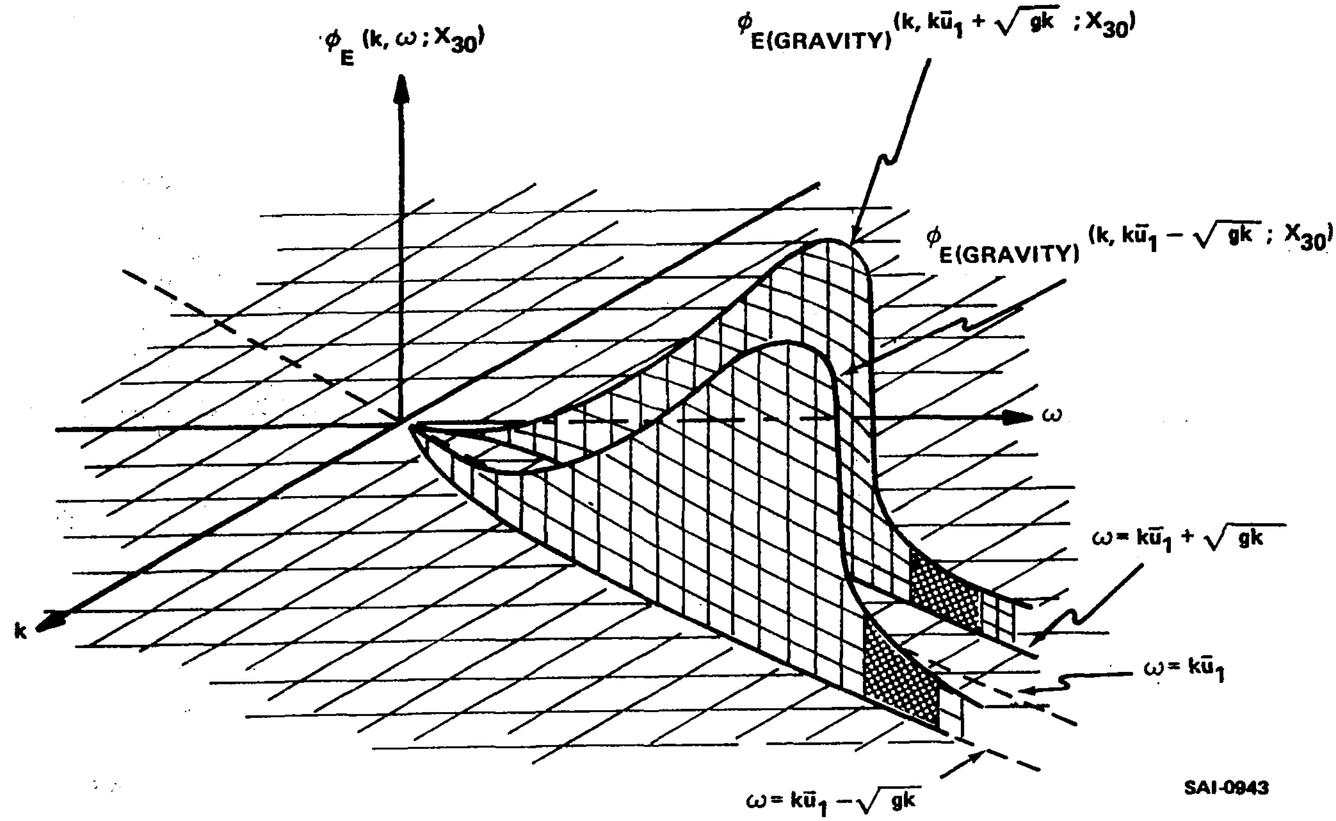

Figure I-5. Eulerian Space-Time Power Spectrum for Gravity Waves

As before the more heavily shaded portions of the plot indicates the part of the spectrum in which gravity waves most likely will occur.

APPENDIX J

Notes on Space-Time Spectrum ψ_L (K, Ω; X_{30})

It is desirable to introduce a two-dimensional space-time spectrum ψ_L (K, Ω; X_{30}) which satisfies the relation

$$\Psi_L (\Omega; X_{30}) = \int_{\infty}^{\infty} \psi_L (K, \Omega : X_{30}) \, dK \qquad \text{(J-1)}$$

The function ψ_L (K,$-\Omega$; X_{30}) is the counterpart of ϕ_E (k, ω; X_{30}). Each of the five figures given in Appendix I could be redrawn to represent ψ_L (K, Ω; X_{30}) as a function of K, Ω. For the sake of brevity only the three specific cases, illustrated by Figures I-2, I-4 and I-5, will be developed.

For the case involving Taylor's hypothesis,

$$\Omega = 0 \qquad \text{(J-2)}$$

ψ_L as a function of K and Ω is shown in Figure J-1.

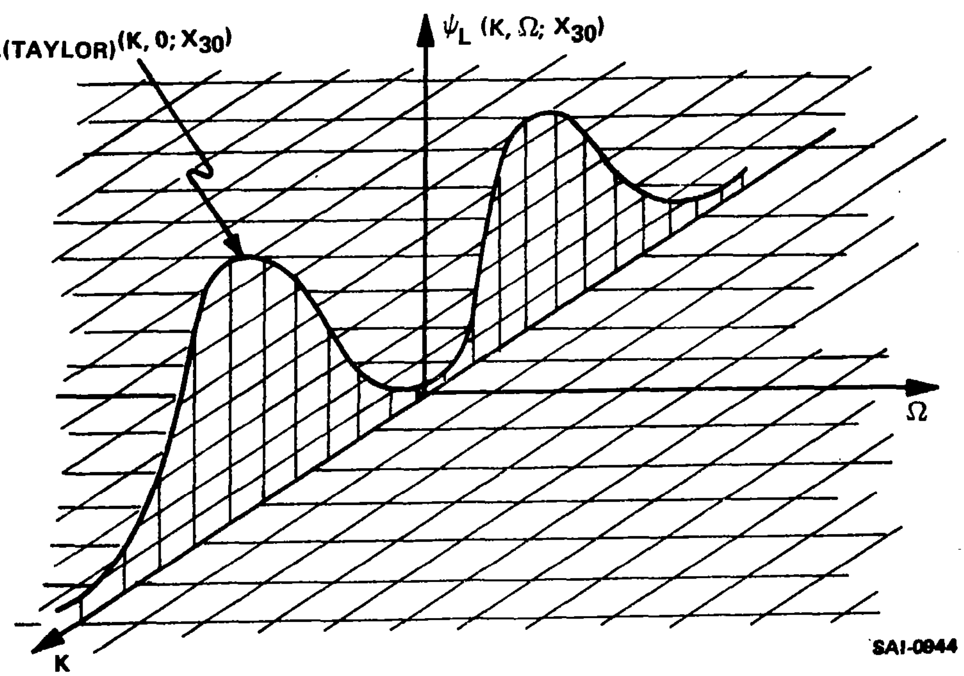

Figure J-1. Lagrangian Space-Time Power Spectrum According to Taylor's Hypothesis

A comparison of Figures I-2 and J-1 reveals that as $\tilde{u}_1$ approaches zero, $\psi_{L(TAYLOR)}(K, -\Omega; X_{30})$ approaches $\phi_{E(TAYLOR)}(k, \omega; X_{30})$.

For the case involving the Rossby wave,

$$\Omega = \beta/K \tag{J-3}$$

or

$$K = \beta/\Omega \tag{J-4}$$

The variation of $\psi_{L(ROSSBY)}(K, \Omega ; X_{30})$ with K and Ω is shown in Figure J-2. As before the more heavily shaded regions indicate

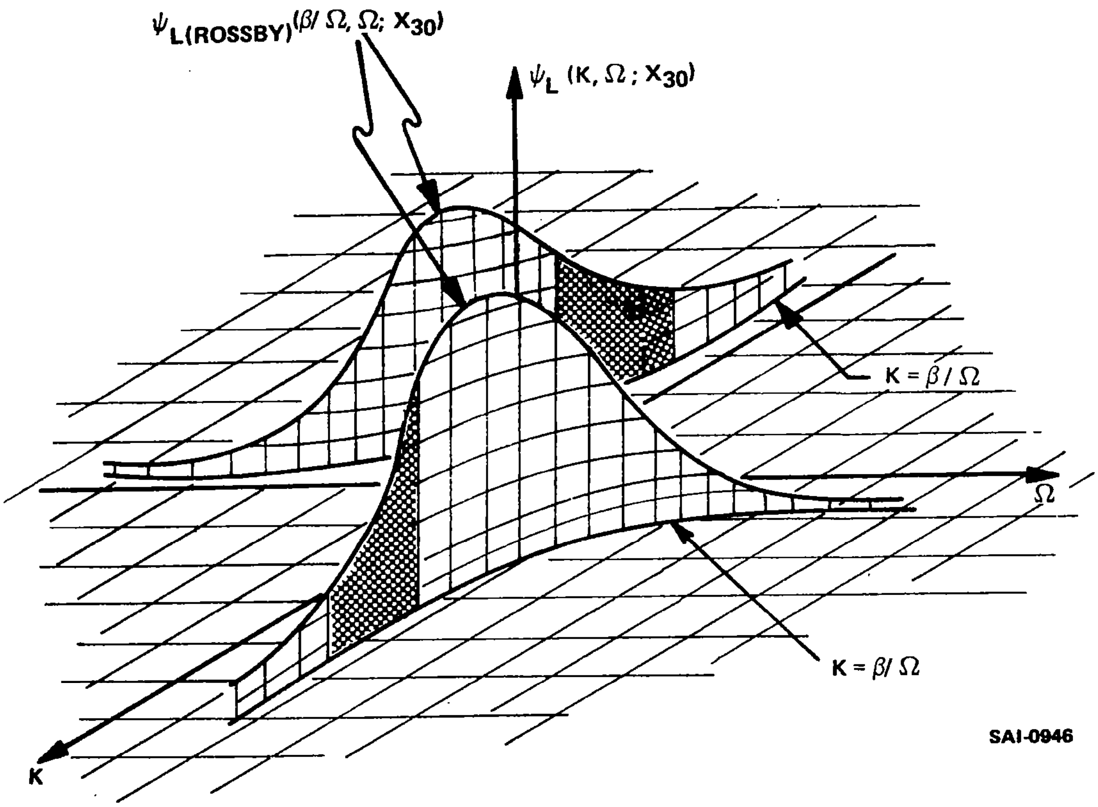

Figure J-2. Lagrangian Space-Time Power Spectrum for Rossby Waves that portion of the spectrum where Rossby waves are more likely to occur. A comparison of Figures I-4 and J-2 indicates that as $\bar{u}_1$ approaches zero, $\psi_{L(ROSSBY)}$ $(K, -\Omega; X_{30})$ approaches $\phi_{E(ROSSBY)}$ $(k, \omega; X_{30})$

In addition, inspection of the shaded portion of Figure J-2 reveals that in that portion of the spectrum where Rossby waves occur, $\psi_{L(ROSSBY)}$ increases with increasing Ω while, as shown in Figure I-4, $\phi_{E(ROSSBY)}$ decreases with increasing k. This provides a slightly better understanding of the relationship between $\phi_{E(ROSSBY)}$ and $\psi_{L(ROSSBY)}$ which was originally presented in Appendix H.

For the case involving gravity waves,

$$\Omega = \mp \sqrt{gK} \tag{J-5}$$

and

$$K = \frac{\Omega^2}{g} \tag{J-6}$$

The variation of $\psi_{L(GRAVITY)}$ $(k, \Omega; X_{30})$ with K and Ω is shown in Figure J-3.

The more heavily shaded portion of the spectrum represents the region in which gravity waves normally occur. Comparison of Figures I-5 and J-3 reveals, that as $\bar{u}_1$ approaches zero, $\psi_{L(GRAVITY)}$ $(K - \Omega; X_{30})$ approaches $\phi_{E(GRAVITY)}$ $(k, \omega; X_{30})$. Furthermore, although difficult to determine quantitatively from Figure I-5 and J-3, it is possible to observe qualitatively that $\psi_{L(GRAVITY)}$ decreases more rapidly with increasing Ω than $\phi_{E(GRAVITY)}$ decreases with increasing k.

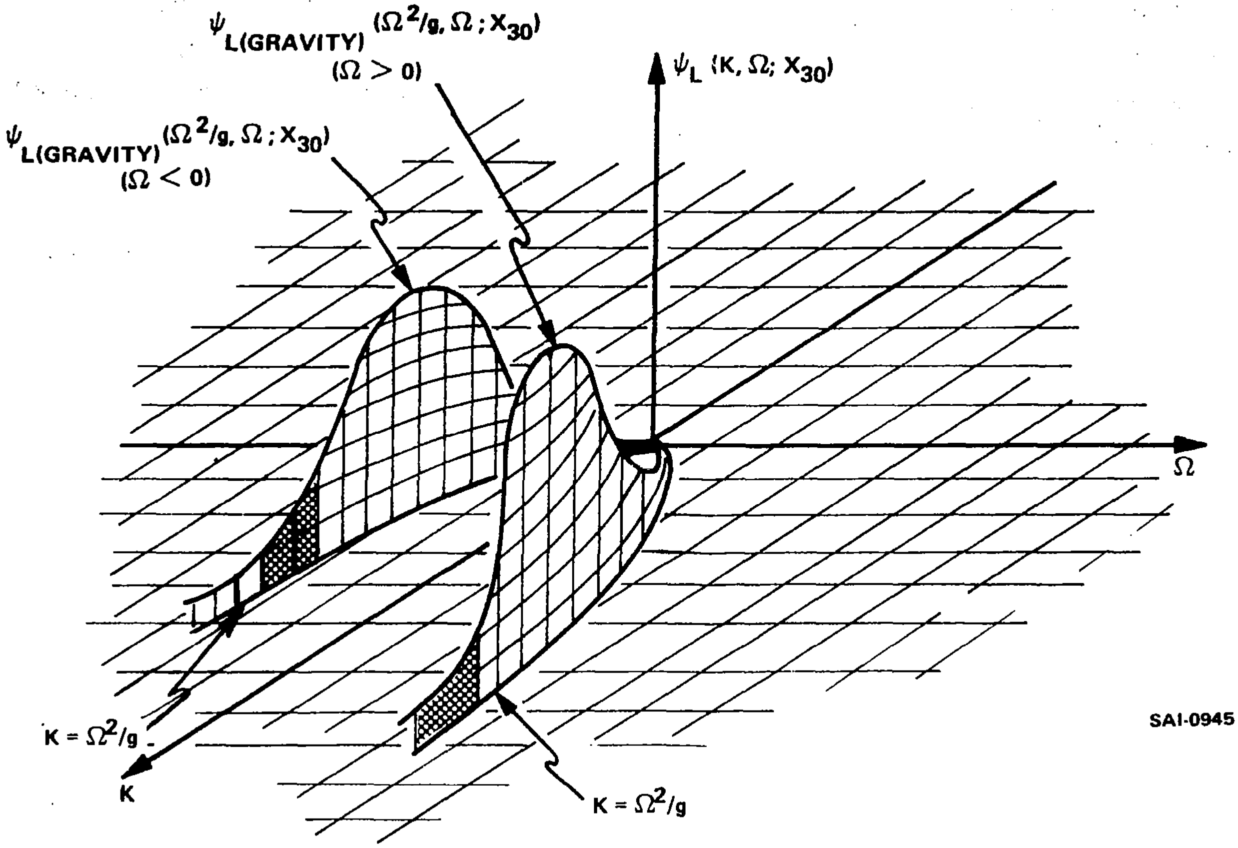

Figure J-3. Lagrangian Space-Time Power Spectrum for Gravity Waves

APPENDIX K

Source Listing for BALLOON Program

Balloon is written in FORTRAN IV for the Univac 1108 Computer. The listing which follows represents the current form of the program.

```
      COMMON/CONS/PI,D,SIGMA,AP,M,                              VOL,
     *MUREF,TEMREF,          TEMPO,TEMLAP,X30,R,GSRTL,G(3),PO,X33
      COMMON/TERMS/FDRAG(3),FAP1(3),FAP2(3),FBUOY(3),FBASS(3),
     *MA,NU,MU,RHO,TEMP,X(3),FACTOR,RE
      COMMON/VELOC/U(3),V(3),UMAG,VMAG,MAGDIF
      COMMON/INTL/K(3),THETA(3),OMEGA,UB(3),A,B,C
      DIMENSION FU(3),FV(3),VDU(3)
      DIMENSION XD(5),XN(7)
      DIMENSION WRA(50,11),WRB(50,6),WRC(50,17)
      DIMENSION BCDX(12),BCDY1(12),BCDY2(12),BCDY3(12) ,FLDY1(12),FLDY2(
     112),FLDY3(12)
      DIMENSION PT(500),PX(500),PY(500),PZ(500),PY1(500),PY2(500),PY3(50
     10),PZ1(500),PZ2(500),PZ3(500)
      EQUIVALENCE(K(1),K1),(K(2),K2),(K(3),K3),(THETA(1),THETAA),(THETA(
     12),THETAB),(THETA(3),THETAC)
      REAL M,L,K
      REAL MA,NU,MU,MUREF
      REAL MAGDIF
      NAMELIST/INPUT/G,X,K,THETA,UB,V,A,OMEGA,SIGMA,D,MUREF,TEMREF,T,
     *TLIM,DELTAT,TEMPO,PO,TEMLAP,R,X30
      PI=3.141592654
      READ(5,7002) NNN
      READ(5,7001) BCDX,BCDY1,BCDY2,BCDY3,FLDY1,FLDY2,FLDY3
      READ(5,100) G,X,K,THETA,UB,V
      READ(5,100) A,OMEGA,SIGMA,D,MUREF,TEMREF,T,TLIM,DELTAT,
     *TEMPO,PO,TEMLAP,R,X30
  100 FORMAT(8E10.3)
 7001 FORMAT(12A6,8X)
 7002 FORMAT(I2)
      DO 20 I=1,3
      FBASS(I) = 0.
   20 V(I) = UB(I)
      DGTORD=PI/180.
      THETA1=THETAA*DGTORD
      THETA2=THETAB*DGTORD
      THETA3=THETAC*DGTORD
      IF(THETA1.EQ.0.AND.THETA2.EQ.0) GO TO 1
      C=-A*K1*(SIN(THETA1)-COS(THETA1)*TAN(THETA2))/K3/(SIN(THETA3)
     * -COS(THETA3)*TAN(THETA2))
      B=-A*K1*(SIN(THETA1)-COS(THETA1)*TAN(THETA3))/K2/(SIN(THETA2)
     * -COS(THETA2)*TAN(THETA3))
```

```
      GO TO 2
    1 B=-A*K1*.5/K2
      C=-A*K1*.5/K3
    2 CONTINUE
      WRITE(6,9004) A,B,C
 9004 FORMAT(///10X,1P3E12.4)
      UCON = UB(1)/A
      DO 1001 L1=1,NNN
      READ(5,101) XD(2),XD(5),BCDX(11),BCDX(12),T,TLIM,DELTAT,IDT,IDS
  101 FORMAT(2E10.3,10X,2A6,8X,3F5.0,2I5)
      TRF = T
      TRLIM = TLIM
      K(1) = XD(2)/D
      K(2) = K(1)
      K(3) = K(1)
      OMEGA = XD(5)*A/D
      ETA = 1.0E-30
      DO 10 I=1,3
      K(I) = AMAX1(K(I),ETA)
   10 CONTINUE
      CALL GEOMET
      CALL PROPTY(X)
      GR = -G(3)
      GAM = GR/R/4.184E+7
      XD(1) = (12.*NU)/(A*D)
      XD(3) = .6666667*GR*D*D*(GAM-TEMLAP)/(A*A*TEMP0)
      XD(4) = UCON
      WRITE(6,9015) BCDX(11),BCDX(12),(XD(L2),L2=1,5)
      WRITE(6,INPUT)
 9015 FORMAT(1H1,25X,'TEST CASE'2A6//' DIMENSIONLESS GROUPS'//' N7='1PE1
     12.4/' N8='E12.4/              ' N9='E12.4/' N10='E12.4/' N11='E12.4)
      CALL IDENT (8,1)
      DO 1002 LS = 1,IDS
      ID = 0
      IDX = 0
    5 CALL INTEG(T,V,X,DELTAT,IDT)
      DO 200 I = 1,3
      FU(I) = U(I)/A
      FV(I) = V(I)/A
      VDU(I) = V(I)/U(I)
  200 CONTINUE
      AKT = A*K(1)*T
      DZ = X(3) - X30
      ID = ID + 1
      IDX = IDX + 1
      PX(IDX) = X(1)
      PY(IDX) = X(2)
      PZ(IDX) = DZ
      PY1(IDX) = FU(1)
      PY2(IDX) = FU(2)
      PY3(IDX) = FU(3)
      PZ1(IDX) = FV(1)
      PZ2(IDX) = FV(2)
      PZ3(IDX) = FV(3)
      WRA(ID,1) = T
      WRB(ID,1) = T
```

```
      WRC(ID,1) = T
      WRA(ID,2) = AKT
      WRB(ID,2) = AKT
      WRC(ID,2) = AKT
      PT(IDX) = AKT
      WRB(ID,3) = X(1)
      WRB(ID,4) = X(2)
      WRB(ID,5) = DZ
      WRB(ID,6) = RE
      DO 300 I=1,3
      WRA(ID,I+2) = FU(I)
      WRA(ID,I+5) = FV(I)
      WRA(ID,I+8) = VDU(I)
      WRC(ID,I+2) = FDRAG(I)
      WRC(ID,I+5) = FAP1(I)
      WRC(ID,I+8) = FAP2(I)
      WRC(ID,I+11) = FBUOY(I)
      WRC(ID,I+14) = FBASS(I)
  300 CONTINUE
      IF(ID - 50) 305,302,302
  302 CONTINUE
      WRITE(6,9002)
      WRITE(6,9003) ((WRA(I,J),J=1,11),I=1,50)
      WRITE(6,9008)
      WRITE(6,9009) ((WRB(I,J),J=1,6),I=1,50)
      WRITE(6,9006)
      WRITE(6,9007) ((WRC(I,J),J=1,17),I=1,50)
 9002 FORMAT('1 TIME  SCALED TIME      SCALED ATMOSPHERIC WIND
     1SCALED BALLOON VELOCITIES      VELOCITY RATIOS'//)
 9003 FORMAT(1X,0PF8.2,1P10E11.3)
 9008 FORMAT('1 TIME  SCALED TIME       X            Y            DZ            RE
     1'//)
 9009 FORMAT(1X,0PF8.2,1P5E11.3)
 9006 FORMAT('1 TIME  SCALED TIME                 FDRAG/FBUOY
     1       FAP1/FBASS                          FAP2'//)
 9007 FORMAT(1X,0PF8.2,1P10E11.3/20X,1P6E11.3)
      ID = 0
  305 CONTINUE
      IF(T.LT.TLIM) GO TO 5
      XL = A*K(1)*TRF
      XR = A*K(1)*TLIM
      YB = 8.8
      YT = 11.2
      CALL QUIK3L(-1,XL,XR,YB,YT,1H+,BCDX,BCDY1,-IDX,PT,PY1)
      CALL QUIK3L(0,XL,XR,YB,YT,1H0,BCDX,BCDY1,-IDX,PT,PZ1)
      YB = -1.5
      YT = 1.5
      CALL QUIK3L(-1,XL,XR,YB,YT,1H+,BCDX,BCDY2,-IDX,PT,PY2)
      CALL QUIK3L(0,XL,XR,YB,YT,1H0,BCDX,BCDY2,-IDX,PT,PZ2)
      CALL QUIK3L(-1,XL,XR,YB,YT,1H+,BCDX,BCDY3,-IDX,PT,PY3)
      CALL QUIK3L(0,XL,XR,YB,YT,1H0,BCDX,BCDY3,-IDX,PT,PZ3)
      CALL QUIK3V(-1,1H0,BCDX,FLDY2,-IDX,PT,PY)
      CALL QUIK3V(-1,1H0,BCDX,FLDY3,-IDX,PT,PZ)
      TRF = T
      TLIM = TLIM + TRLIM
 1002 CONTINUE
```

```
      CALL ENDJOB
      T = 0.
      X(1) = 0.
      X(2) = 0.
      X(3) =X30
      V(1) = UB(1)
      V(2) = UB(2)
      V(3) = UB(3)
 1001 CONTINUE
      STOP
      END
```

```
      SUBROUTINE ACCEL(T,VI,XI,DVDT,DELTAT,S)
      COMMON/CONS/PI,D,SIGMA,AP,M,                                VOL,
     *MUREF,TEMREF,        TEMPO,TEMLAP,X30,R,GSRTL,G(3),PO,X33
      COMMON/TERMS/FDRAG(3),FAP1(3),FAP2(3),FBUOY(3),FBASS(3),
     *MA,NU,MU,RHO,TEMP,X(3),FACTOR
      COMMON/VELOC/U(3),V(3),UMAG,VMAG,MAGDIF
      REAL M,L,K
      REAL MA,NU,MU,MUREF
      REAL MAGDIF
      REAL MEFF
      DIMENSION VI(3),XI(3),DVDT(3)
      CALL PROPTY(XI)
      CALL BUOYNT
      CALL APARNT(T,XI,VI)
      VMAG=SQRT(VI(1)**2+VI(2)**2+VI(3)**2)
      UMAG=SQRT(U(1)**2+U(2)**2+U(3)**2)
      SUM=0.
      DO 5 I=1,3
 5    SUM=SUM+(VI(I)-U(I))**2
      MAGDIF=SQRT(SUM)
      CALL DRAG(VI)
      B=FACTOR*SQRT(DELTAT*S)
      MEFF=M+MA
      DO 10 I=1,3
      DVDT(I)=(FDRAG(I)+FAP1(I)+FAP2(I)+FBUOY(I)+FBASS(I))/(MEFF+B)
   10 CONTINUE
      RETURN
      END
```

```
      SUBROUTINE APARNT(T,XI,VI)
      DIMENSION XI(3),VI(3)
C     THIS ROUTINE CALCULATE FORCES RESULTING FROM APPARENT MASS AND FLUID
      COMMON/CONS/PI,D,SIGMA,AP,M,                            VOL,
     *MUREF,TEMREF,           TEMPO,TEMLAP,X30,R,GSRTL,G(3),PO,X33
      COMMON/TERMS/FDRAG(3),FAP1(3),FAP2(3),FBUOY(3),FBASS(3),
     *MA,NU,MU,RHO,TEMP,X(3),FACTOR
      COMMON/VELOC/U(3),V(3),UMAG,VMAG,MAGDIF
      COMMON/DERV/PDUDX(3,3),PDUDT(3)
      COMMON/TIME/N
      DIMENSION DUDTF(3)
      REAL M,L,K
      REAL MA,NU,MU,MUREF
      REAL MAPMRS
      REAL MAGDIF
      MAPMRS=MA+M*RHO/SIGMA
      XI3 = XI(3)- X30
      CALL POTFLU(T,XI(1),XI(2),XI3)
      DO 10 I=1,3
      UDUDX=DVAL(U,0.,I)
      DUDTF(I)=PDUDT(I)+UDUDX
      FAP1(I)=MAPMRS*DUDTF(I)
      FAP2(I) = MA*DVAL(VI,U,I)
   10 CONTINUE
      RETURN
      END




      SUBROUTINE BUOYNT
      COMMON/CONS/PI,D,SIGMA,AP,M,                            VOL,
     *MUREF,TEMREF,           TEMPO,TEMLAP,X30,R,GSRTL,G(3),PO,X33
      COMMON/TERMS/FDRAG(3),FAP1(3),FAP2(3),FBUOY(3),FBASS(3),
     *MA,NU,MU,RHO,TEMP,X(3),FACTOR
C
      REAL M,L,K
      REAL MA,NU,MU
      REAL MROSIG
      MROSIG=M*(1.-RHO/SIGMA)
      DO 10 I=1,3
   10 FBUOY(I)=G(I)*MROSIG
      RETURN
      END
```

```
      SUBROUTINE DRAG(VI)
      COMMON/CONS/PI,D,SIGMA,AP,M,                              VOL,
     *MUREF,TEMREF,         TEMPO,TEMLAP,X30,R,GSRTL,G(3),PO,X33
      COMMON/TERMS/FDRAG(3),FAP1(3),FAP2(3),FBUOY(3),FBASS(3),
     *MA,NU,MU,RHO,TEMP,X(3),FACTOR,RE
      COMMON/VELOC/U(3),V(3),UMAG,VMAG,MAGDIF
      DIMENSION RTABL(8),REN(8)
      DIMENSION VI(3)
      REAL M,L,K
      REAL MA,NU,MU,MUREF
      REAL MAGDIF
      DATA RTABL/7.74066,5.2983,3.13549,1.5,.09531,-.693147,
     *-1.23787,-.544727/,NREN/8/,EPS/.01/,REN/-4.6052,-2.3026,0.,
     *2.3026,4.6052,6.9078,9.2103,11.5129/
C
      RE=     MAGDIF*D/NU
      REZ = RE + 1.00E-30
      CD = 24./REZ + 0.50
      VI1=VI(1)
      VI2=VI(2)
      VI3=VI(3)
      HALFRO=.5*RHO
      CDAPMD=CD*AP*MAGDIF
      HACD=HALFRO*CDAPMD
      DO 10 I=1,3
      FDRAG(I)=HACD*(U(I)-VI(I))
   10 CONTINUE
      RETURN
      END
```

```
      FUNCTION DVAL(W,Z,I)
      COMMON/DERV/PDUDX(3,3),PDUDT(3)
      DIMENSION W(3),Z(3)
      DVAL=0.
      DO 10 J=1,3
10    DVAL=DVAL+(W(J)-Z(J))*PDUDX(I,J)
      RETURN
      END
```

```
      SUBROUTINE GEOMET
C     THIS ROUTINE CALCULATES TIME INDEPENDENT GEOMETRIC VALUES
      COMMON/CONS/PI,D,SIGMA,AP,M,                              VOL,
     *MUREF,TEMREF,         TEMPO,TEMLAP,X30,R,GSRTL,G(3),PO,X33
      REAL M,L,K,MUREF
      VOL=PI*D**3/6.
      M=VOL*SIGMA
      AP=PI*D**2/4.0
      IF(TEMLAP) 10,20,10
   10 CONTINUE
      GSRTL=ABS(G(3))/(R*TEMLAP)/4.184E+7
      GO TO 30
   20 CONTINUE
      GSRTL=ABS(G(3))/(R*TEMPO )/4.184E+7
   30 CONTINUE
      RETURN
      END
```

```
      SUBROUTINE INTEG(T,V,X,DELTAT,IDT)
      DIMENSION X(3),V(3),DV1(3),DV2(3),DV4(3),DV5(3),
     *VI(3),XI(3),DVDT(3),DV3(3)
      DIMENSION DX1(3),DX2(3),DX3(3),DX4(3),DX5(3),E(3),EX(3)
      COMMON/TIME/N
      DATA ACCUR/1./
      DO 2000 L1=1,IDT
3     CALL ACCEL(T,V,X,DVDT,DELTAT,1.)
    4 DO 5 I=1,3
      DV1(I)=DELTAT*DVDT(I)/3.
      DX1(I)=DELTAT*V(I)/3.
      VI(I)=V(I)+DV1(I)
    5 XI(I)=X(I)+DX1(I)
      CALL ACCEL(T+DELTAT/3.,VI,XI,DVDT,DELTAT,.3333333333)
      DO 6 I=1,3
      DV2(I)=DELTAT*DVDT(I)/3.
      DX2(I)=DELTAT*VI(I)/3.
      VI(I)=V(I)+.5*DV1(I)+.5*DV2(I)
    6 XI(I)=X(I)+.5*DX1(I)+.5*DX2(I)
      CALL ACCEL(T+DELTAT/3.,VI,XI,DVDT,DELTAT,.3333333333)
      DO 7 I=1,3
      DV3(I)=DELTAT*DVDT(I)/3.
      DX3(I)=DELTAT*VI(I)/3.
      VI(I)=V(I)+0.375*DV1(I)+1.125*DV3(I)
    7 XI(I)=X(I)+0.375*DX1(I)+1.125*DX3(I)
      CALL ACCEL(T+DELTAT/2.,VI,XI,DVDT,DELTAT,.5)
      DO 8 I=1,3
      DV4(I)=DELTAT*DVDT(I)/3.
      DX4(I)=DELTAT*VI(I)/3.
      VI(I)=V(I)+1.5*DV1(I)-4.5*DV3(I)+6.0*DV4(I)
```

```
    8 XI(I)=X(I)+1.5*DX1(I)-4.5*DX3(I)+6.0*DX4(I)
      CALL ACCEL(T+DELTAT,VI,XI,DVDT,DELTAT,1.)
      TEST=0.0
      DO 9 I=1,3
      DV5(I)=DELTAT*DVDT(I)/3.
      DX5(I)=DELTAT*VI(I)/3.
      E(I)=0.2*DV1(I)-.9*DV3(I)+.8*DV4(I)-.1*DV5(I)
      EX(I)=0.2*DX1(I)-.9*DX3(I)+.8*DX4(I)-.1*DX5(I)
    9 TEST=AMAX1(TEST,ABS(E(I)),ABS(EX(I)))
      IF(TEST.LT.ACCUR) GO TO 10
      WRITE(6,1000)
 1000 FORMAT(10X,38H***ACCURACY TEST FAILED IN INTEGRATION)
   10 DO 11 I=1,3
      V(I)=V(I)+.5*DV1(I)+2.*DV4(I)+.5*DV5(I)
   11 X(I)=X(I)+.5*DX1(I)+2.*DX4(I)+.5*DX5(I)
      T=T+DELTAT
 2000 CONTINUE
      RETURN
      END
```

```
      REAL FUNCTION MREF(TEMP,MUREF,TEMREF)
      REAL MUREF
      A=MUREF*(TEMP/TEMREF)**1.5
      B=1.505*TEMREF
      C=TEMP+.505*TEMREF
      MREF=A*B/C
      RETURN
      END
```

```
      SUBROUTINE POTFLU(T,X,Y,Z)
      COMMON/INTL/K1,K2,K3,THETA1,THETA2,THETA3,OMEGA,UB,VB,WB,A,B,C
      COMMON/DERV/DUDX,DVDX,DWDX,DUDY,DVDY,DWDY,DUDZ,DVDZ,DWDZ,DUDT,
     *DVDT,DWDT
      COMMON/VELOC/U,V,W,DUMY(6)
      REAL L1,L2,L3,K1,K2,K3
      XI=K1*X+K2*Y+K3*Z
      XIMOMT=XI-OMEGA*T
      COS1=COS(XIMOMT+THETA1)
      COS2=COS(XIMOMT+THETA2)
      COS3=COS(XIMOMT+THETA3)
      U=UB+A*SIN(XIMOMT+THETA1)
      V=VB+B*SIN(XIMOMT+THETA2)
      W=WB+C*SIN(XIMOMT+THETA3)
      DUDX=A*K1*COS1
      DUDY=A*K2*COS1
      DUDZ=A*K3*COS1
```

```
      DVDX=B*K1*COS2
      DVDY=B*K2*COS2
      DVDZ=B*K3*COS2
      DWDX=C*K1*COS3
      DWDY=C*K2*COS3
      DWDZ=C*K3*COS3
      DUDT=-A*OMEGA*COS1
      DVDT=-B*OMEGA*COS2
      DWDT=-C*OMEGA*COS3
   20 CONTINUE
      RETURN
      END
```

```
      SUBROUTINE PROPTY(XI)
C     THIS ROUTINE CALCULATES TEMPERATURE AND DENSITY FROM
C     TABULATED FUNCTIONS OF ALTITUDE (X(3) OR ALT).  DYNAMIC
C     VISCOSITY,MU, AND KINEMATIC VISCOSITY,NU,ARE CALCULATED.
C     PRESSURE = PO = DYNES/CM**2
C     DENSITY = RHO = GMS/C**3
      DIMENSION XI(3)
      COMMON/CONS/PI,D,SIGMA,AP,M,                           VOL,
     *MUREF,TEMREF,        TEMPO,TEMLAP,X30,R,GSRTL,G(3),PO,X33
      COMMON/TERMS/FDRAG(3),FAP1(3),FAP2(3),FBUOY(3),FBASS(3),
     *MA,NU,MU,RHO,TEMP,X(3),FACTOR
      REAL M,L,K
      REAL MA,NU,MU,MUREF
      REAL MREF
      TEMP=TEMPO-TEMLAP*(XI(3)-X30)
      MU=MREF(TEMP,MUREF,TEMREF)
 1000 FORMAT(10X,5HTEMP=,E10.4)
 2000 FORMAT(10X,3HMU=,E10.4)
      IF(TEMLAP) 10,20,10
   10 CONTINUE
      P=PO*(TEMP/TEMPO)**GSRTL
      GO TO 30
   20 CONTINUE
      P = PO*EXP(-GSRTL*(XI(3)-X30))
   30 CONTINUE
      RHO=P/(R*TEMP)/4.184E+7
      NU=MU/RHO
      MA=VOL*RHO*.5
  100 FORMAT(//10X,16HPROPTY VARIABLES)
  200 FORMAT(10X,5HTEMP=,E10.4/10X,3HXI=,3E10.4/10X,4HX30=,E10.4/
     *10X,3HMU=,E10.4/10X,2HP=,E10.4/10X,6HGSRTL=,E10.4/
     *10X,3HNU=,E10.4/10X,3HMA=,E10.4/10X,2HM=,E10.4/10X,4HVOL=,E10.4//)
      RETURN
      END
```

APPENDIX L

Samples for Blocks #1, #2 & #3 Outputs

The sample outputs which follow correspond to Blocks #1, #2 and #3 Outputs which are described in Section 4.2. These outputs are for the most part labeled and thus are self-explanatory. Where three components of a vector are printed out, the sequence always corresponds to the order x_1, x_2, x_3.

L.1 Block #1 Output (Sample)

```
1.0000+02     1.0000+02     1.0000+02
```

L.2 Block #2 Output (Sample)

```
                              TEST CASETEST (1.1)

DIMENSIONLESS GROUPS

N7=     3.5914-04
N8=     8.1681-04
N9=     1.7317-03
N10=     1.0000+01
N11=     8.1681-03
$INPUT
G       =      .00000000E+00,    .00000000E+00,   -.98066500E+03
X       =      .00000000E+00,    .00000000E+00,    .11000000E+07
K       =      .62831538E-05,    .62831538E-05,    .62831538E-05
THETA   =      .00000000E+00,    .12000000E+03,    .24000000E+03
UB      =      .10000000E+04,    .00000000E+00,    .00000000E+00
V       =      .10000000E+04,    .00000000E+00,    .00000000E+00
A       =      .10000000E+03
OMEGA   =      .62831538E-02
SIGMA   =      .36149400E-03
D       =      .13000000E+03
MUREF   =      .17080000E-03
TEMREF  =      .27315000E+03
T       =      .00000000E+00
TLIM    =      .10000000E+05
DELTAT  =      .25000000E+01
TEMPO   =      .21800000E+03
PO      =      .22619000E+06
TEMLAP  =      .00000000E+00
R       =      .68600000E-01
X30     =      .11000000E+07
```

L.3 Block #3 Output (Sample - next four pages)

TIME	SCALED TIME	SCALED ATMOSPHERIC WIND			SCALED BALLOON VELOCITIES			VELOCITY RATIOS		
50.00	3.142-02	1.003+01	6.087-01	9.562-01	1.004+01	5.924-01	5.837-01	1.000+00	9.733-01	6.104-01
100.00	6.283-02	1.007+01	6.375-01	9.664-01	1.007+01	6.389-01	4.319-01	1.000+00	1.002+00	4.469-01
150.00	9.425-02	1.011+01	6.645-01	9.749-01	1.011+01	6.661-01	3.476-01	1.000+00	1.002+00	3.566-01
200.00	1.257-01	1.014+01	6.934-01	9.821-01	1.014+01	6.919-01	2.887-01	1.000+00	1.002+00	2.940-01
250.00	1.571-01	1.018+01	7.157-01	9.882-01	1.018+01	7.172-01	2.440-01	1.000+00	1.002+00	2.469-01
300.00	1.885-01	1.021+01	7.405-01	9.931-01	1.021+01	7.419-01	2.083-01	1.000+00	1.002+00	2.098-01
350.00	2.199-01	1.025+01	7.649-01	9.968-01	1.025+01	7.662-01	1.789-01	1.000+00	1.002+00	1.794-01
400.00	2.513-01	1.029+01	7.889-01	9.991-01	1.029+01	7.902-01	1.538-01	1.000+00	1.002+00	1.539-01
450.00	2.827-01	1.032+01	8.124-01	1.000+00	1.032+01	8.136-01	1.318-01	1.000+00	1.002+00	1.318-01
500.00	3.142-01	1.036+01	8.354-01	9.993-01	1.036+01	8.365-01	1.119-01	1.000+00	1.001+00	1.120-01
550.00	3.456-01	1.040+01	8.576-01	9.969-01	1.040+01	8.587-01	9.366-02	1.000+00	1.001+00	9.396-02
600.00	3.770-01	1.044+01	8.790-01	9.925-01	1.044+01	8.801-01	7.638-02	1.000+00	1.001+00	7.696-02
650.00	4.084-01	1.048+01	8.994-01	9.861-01	1.048+01	9.003-01	5.969-02	1.000+00	1.001+00	6.064-02
700.00	4.398-01	1.052+01	9.185-01	9.774-01	1.052+01	9.194-01	4.329-02	1.000+00	1.001+00	4.429-02
750.00	4.712-01	1.056+01	9.362-01	9.663-01	1.056+01	9.369-01	2.693-02	1.000+00	1.001+00	2.787-02
800.00	5.027-01	1.060+01	9.521-01	9.527-01	1.060+01	9.528-01	1.044-02	1.000+00	1.001+00	1.096-02
850.00	5.341-01	1.064+01	9.661-01	9.365-01	1.064+01	9.667-01	-6.300-03	1.000+00	1.001+00	-6.728-03
900.00	5.655-01	1.068+01	9.780-01	9.175-01	1.068+01	9.784-01	-2.336-02	1.000+00	1.000+00	-2.546-02
950.00	5.969-01	1.071+01	9.874-01	8.957-01	1.071+01	9.878-01	-4.070-02	1.000+00	1.000+00	-4.544-02
1000.00	6.283-01	1.075+01	9.944-01	8.710-01	1.075+01	9.946-01	-5.828-02	1.000+00	1.000+00	-6.691-02
1050.00	6.597-01	1.078+01	9.986-01	8.436-01	1.078+01	9.987-01	-7.599-02	1.000+00	1.000+00	-9.007-02
1100.00	6.911-01	1.081+01	1.000+00	8.135-01	1.082+01	1.000+00	-9.367-02	1.000+00	1.000+00	-1.151-01
1150.00	7.226-01	1.085+01	9.985-01	7.808-01	1.085+01	9.984-01	-1.111-01	1.000+00	9.999-01	-1.423-01
1200.00	7.540-01	1.087+01	9.940-01	7.455-01	1.087+01	9.937-01	-1.281-01	1.000+00	9.998-01	-1.719-01
1250.00	7.854-01	1.090+01	9.865-01	7.080-01	1.090+01	9.861-01	-1.444-01	1.000+00	9.997-01	-2.040-01
1300.00	8.168-01	1.092+01	9.760-01	6.683-01	1.092+01	9.756-01	-1.597-01	1.000+00	9.996-01	-2.389-01
1350.00	8.482-01	1.094+01	9.627-01	6.268-01	1.094+01	9.622-01	-1.736-01	1.000+00	9.994-01	-2.770-01
1400.00	8.796-01	1.096+01	9.467-01	5.837-01	1.096+01	9.460-01	-1.859-01	1.000+00	9.993-01	-3.185-01
1450.00	9.111-01	1.097+01	9.280-01	5.392-01	1.097+01	9.272-01	-1.963-01	1.000+00	9.992-01	-3.640-01
1500.00	9.425-01	1.098+01	9.069-01	4.937-01	1.098+01	9.060-01	-2.043-01	1.000+00	9.990-01	-4.139-01
1550.00	9.739-01	1.099+01	8.834-01	4.472-01	1.099+01	8.825-01	-2.097-01	1.000+00	9.989-01	-4.690-01
1600.00	1.005+00	1.100+01	8.579-01	4.002-01	1.100+01	8.569-01	-2.122-01	1.000+00	9.988-01	-5.303-01
1650.00	1.037+00	1.100+01	8.305-01	3.528-01	1.100+01	8.294-01	-2.115-01	1.000+00	9.986-01	-5.995-01
1700.00	1.068+00	1.100+01	8.014-01	3.052-01	1.100+01	8.001-01	-2.072-01	1.000+00	9.984-01	-6.789-01
1750.00	1.100+00	1.100+01	7.707-01	2.575-01	1.100+01	7.694-01	-1.990-01	1.000+00	9.983-01	-7.725-01
1800.00	1.131+00	1.099+01	7.387-01	2.100-01	1.099+01	7.372-01	-1.864-01	1.000+00	9.981-01	-8.873-01
1850.00	1.162+00	1.099+01	7.054-01	1.628-01	1.099+01	7.039-01	-1.689-01	1.000+00	9.979-01	-1.038+00
1900.00	1.194+00	1.098+01	6.710-01	1.158-01	1.098+01	6.694-01	-1.458-01	1.000+00	9.977-01	-1.259+00
1950.00	1.225+00	1.097+01	6.355-01	6.916-02	1.097+01	6.339-01	-1.157-01	1.000+00	9.974-01	-1.673+00
2000.00	1.257+00	1.095+01	5.990-01	2.279-02	1.095+01	5.973-01	-7.555-02	9.999-01	9.972-01	-3.316+00
2050.00	1.288+00	1.094+01	5.613-01	-2.354-02	1.094+01	5.595-01	-1.591-02	9.999-01	9.969-01	6.760-01
2100.00	1.319+00	1.092+01	5.222-01	-6.998-02	1.092+01	5.270-01	1.837-02	1.000+00	9.996-01	-2.625-01
2150.00	1.351+00	1.090+01	4.838-01	-1.142-01	1.090+01	4.848-01	-1.921-02	1.000+00	1.002+00	1.682-01
2200.00	1.382+00	1.088+01	4.468-01	-1.556-01	1.088+01	4.484-01	-3.577-02	1.000+00	1.004+00	2.298-01
2250.00	1.414+00	1.086+01	4.109-01	-1.948-01	1.086+01	4.127-01	-3.871-02	1.000+00	1.005+00	1.987-01
2300.00	1.445+00	1.084+01	3.759-01	-2.319-01	1.085+01	3.779-01	-4.323-02	1.000+00	1.005+00	1.864-01
2350.00	1.477+00	1.082+01	3.422-01	-2.669-01	1.083+01	3.442-01	-4.804-02	1.000+00	1.006+00	1.799-01
2400.00	1.508+00	1.080+01	3.097-01	-2.999-01	1.081+01	3.118-01	-5.213-02	1.000+00	1.007+00	1.738-01
2450.00	1.539+00	1.078+01	2.786-01	-3.308-01	1.079+01	2.807-01	-5.547-02	1.000+00	1.007+00	1.677-01
2500.00	1.571+00	1.076+01	2.487-01	-3.598-01	1.077+01	2.508-01	-5.813-02	1.000+00	1.008+00	1.615-01

TIME	SCALED TIME	X	Y	DZ	RE
50.00	3.142-02	5.009+04	2.372+03	3.093+03	1.240+04
100.00	6.283-02	1.004+05	5.475+03	5.580+03	1.770+04
150.00	9.425-02	1.508+05	8.738+03	7.514+03	2.071+04
200.00	1.257-01	2.015+05	1.213+04	9.097+03	2.284+04
250.00	1.571-01	2.523+05	1.566+04	1.042+04	2.446+04
300.00	1.885-01	3.033+05	1.930+04	1.155+04	2.575+04
350.00	2.199-01	3.544+05	2.307+04	1.252+04	2.680+04
400.00	2.513-01	4.058+05	2.697+04	1.335+04	2.766+04
450.00	2.827-01	4.573+05	3.098+04	1.406+04	2.838+04
500.00	3.142-01	5.090+05	3.510+04	1.467+04	2.898+04
550.00	3.456-01	5.609+05	3.934+04	1.518+04	2.947+04
600.00	3.770-01	6.130+05	4.369+04	1.560+04	2.987+04
650.00	4.084-01	6.653+05	4.814+04	1.594+04	3.019+04
700.00	4.398-01	7.178+05	5.269+04	1.620+04	3.043+04
750.00	4.712-01	7.705+05	5.733+04	1.637+04	3.059+04
800.00	5.027-01	8.234+05	6.205+04	1.647+04	3.068+04
850.00	5.341-01	8.765+05	6.685+04	1.648+04	3.070+04
900.00	5.655-01	9.298+05	7.172+04	1.640+04	3.064+04
950.00	5.969-01	9.833+05	7.663+04	1.625+04	3.050+04
1000.00	6.283-01	1.037+06	8.159+04	1.600+04	3.028+04
1050.00	6.597-01	1.091+06	8.658+04	1.566+04	2.998+04
1100.00	6.911-01	1.145+06	9.157+04	1.524+04	2.960+04
1150.00	7.226-01	1.199+06	9.657+04	1.473+04	2.912+04
1200.00	7.540-01	1.253+06	1.016+05	1.413+04	2.855+04
1250.00	7.854-01	1.308+06	1.065+05	1.345+04	2.789+04
1300.00	8.168-01	1.362+06	1.114+05	1.269+04	2.712+04
1350.00	8.482-01	1.417+06	1.163+05	1.185+04	2.625+04
1400.00	8.796-01	1.472+06	1.210+05	1.096+04	2.528+04
1450.00	9.111-01	1.526+06	1.257+05	9.999+03	2.419+04
1500.00	9.425-01	1.581+06	1.303+05	8.997+03	2.300+04
1550.00	9.739-01	1.636+06	1.348+05	7.962+03	2.168+04
1600.00	1.005+00	1.691+06	1.391+05	6.906+03	2.024+04
1650.00	1.037+00	1.746+06	1.433+05	5.845+03	1.868+04
1700.00	1.068+00	1.801+06	1.474+05	4.798+03	1.699+04
1750.00	1.100+00	1.856+06	1.513+05	3.781+03	1.516+04
1800.00	1.131+00	1.911+06	1.551+05	2.816+03	1.319+04
1850.00	1.162+00	1.966+06	1.587+05	1.926+03	1.105+04
1900.00	1.194+00	2.021+06	1.621+05	1.137+03	8.727+03
1950.00	1.225+00	2.076+06	1.654+05	4.806+02	6.172+03
2000.00	1.257+00	2.131+06	1.685+05	-2.281+00	3.286+03
2050.00	1.288+00	2.185+06	1.714+05	-2.429+02	2.624+02
2100.00	1.319+00	2.240+06	1.741+05	-1.885+02	2.953+03
2150.00	1.351+00	2.295+06	1.766+05	-1.883+02	3.176+03
2200.00	1.382+00	2.349+06	1.789+05	-3.372+02	4.007+03
2250.00	1.414+00	2.403+06	1.811+05	-5.232+02	5.221+03
2300.00	1.445+00	2.458+06	1.830+05	-7.269+02	6.313+03
2350.00	1.477+00	2.512+06	1.848+05	-9.548+02	7.326+03
2400.00	1.508+00	2.566+06	1.865+05	-1.205+03	8.294+03
2450.00	1.539+00	2.620+06	1.880+05	-1.474+03	9.222+03
2500.00	1.571+00	2.674+06	1.893+05	-1.758+03	1.011+04

TIME	SCALED TIME	FDRAG/FBUOY			FAP1/FMASS			FAP2		
50.00	3.142-02	-1.057+01	7.275+01	1.665+03	6.236+01	4.951+01	1.826+01	-5.021+00	-3.986+00	-1.470+00
		0.000	0.000	-1.972+03	0.000	0.000	0.000			
100.00	6.283-02	-1.350+01	-9.145+00	3.406+03	6.493+01	5.015+01	1.674+01	-6.858+00	-5.297+00	-1.768+00
		0.000	0.000	-3.551+03	0.000	0.000	0.000			
150.00	9.425-02	-1.568+01	-1.184+01	4.676+03	6.726+01	5.055+01	1.506+01	-8.005+00	-6.017+00	-1.793+00
		0.000	0.000	-4.774+03	0.000	0.000	0.000			
200.00	1.257-01	-1.719+01	-1.262+01	5.698+03	6.940+01	5.072+01	1.319+01	-8.794+00	-6.427+00	-1.671+00
		0.000	0.000	-5.773+03	0.000	0.000	0.000			
250.00	1.571-01	-1.828+01	-1.303+01	6.549+03	7.138+01	5.066+01	1.111+01	-9.369+00	-6.649+00	-1.458+00
		0.000	0.000	-6.608+03	0.000	0.000	0.000			
300.00	1.885-01	-1.908+01	-1.318+01	7.269+03	7.320+01	5.034+01	8.784+00	-9.794+00	-6.737+00	-1.175+00
		0.000	0.000	-7.316+03	0.000	0.000	0.000			
350.00	2.199-01	-1.965+01	-1.313+01	7.883+03	7.483+01	4.977+01	6.210+00	-1.011+01	-6.721+00	-8.387-01
		0.000	0.000	-7.922+03	0.000	0.000	0.000			
400.00	2.513-01	-2.004+01	-1.291+01	8.409+03	7.627+01	4.891+01	3.369+00	-1.032+01	-6.620+00	-4.561-01
		0.000	0.000	-8.441+03	0.000	0.000	0.000			
450.00	2.827-01	-2.027+01	-1.256+01	8.861+03	7.748+01	4.773+01	2.510-01	-1.046+01	-6.446+00	-3.390-02
		0.000	0.000	-8.887+03	0.000	0.000	0.000			
500.00	3.142-01	-2.037+01	-1.207+01	9.246+03	7.843+01	4.623+01	-3.151+00	-1.053+01	-6.206+00	4.230-01
		0.000	0.000	-9.267+03	0.000	0.000	0.000			
550.00	3.456-01	-2.033+01	-1.148+01	9.571+03	7.908+01	4.436+01	-6.837+00	-1.053+01	-5.906+00	9.101-01
		0.000	0.000	-9.587+03	0.000	0.000	0.000			
600.00	3.770-01	-2.018+01	-1.078+01	9.840+03	7.940+01	4.213+01	-1.080+01	-1.046+01	-5.550+00	1.423+00
		0.000	0.000	-9.852+03	0.000	0.000	0.000			
650.00	4.084-01	-1.991+01	-9.986+00	1.006+04	7.935+01	3.950+01	-1.503+01	-1.033+01	-5.144+00	1.958+00
		0.000	0.000	-1.006+04	0.000	0.000	0.000			
700.00	4.398-01	-1.952+01	-9.112+00	1.022+04	7.889+01	3.647+01	-1.950+01	-1.015+01	-4.690+00	2.508+00
		0.000	0.000	-1.022+04	0.000	0.000	0.000			
750.00	4.712-01	-1.903+01	-8.151+00	1.033+04	7.799+01	3.304+01	-2.419+01	-9.899+00	-4.194+00	3.070+00
		0.000	0.000	-1.033+04	0.000	0.000	0.000			
800.00	5.027-01	-1.843+01	-7.118+00	1.040+04	7.663+01	2.922+01	-2.904+01	-9.594+00	-3.659+00	3.636+00
		0.000	0.000	-1.039+04	0.000	0.000	0.000			
850.00	5.341-01	-1.772+01	-6.031+00	1.041+04	7.478+01	2.503+01	-3.402+01	-9.234+00	-3.091+00	4.200+00
		0.000	0.000	-1.040+04	0.000	0.000	0.000			
900.00	5.655-01	-1.692+01	-4.894+00	1.036+04	7.244+01	2.050+01	-3.906+01	-8.819+00	-2.496+00	4.756+00
		0.000	0.000	-1.035+04	0.000	0.000	0.000			
950.00	5.969-01	-1.603+01	-3.719+00	1.027+04	6.960+01	1.566+01	-4.410+01	-8.354+00	-1.880+00	5.293+00
		0.000	0.000	-1.025+04	0.000	0.000	0.000			
1000.00	6.283-01	-1.506+01	-2.520+00	1.012+04	6.628+01	1.057+01	-4.907+01	-7.842+00	-1.251+00	5.806+00
		0.000	0.000	-1.010+04	0.000	0.000	0.000			
1050.00	6.597-01	-1.400+01	-1.313+00	9.915+03	6.250+01	5.289+00	-5.389+01	-7.269+00	-6.166-01	6.284+00
		0.000	0.000	-9.889+03	0.000	0.000	0.000			
1100.00	6.911-01	-1.289+01	-1.125-01	9.655+03	5.830+01	-1.160-01	-5.849+01	-6.699+00	1.333-02	6.721+00
		0.000	0.000	-9.625+03	0.000	0.000	0.000			
1150.00	7.226-01	-1.172+01	1.064+00	9.340+03	5.373+01	-5.570+00	-6.280+01	-6.080+00	6.303-01	7.106+00
		0.000	0.000	-9.305+03	0.000	0.000	0.000			
1200.00	7.540-01	-1.051+01	2.200+00	8.970+03	4.884+01	-1.100+01	-6.675+01	-5.439+00	1.225+00	7.433+00
		0.000	0.000	-8.932+03	0.000	0.000	0.000			
1250.00	7.854-01	-9.275+00	3.279+00	8.548+03	4.371+01	-1.631+01	-7.027+01	-4.786+00	1.786+00	7.695+00
		0.000	0.000	-8.505+03	0.000	0.000	0.000			
1300.00	8.168-01	-8.034+00	4.280+00	8.077+03	3.839+01	-2.145+01	-7.332+01	-4.129+00	2.306+00	7.886+00
		0.000	0.000	-8.029+03	0.000	0.000	0.000			
1350.00	8.482-01	-6.796+00	5.189+00	7.558+03	3.298+01	-2.633+01	-7.585+01	-3.477+00	2.775+00	7.996+00

		0.000	0.000	-7.507+03	0.000	0.000	0.000			
1400.00	8.796-01	-5.588+00	5.990+00	6.998+03	2.754+01	-3.088+01	-7.783+01	-2.840+00	3.184+00	8.024+00
		0.000	0.000	-6.942+03	0.000	0.000	0.000			
1450.00	9.111-01	-4.423+00	6.662+00	6.401+03	2.216+01	-3.506+01	-7.925+01	-2.228+00	3.526+00	7.969+00
		0.000	0.000	-6.341+03	0.000	0.000	0.000			
1500.00	9.425-01	-3.316+00	7.196+00	5.774+03	1.689+01	-3.882+01	-8.010+01	-1.650+00	3.791+00	7.824+00
		0.000	0.000	-5.710+03	0.000	0.000	0.000			
1550.00	9.739-01	-2.289+00	7.575+00	5.125+03	1.182+01	-4.211+01	-8.039+01	-1.115+00	3.976+00	7.589+00
		0.000	0.000	-5.057+03	0.000	0.000	0.000			
1600.00	1.005+00	-1.357+00	7.788+00	4.462+03	6.979+00	-4.492+01	-8.012+01	-6.327-01	4.072+00	7.264+00
		0.000	0.000	-4.390+03	0.000	0.000	0.000			
1650.00	1.037+00	-5.366-01	7.821+00	3.795+03	2.434+00	-4.722+01	-7.932+01	-2.101-01	4.076+00	6.848+00
		0.000	0.000	-3.719+03	0.000	0.000	0.000			
1700.00	1.068+00	1.484-01	7.670+00	3.134+03	-1.779+00	-4.901+01	-7.802+01	1.446-01	3.984+00	6.342+00
		0.000	0.000	-3.055+03	0.000	0.000	0.000			
1750.00	1.100+00	6.991-01	7.321+00	2.493+03	-5.627+00	-5.029+01	-7.626+01	4.240-01	3.790+00	5.747+00
		0.000	0.000	-2.409+03	0.000	0.000	0.000			
1800.00	1.131+00	1.090+00	6.761+00	1.884+03	-9.086+00	-5.106+01	-7.407+01	6.210-01	3.490+00	5.062+00
		0.000	0.000	-1.796+03	0.000	0.000	0.000			
1850.00	1.162+00	1.309+00	5.982+00	1.322+03	-1.214+01	-5.135+01	-7.148+01	7.279-01	3.079+00	4.286+00
		0.000	0.000	-1.229+03	0.000	0.000	0.000			
1900.00	1.194+00	1.336+00	4.957+00	8.242+02	-1.477+01	-5.116+01	-6.853+01	7.361-01	2.549+00	3.415+00
		0.000	0.000	-7.263+02	0.000	0.000	0.000			
1950.00	1.225+00	1.148+00	3.668+00	4.128+02	-1.698+01	-5.051+01	-6.526+01	6.338-01	1.885+00	2.435+00
		0.000	0.000	-3.070+02	0.000	0.000	0.000			
2000.00	1.257+00	7.098-01	2.039+00	1.177+02	-1.877+01	-4.941+01	-6.169+01	3.998-01	1.053+00	1.314+00
		0.000	0.000	1.495+00	0.000	0.000	0.000			
2050.00	1.288+00	7.058-02	1.938-01	-8.500-01	-2.013+01	-4.787+01	-5.782+01	-2.390-02	-5.684-02	-6.866-02
		0.000	0.000	1.553+02	0.000	0.000	0.000			
2100.00	1.319+00	2.154-02	2.501-01	-9.520+01	-2.105+01	-4.589+01	-5.368+01	-4.503-01	-9.819-01	-1.149+00
		0.000	0.000	1.205+02	0.000	0.000	0.000			
2150.00	1.351+00	-6.078-01	-1.171+00	-1.100+02	-2.152+01	-4.363+01	-4.953+01	-5.447-01	-1.104+00	-1.254+00
		0.000	0.000	1.204+02	0.000	0.000	0.000			
2200.00	1.382+00	-1.202+00	-2.332+00	-1.745+02	-2.160+01	-4.120+01	-4.549+01	-7.496-01	-1.430+00	-1.579+00
		0.000	0.000	2.156+02	0.000	0.000	0.000			
2250.00	1.414+00	-1.910+00	-3.553+00	-2.953+02	-2.134+01	-3.862+01	-4.155+01	-1.047+00	-1.695+00	-2.039+00
		0.000	0.000	3.346+02	0.000	0.000	0.000			
2300.00	1.445+00	-2.561+00	-4.533+00	-4.310+02	-2.079+01	-3.593+01	-3.771+01	-1.345+00	-2.325+00	-2.440+00
		0.000	0.000	4.649+02	0.000	0.000	0.000			
2350.00	1.477+00	-3.181+00	-5.376+00	-5.795+02	-1.999+01	-3.317+01	-3.402+01	-1.646+00	-2.731+00	-2.801+00
		0.000	0.000	6.107+02	0.000	0.000	0.000			
2400.00	1.508+00	-3.799+00	-6.165+00	-7.420+02	-1.900+01	-3.039+01	-3.050+01	-1.953+00	-3.125+00	-3.135+00
		0.000	0.000	7.710+02	0.000	0.000	0.000			
2450.00	1.539+00	-4.420+00	-6.923+00	-9.163+02	-1.784+01	-2.762+01	-2.714+01	-2.264+00	-3.506+00	-3.445+00
		0.000	0.000	9.432+02	0.000	0.000	0.000			
2500.00	1.571+00	-5.043+00	-7.651+00	-1.100+03	-1.655+01	-2.489+01	-2.397+01	-2.575+00	-3.872+00	-3.730+00
		0.000	0.000	1.125+03	0.000	0.000	0.000			

APPENDIX M

Initial Testing of Balloon Program

In general according to first-order theory, the equation for a balloon in a stationary atmosphere can be written as

$$\left(\frac{m + m_a}{m}\right)\frac{dv_3}{dt} + 2\alpha\, v_3 + N^2 x_3' = G_1 \;|v_3|\; v_3 + F_B \qquad \text{(M-1)}$$

In this equation, the vertical displacement from equilibrium is x'_3 ($=x_3 - x_{30}$). The mass of the balloon is m, and the apparent mass of the displaced fluid is m_a. In general, for a spherical balloon displaced a small distance from equilibrium, $(m + m_a)/m=3/2$.

In Equation (M-1) α is the linear drag and G_1 is the non-linear contribution to the drag term based on the following approximation for drag coefficient

$$C_D = \frac{24}{Re} + C_{D\ell} \qquad \text{(M-2)}$$

where $C_{D\ell}$ is a constant and Re is the Reynolds number $\left(Re \propto |v_3|\right)$

In Equation (M-1) the term F_B represents the Basset force which arises in a transient flow at low Reynolds numbers.

The buoyancy term N^2 has been reduced to its linear component. Perturbation techniques used to evaluate the nonlinear contributions show that the first-order term contributes a modification of about 1 cm in 10 m to the amplitude of the oscillation and a subharmonic term of similar amplitude. These nonlinear contributions should be observed using a small time step and careful analysis. The perturbation technique cannot be used to solve the linear oscillator in general, as the solution does not converge due to secular terms which arise in solutions higher than first-order. However, the technique seems applicable here to determine, the order of magnitude of the nonlinear contribution since no resonance phenomena are expected in the unforced system.

In the first four tests respectively the following simplifications were made:

(1) $(m + m_a)/m = 1$, $\alpha = 0$, $F_B = 0$, $G_1 = 0$
(2) $(m + m_a)/m = 1$, $\alpha \neq 0$, $F_B = 0$, $G_1 = 0$
(3) $(m + m_a)/m = 3/2$, $\alpha = 0$, $F_B = 0$, $G_1 = 0$
(4) $(m + m_a)/m = 1$, $\alpha = 0$, $F_B \neq 0$, $G_1 = 0$

For test case #1 the governing equation is the same as that for a parcel of air displaced from its equilibrium position in the absence drag forces, Basset forces, apparent mass forces and fluid acceleration forces. With these simplifications the governing equation is

$$\frac{dv_3}{dt} = - \frac{\partial p}{\partial x_3} - g \qquad \text{(M-3)}$$

where the terms have their usual meaning.

For the atmosphere, by means of the hydrostatic equation,

$$0 = - \frac{1}{\rho}\frac{\partial p}{\partial x_3} - g. \qquad \text{(M-4)}$$

The atmospheric temperature is assumed to vary linearly with altitude according to the relation.

$$T = T_o - \gamma\, x_3' \qquad \text{(M-5)}$$

The temperature of the parcel is also assumed to vary linearly with altitude according to the relation

$$T_p = T_o - \gamma_p\, x_3' \qquad \text{(M-6)}$$

As shown by Hess [181], based on the four preceding equations combined with the ideal gas law, by first-order theory the oscillation of the air parcel can be predicted. The period of oscillation is

$$\tau = \frac{2\pi}{\sqrt{g/T_o\,(\gamma_p - \gamma)}} \qquad \text{(M-7)}$$

Normally γ_p is assumed to be equal to the adiabatic lapse rate, Γ_s, and the resulting relation is

$$\tau_{B.V.} = \frac{2\,\pi}{\sqrt{g/T_o\,(\Gamma_s - \gamma)}} \qquad \text{(M-8)}$$

where the subscript B.V. refers to Brunt-Väisälä.

As pointed out by Angell and Pack [131], if γ_p is set equal to the constant density lapse rate, Γ_ρ, (instead of the adiabatic lapse rate), the motion of the air parcel is the same as that of a constant volume balloon with a period of oscillation of

$$\tau_{CVB} = \frac{2\pi}{\sqrt{g/T_o \; (\Gamma_\rho - \gamma)}} \tag{M-9}$$

Now

$$\Gamma_\rho = -.0341 \; {}^oK/m \tag{M-10}$$

which is about six times larger than the lapse rate normally observed in the lower atmosphere. For the case of an isothermal atmosphere,

$$\tau_{CVB} = \frac{2\pi}{\sqrt{g/T_o \; \Gamma_\rho}}$$

$$= 10.85 \sqrt{T_o} \tag{M-11}$$

Equation (M-11) closely agrees with the relation given by Lally [58].

Now for the test case #1, with an isothermal atmosphere,

$$\gamma = 0 \tag{M-12}$$

and

$$T_o = 218^oK \tag{M-13}$$

the time period is

$$\tau_{CVB} = 160.20 \text{ sec.} \tag{M-14}$$

The balloon displacement as a function of time, based on the computer program is presented in Table (M-1). Inspection of this table reveals a time period of 160 seconds, in close agreement with Equation (M-12).

For the case #2, the solution to Equation (M-1) is

$$x_3' = Ae^{-\alpha t} \cos \lambda t \tag{M-15}$$

where

$$\lambda = (N^2 - \alpha^2)^{\frac{1}{2}} \tag{M-16}$$

TABLE M-1

Predicted Displacement History of Constant-Volume Balloon in a Stationary Isothermal Atmosphere (Test Case #1) *

Time Step N	Vertical Displacement x_3-x_{30}(m)	Time t (sec)	Time Step N	Vertical Displacement x_3-x_{30}(m)	Time t (sec)
1	10.	0	22	-10.39	105
2	9.74	5	23	- 8.14	10
3	8.93	10	24	- 5.69	15
4	7.76	15	25	- 3.13	20
5	6.12	20	26	- .57	25
6	4.13	25	27	+ 1.89	30
7	1.86	30	28	4.15	35
8	- .59	35	29	6.13	40
9	- 3.14	40	30	7.77	45
10	- 5.69	45	31	8.99	150
11	- 8.14	50	32	9.74	55
12	-10.40	55	33	10.00	60
13	-12.38	60	34	9.77	65
14	-14.00	65	35	9.05	70
15	-15.21	70	36	7.86	175
16	-15.95	75	37	6.25	80
17	-16.20	80	38	4.28	85
18	-15.95	85	39	2.02	90
19	-15.21	90	40	- .43	95
20	-14.00	95	41	- 2.98	200
21	-12.37	100			

* Note: An error in the balloon density places the equilibrium position at $x_3 - x_{30} \cong - 3$ m.

TABLE M-1 (con't)

Time Step N	Vertical Displacement $x_3 - x_{30}$ (m)	Time t (sec)	Time Step N	Vertical Displacement $x_3 - x_{30}$ (m)	Time t (sec)
42	- 5.53	205	62	7.67	305
43	- 7.99	10	63	8.92	10
44	-10.27	15	64	9.71	15
45	-12.27	20	65	10.00	20
46	-13.92	225	66	9.79	325
47	-15.15	30	67	9.09	30
48	-15.92	35	68	7.93	35
49	-16.21	40	69	6.34	40
50	-15.99	45	70	4.39	45
51	-15.27	250	71	2.16	350
52	-14.09	55	72	- .27	55
53	-12.49	60	73	- 2.82	60
54	-10.53	65	74	- 5.37	65
55	- 8.29	70	75	- 7.83	70
56	- 5.85	275	76	-10.11	375
57	- 3.30	80	77	-12.12	80
58	- .74	85	78	-13.79	85
59	+ 1.73	90	79	-15.06	90
60	4.02	95	80	-15.87	95
61	6.02	300	81		400

In the case studied, it was found that $\alpha^2 << N^2$. Consequently the period

$$\tau = \frac{\tau_o}{\sqrt{1 - \tau_o^{\,2}/\tau_\alpha^{\,2}}}$$

$$\simeq \tau_o \tag{M-17}$$

where

$$\tau_o = 2\pi/N \tag{M-18}$$

$$\tau_\alpha = 2\pi/\alpha \tag{M-19}$$

$$N = \sqrt{\frac{g}{T_o\ (\gamma_o - \gamma)}} \tag{M-20}$$

Hence, no change in this period was observed in the numerical solution due to the dissipation term. However, the amplitude damping in the numerical solution was found to correspond almost exactly to the theoretical value.

In the Case #3 test, it was observed that the period τ given by the numerical solution corresponded closely to the first-order solution which required

$$\tau = \sqrt{\frac{3}{2}}\ \tau_o \tag{M-21}$$

In the fourth test, the Basset force was non-zero,

$$F_B \propto \int_o^t \frac{dv_3/dt'}{\sqrt{t - t'}} dt' \tag{M-22}$$

No attempt was made to obtain a solution to the integral equation. The results of the test suggested that the Basset term behaves like a term, of the form,

$$F_B = 2a\ \ v_3 - b^2 x_3' \tag{M-23}$$

leading to an equation of the form

$$\frac{dv_3}{dt} + 2a\ \ v_3 + (N^2 - b^2)\ x_3' = 0 \tag{M-24}$$

where the fundamental period was altered and the motion dampened. The oscillation was regular over two periods leading to the supposition that

$$a, b \neq f(x_3') \tag{M-25}$$

The value of "a" was of the same order of magnitude as the coefficient of the integral. However, "b^2" was found to be an order of magnitude greater;

$$b^2 \sim 10\, a \sim 10^{-2} \tag{M-26}$$

All of the preceding tests were conducted assuming an isothermal atmosphere with the natural period given by the relation

$$\tau_o = T_o \sqrt{\frac{g}{\gamma_o}} \tag{M-27}$$

instead of the more general relation

$$\tau = T_o \sqrt{\frac{g}{\gamma_o - \gamma}} \tag{M-28}$$

One additional test case (#5) was run to ensure that $\gamma = 0$ was not a special case. The period of this test case and the period obtained from the analytic solution of the equation were again nearly identical.

APPENDIX N

Results of Test Runs #6 - #11

Based on the numerical solution produced by BALLOON, the variation of the vertical component of velocity (for the wind and the balloon) versus time is presented in Figures N-1 through N-5 for test cases #6 - #11.

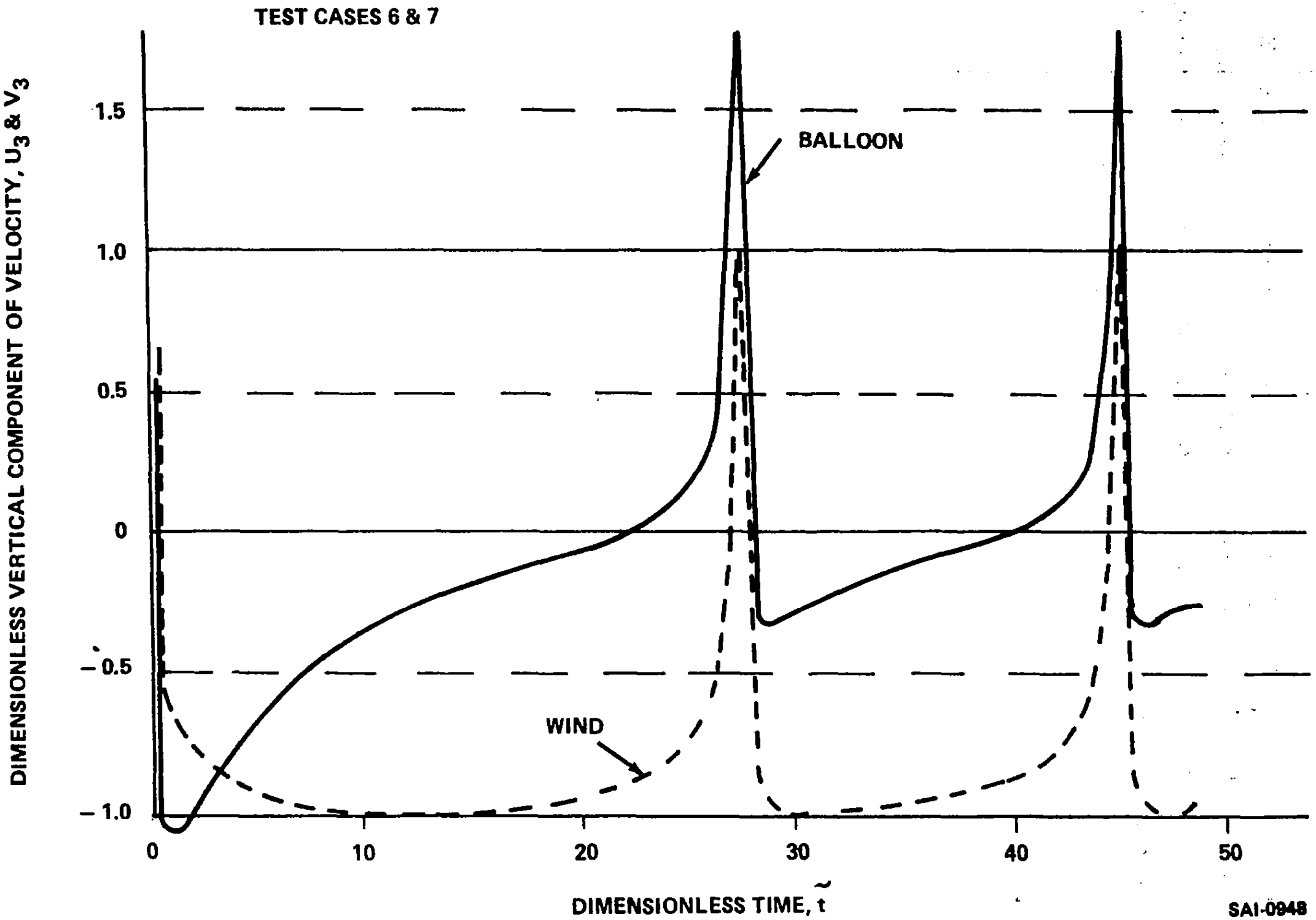

Figure N-1. Vertical Component of Velocity Versus Time, Test Cases #6 and #7

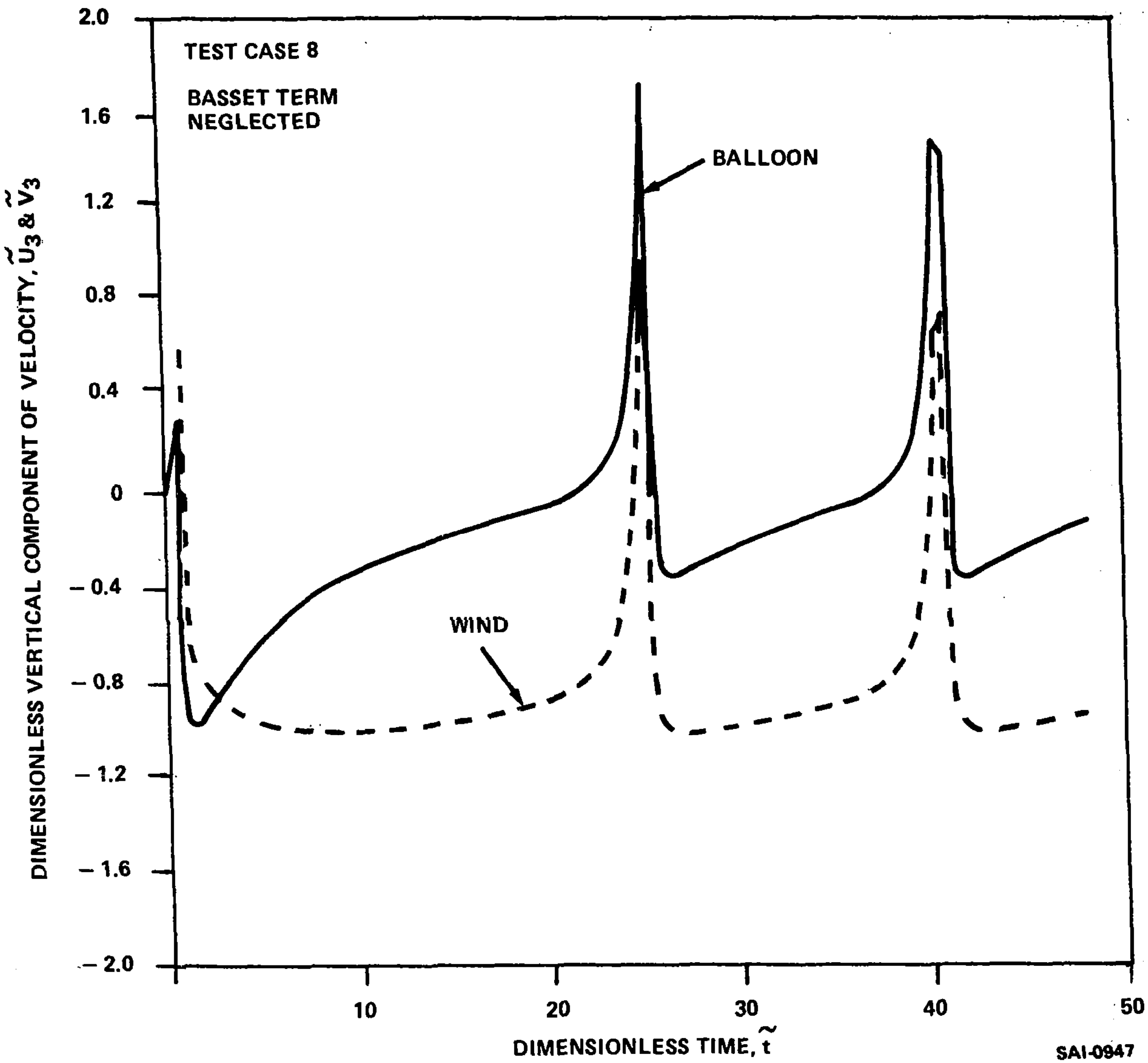

Figure N-2. Vertical Component of Velocity Versus Time, Test Case #8

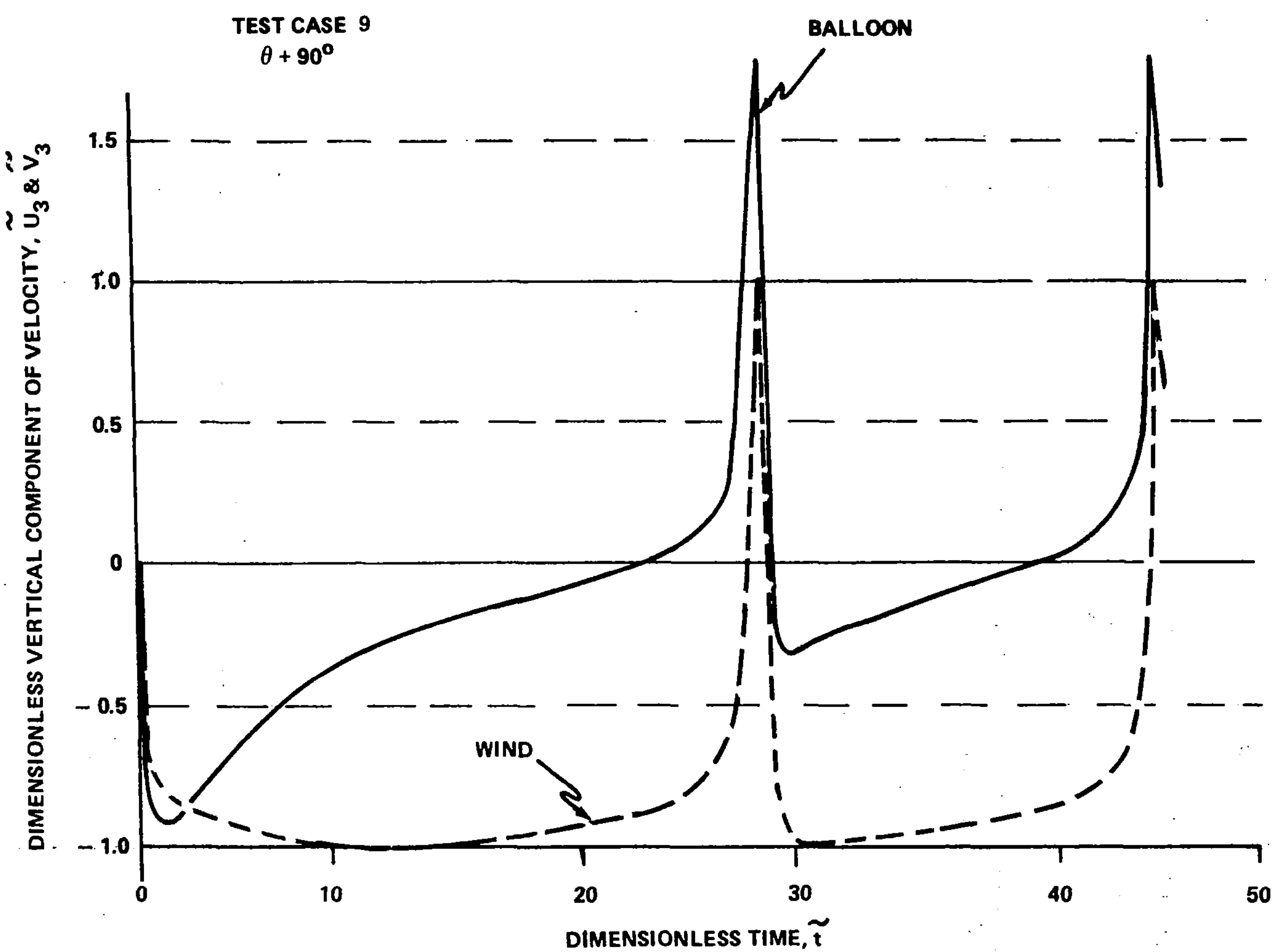

Figure N-3. Vertical Component of Velocity Versus Time, Test Case #9

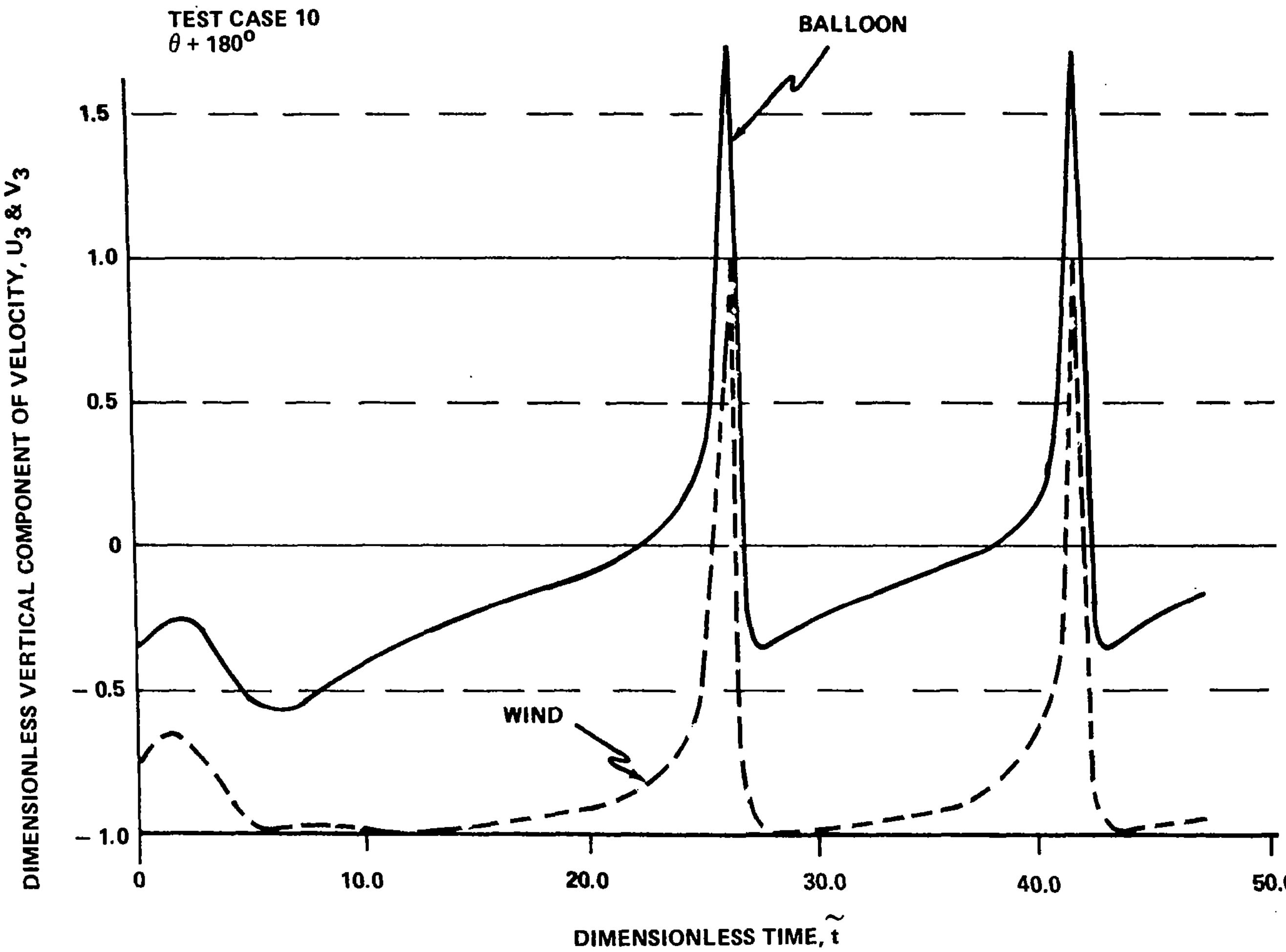

1-75-1566

Figure N-4. Vertical Component of Velocity Versus Time, Test Case #10

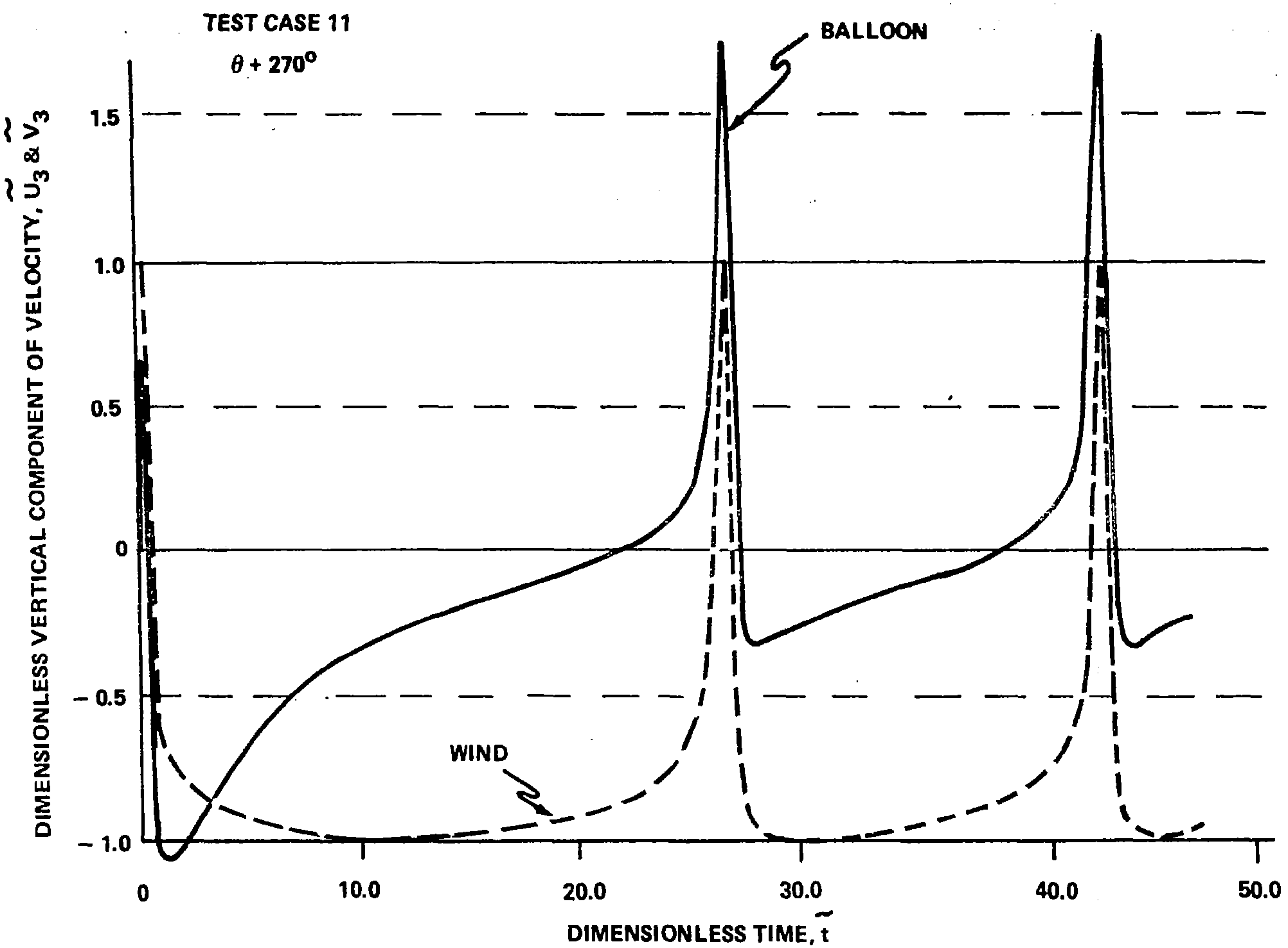

1-75-1565

Figure N-5. Vertical Component of Velocity Versus Time, Test Case #11

APPENDIX O

Analysis of Numerical Results, Phase I (16 Original Runs)

For each of the sixteen runs which were initially performed as part of Phase I a set of 6 position and velocity plots was generated. These plots are not included in the report because of the considerable bulk which they represent. They have been collected and bound in a separate document [1] for reference purposes.

For each of the sixteen runs special attention was given to the length of the time interval over which the numerical integration was carried out. The time interval used along with the time period of the associated flow field are presented in Figure O-1.

Figure O-2 presents the linear period, the observed period and the observed phase lag in the balloon velocity for the 16 runs. The wind is given by:

$$u_i = \bar{u}_i + A \sin (k_j x_j - \omega t + \theta_i) \qquad \text{(O-1)}$$

Based on the assumption

$$x_i = \bar{u}_i t \qquad \text{(O-2)}$$

then the linear period is given by

$$\tau = \frac{2\pi}{k\,|\bar{u}_1 - c|} \qquad \text{(O-3)}$$

since $k_i = k$ and $\bar{u}_i = \bar{u}_i \delta_{i1}$, and

$$c = \frac{\omega}{k} \qquad \text{(O-4)}$$

is the phase velocity. The observed periods are taken directly from the data represented in Figures 5-4 through 5-6.

In Figure O-2 values to the right of the principal diagonal represent cases where $\bar{u}_1 > c$ and to the left where $\bar{u}_1 < c$. Of course, on the diagonal, $\bar{u}_1 = c$, corresponding to Taylor's hypothesis. Off the diagonal the equation for vertical motion has the form

ω (sec^{-1}) \ k (cm^{-1})	6.28×10^{-6}	6.28×10^{-5}	6.28×10^{-4}	6.28×10^{-3}
6.28×10^{-3}	A_{11} 20000 ∞	A_{12} 4000 111	A_{13} 600 10.1	A_{14} 80 1.00
6.28×10^{-2}	A_{21} 4000 111	A_{22} 4000 ∞	A_{23} 600 11.1	A_{24} 80 1.01
6.28×10^{-1}	A_{31} 600 10.1	A_{32} 600 11.1	A_{33} 600 ∞	A_{34} 80 1.11
6.28	A_{41} 80 1.00	A_{42} 80 1.01	A_{43} 80 1.11	A_{44} 80 ∞

NOTE: Associated with each element in the array there are two numbers. The top number is the total time interval over which the particular case was integrated, and the bottom number is the linear period due to the forcing function. Both time periods have units of seconds.

Figure O-1. Total Time Intervals and Linear Periods for 16 Original Runs of Phase I

ω (sec^{-1}) \ k (cm^{-1})	6.28×10^{-6}	6.28×10^{-5}	6.28×10^{-4}	6.28×10^{-3}
6.28×10^{-3}	A_{11} ∞ ∞ (?)	A_{12} 111 114 (+5)	A_{13} 10.1 10.3 (0)	A_{14} 1.00 1.06 (0)
6.28×10^{-2}	A_{21} 111 111 (+10)	A_{22} ∞ ∞ (?)	A_{23} 11.1 12 (0)	A_{24} 1.01 1.09 (0)
6.28×10^{-1}	A_{31} 10.1 10.1 (0)	A_{32} 11.1 11.4 (0)	A_{33} ∞ ∞ (?)	A_{34} 1.11 1.23 (0)
6.28	A_{41} 1.00 1.00 (-0)	A_{42} 1.01 1.01 (0)	A_{43} 1.11 1.10 (0)	A_{44} ∞ ∞ (?)

NOTE: Associated with each element in the array there are three numbers. The upper number is the theoretical (linear) period, the middle number is the observed period, and the lower number is the phase lag. Positive values of the phase lag indicate the balloon lags of the wind. All values are in seconds.

Figure O-2. Periods of Oscillation and Phase Lag for 16 Original Runs of Phase I

$$\frac{dv_3}{dt} + 2\alpha\, v_3 + N^2 x_3' = C \cos (k_j x_j - \omega t + \theta_3) + G \qquad (O-5)$$

where the left-hand-side of the equation is the usual equation for a damped oscillator. The first term on the right-hand-side is the forcing function due to the pressure forces where C is assumed to be a constant, and G is a function which is nonlinear in dx_3/dt. If the function G is neglected, the balloon would be expected to oscillate with the period of the forcing function given by Equation (O-3). This expectation is borne out by the test case results. The largest observed deviation from the linear period occurs along the fourth column in Figure O-2 where the wave number is a maximum and not necessarily where $|u - c|$ approaches a minimum.

Along the diagonal of the experiment matrix, the cosine of Equation (O-5) becomes a constant. For these cases the oscillations should be expected to damp out as was observed in the A_{11} case. In these cases, the balloon approximately matched the flow after the initial transient motion was suppressed and the forces balanced to hold it in this position. Thus for case A_{11}, the balloon was observed to reach equilibrium about 120 m below its equilibrium level and, was observed to continue to have a lateral motion. This lateral motion persists for longer time intervals, causing an ever-increasing lateral displacement of the balloon. Therefore, one would observe no vertical motion but a mean lateral motion.

The vertical displacement typically displayed two modes of oscillation. The short-period oscillation corresponded to the forced oscillation. The long-period oscillation resulted from the initial conditions and was found to be damped as expected.

Figure O-3 shows case A_{31} where a very long total time interval for numerical integration was employed. This case clearly shows the damping in the transient mode of oscillation.

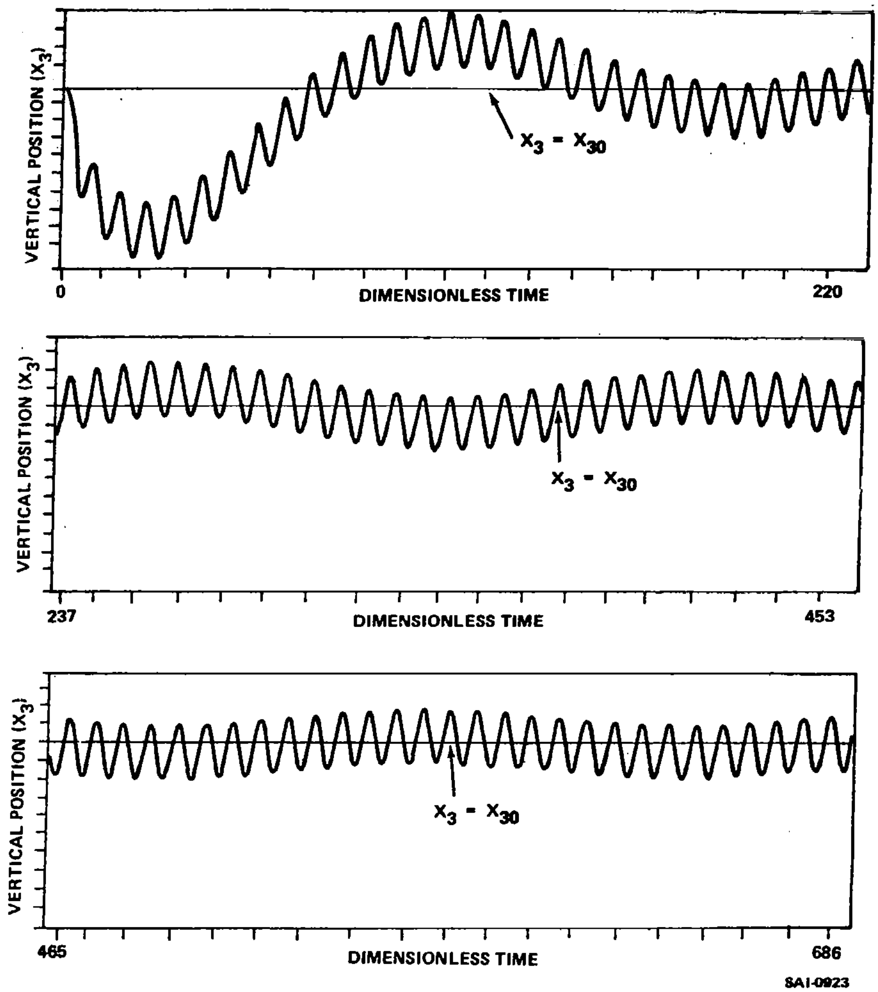

Figure O-3. Run A_{31}. Vertical Position of Balloon as a Function of Time.

APPENDIX P

Analysis of Numerical Results Phase I - Cruciform Runs

P.1 Cruciform C_{22}

Twenty-four runs were carried out in the Cruciform C_{22} arrangement shown in Figure P-1. The values of k and ω for each run are given in Figure P-1. For each run, a set of six position and velocity histories are generated. These plots are not included in the report, because of the considerable bulk which they represent. Such plots have been collected and bound in a separate document [1] for reference pusposes.

Analysis of the numerical results of the 24 runs was primarily concerned with comparing the first-order theoretical time period with the observed value. The results of this comparison are presented in Figure P-2. In general, as the conditions corresponding to A_{22} are approached along any one of the four branches of the cruciform the first-order theoretical period and the observed period agree less and less, with the observed value increasing more rapidly than the first-order theoretical value. This indicates that first-order theory, which is linear, is not sufficient to predict the balloon motion under conditions where Taylor's hypothesis is (nearly) satisfied.

P.2 Cruciform C_{33}

Twelve runs were carried in the Cruciform C_{33} arrangement as shown in Figure P-3 . The values of k and ω for these runs are presented in Figure P-3. As with the C_{22} runs, a set of six position and velocity histories was generated for each run. These plots have been collected and bound in separate documents 1 for reference purposes.

As in the case of the C_{22} runs, analysis of the numerical results of the twelve runs was primarily concerned with comparing the first-order theoretical time period with the observed values. Figure P-4 provides a summary of this comparison. Inspection of this figure reveals the same trend as observed in Cruciform C_{22}. Again, it would appear that first-order theory is not adequate to predict the balloon motion under conditions where Taylor's hypothesis is (nearly) satisfied.

U_{226}	8.168×10^{-3}	4.084×10^{-2}
U_{225}	8.168×10^{-3}	4.901×10^{-2}
U_{224}	8.168×10^{-3}	6.535×10^{-2}
U_{223}	8.168×10^{-3}	7.079×10^{-2}
U_{222}	8.168×10^{-3}	7.351×10^{-2}
U_{221}	8.168×10^{-3}	7.515×10^{-2}

L_{226}	L_{225}	L_{224}	L_{223}	L_{222}	L_{221}	A_{22}	R_{221}	R_{222}	R_{223}	R_{224}	R_{225}	R_{226}
4.084×10^{-3}	4.901×10^{-3}	6.535×10^{-3}	7.079×10^{-3}	7.351×10^{-3}	7.515×10^{-3}	8.168×10^{-3}	8.822×10^{-3}	9.257×10^{-3}	1.144×10^{-2}	1.634×10^{-2}	2.450×10^{-2}	4.084×10^{-2}
8.168×10^{-2}	8.168×10^{-2}	8.168×10^{-2}	8.168×10^{-2}	8.168×10^{-2}	8.168×10^{-2}	8.168×10^{-2}	8.168×10^{-2}	8.168×10^{-2}	8.168×10^{-2}	8.168×10^{-2}	8.168×10^{-2}	8.168×10^{-2}

D_{221}	8.168×10^{-3}	8.822×10^{-2}
D_{222}	8.168×10^{-3}	9.257×10^{-2}
D_{223}	8.168×10^{-3}	1.114×10^{-1}
D_{224}	8.168×10^{-3}	1.634×10^{-1}
D_{225}	8.168×10^{-3}	2.450×10^{-1}
D_{226}	8.168×10^{-3}	4.084×10^{-1}

NOTE: ASSOCIATED WITH EACH ELEMENT IN THE CRUCIFORM THERE ARE TWO NUMBERS. THE UPPER IS $\tilde{k}$ AND THE LOWER IS $\tilde{\omega}$.

SAI-0803

Figure P-1. Values of $\tilde{k}$ and $\tilde{\omega}$ for Cruciform C_{22}

	Upper	Lower
U_{226}	153.9	168.5
U_{225}	192.3	234.7
U_{224}	384.6	—
U_{223}	576.9	> 5750
U_{222}	769.2	—
U_{221}	961.5	> 9160

L_{226}	L_{225}	L_{224}	L_{223}	L_{222}	L_{221}	A_{22}	R_{221}	R_{222}	R_{223}	R_{224}	R_{225}	R_{226}
153.8	192.3	384.6	576.9	7693	961.5	∞	961.5	576.9	192.3	76.9	38.5	19.2
168.5	207.7	707.7	>5660	(?)	> 9190	∞	> 9180	> 5720	273.0	85.4	40.8	20.0

	Upper	Lower
D_{221}	961.5	> 9190
D_{222}	576.9	> 5760
D_{223}	192.3	232.3
D_{224}	76.9	80.0
D_{225}	38.5	38.7
D_{226}	19.2	19.2

NOTE: ASSOCIATED WITH EACH ELEMENT IN THE CRUCIFORM, THERE ARE TWO NUMBERS. THE UPPER NUMBER INDICATES THE THEORETICAL PERIOD AND THE LOWER NUMBER THE OBSERVED PERIOD.

SAI-0804

Figure P-2. Dimensionless Time Periods for Runs in the Cruciform C_{22}

U_{333} $\begin{cases} 8.168 \times 10^{-2} \\ 4.747 \times 10^{-1} \end{cases}$

U_{332} $\begin{cases} 8.168 \times 10^{-2} \\ 7.028 \times 10^{-1} \end{cases}$

U_{331} $\begin{cases} 8.168 \times 10^{-2} \\ 7.484 \times 10^{-1} \end{cases}$

L_{333}	L_{332}	L_{331}	A_{33}	R_{331}	R_{332}	R_{333}
5.757×10^{-2}	7.167×10^{-2}	7.537×10^{-2}	8.168×10^{-2}	8.915×10^{-2}	9.494×10^{-2}	1.406×10^{-1}
8.168×10^{-1}	8.168×10^{-1}	8.168×10^{-1}	8.168×10^{-1}	8.168×10^{-1}	8.168×10^{-1}	8.168×10^{-1}

D_{331} $\begin{cases} 8.168 \times 10^{-2} \\ 8.852 \times 10^{-1} \end{cases}$

D_{332} $\begin{cases} 8.168 \times 10^{-2} \\ 9.309 \times 10^{-1} \end{cases}$

D_{333} $\begin{cases} 8.168 \times 10^{-2} \\ 1.159 \end{cases}$

NOTE: ASSOCIATED WITH EACH ELEMENT IN THE CRUCIFORM THERE ARE TWO NUMBERS. THE UPPER IS $\tilde{k}$ AND THE LOWER IS $\tilde{\omega}$.

SAI-0895

U_{333}: 18.3 / 20.7

U_{332}: 55.1 / > 575.5

U_{331}: 91.8 / > 918.0

L_{333}	L_{332}	L_{331}	A_{33}	R_{331}	R_{332}	R_{333}
26.1	62.8	99.5	∞	84.2	47.4	10.6
31.0	557.9	(?)	∞	> 920.1	> 568.6	12.8

D_{331}: 91.8 / > 918.0

D_{332}: 55.1 / > 575.5

D_{333}: 18.3 / 20.8

NOTE: ASSOCIATED WITH EACH ELEMENT IN THE CRUCIFORM, THERE ARE TWO NUMBERS. THE UPPER NUMBER INDICATES THE THEORETICAL PERIOD AND THE LOWER NUMBER THE OBSERVED PERIOD.

SAI-0896

Figure P-4. Dimensionless Time Periods for Runs in the Cruciform C_{33}

*U.S. GOVERNMENT PRINTING OFFICE: 1977 - 735-004/37